Improved Environmental Characterization to Support Natural Resource Decision Making: (1) Distributed Soil Characterization, and (2) Treatment of Legacy Nutrients

Elyce Buell

Dissertation submitted to the faculty of the Virginia Polytechnic Institute and State University in partial fulfillment of the requirements for the degree of
Doctor of Philosophy
In Biological Systems Engineering

Zachary M. Easton, Chair
Scotland C. Leman
Julie E. Shortridge
Stephen K. Stephenson

August 11th, 2022
Blacksburg, VA

Key words: Soil Physical Properties, Digital Elevation Model (DEM) Resolution, Topographic Index, Specific Catchment Area, Slope, bioreactors, legacy nitrogen, best management practices

Improved Environmental Characterization to Support Natural Resource Decision Making: (1) Distributed Soil Characterization, and (2) Treatment of Legacy Nutrients

Elyce Buell

Academic Abstract

Environmental concerns are becoming increasingly relevant during a period of hemorrhaging ecosystem goods and services. Restoring these would result in positive outcomes for public health and economic benefit. This thesis seeks to address two environmental concerns: (1) accurate soil mapping and (2) treatment of nitrogen to affect water quality change.

The current method of soil mapping, SSURGO (USDA-NRCS Soil survey), is often erroneous and misleading. Two studies in this dissertation are conducted to evaluate the potential that different resolution digital elevation models (DEMs) have to distribute soil characteristics successfully. These studies are conducted in southwest Virginia and western Vermont. The aforementioned studies evaluated 36 and 59 soil samples, respectively. Spatial characteristics, including slope, catchment area, and topographic wetness, are derived from several DEMs. In chapter 2, these characteristics are spatially compared, and we found that small resolution rasters result in narrow flow paths relative to coarser rasters. In chapter 3, we isolate the analysis to focus on resolution size, instead of a mix of both resolution size and generation method. This is done by recursively coarsening small rasters, deriving spatial attributes from said rasters and evaluating their potential to fit the soil characteristics of interest. Here we found that slopes generated from resolutions smaller than 11m were poor predictors of soil characteristics. Both chapters are finished by proposing and evaluating a soil map. Proposed regressions beat SSURGO in all investigated properties. Furthermore, proposed maps consistently beat out uninformed smallest resolution derived maps.

Chesapeake bay water quality managers are struggling to achieve targets for nitrogen loading. This is in part due to the widespread presence of legacy nitrogen. Legacy nitrogen is an emerging issue, and springs exporting high levels of nitrogen are not uncommon in northern Virginia. This thesis explores, in part, a novel concept of treating large loads of nitrogen exported from a spring with a bioreactor. Bioreactors are a young science that most typically pair carbon heavy subterranean receptacles to agricultural drainage. This provides a location for nitrogen fixing bacteria to consume nitrate/nitrite, turning these into inert nitrogen gas. A spring fed bioreactor is studied for 10 months, and bioreactor conditions including influent and effluent nitrogen concentrations, bioreactor flow, and temperature are collected. A model driven by first order reaction equations is found to be most accurate with inputs of temperature and bioreactor age. The resulting marginal effects of these inputs were consistent with previously reported studies.

Improved Environmental Characterization to Support Natural Resource Decision Making: (1) Distributed Soil Characterization, and (2) Treatment of Legacy Nutrients

Elyce Buell

General Audience Abstract

Centuries of industrialization have resulted in widespread human progress but have, at times, adversely impacted the environment. Constituents rely heavily on environmental services, such as clean air and water, to subsist. Environmental degradation has resulted in detrimental effects to public health, and remediation is currently economically viable. As such, there are strong incentives for researchers to understand environmental processes at a fundamental level.

One such process is soil characteristic distribution. The distribution of soil characteristics, such as soil texture or organic matter, is especially important for agriculturalists, hydrologists and geotechnicians. Soil texture and organic matter distribution can affect crop yield, nitrogen export to surface waters, and structural stability of soils. Thus, accurate characterization of measured soil properties is paramount to multiple fields. The most typically used soil map is USDA-NRCS Soil survey (commonly referred to as SSURGO). Currently, the SSURGO database is a poor predictor of soil characteristics. There is an opportunity to improve soil characteristic distribution using digital elevation models (DEMs). As DEMs become cheaper to develop, they are typically available in multiple resolutions and generation methods. In this research, several DEMs are used to better soil maps for watersheds in Southwest Virginia and Western Vermont. Both studies showed that DEMs can better distribute soils when compared to the current SSURGO maps. Additionally, we showed that the finest resolution dataset was not always best, and mixed resolution topographic wetness indices to be most advantageous for distributing soils.

Another such process is remediation of surface waters from high loads of nitrogen and phosphorus. The Haber-Bosch method of producing nitrogen fertilizer is one of the most important human innovations in recent history. This method is likely responsible for the aversion of widespread famine in the early 1900s. However, residents of multiple river systems, including the Chesapeake Bay and the Mississippi River, are suffering from the adverse effects of widespread hypoxic/anoxic (with little/no oxygen, respectively) zones within water. These have partially been responsible for the decline of commercial ventures such as fisheries and tourism. These zones are caused by eutrophication, a process of unsustainable plant growth in the presence of nitrogen and phosphorus. Water quality managers typically target agricultural runoff and point source polluters when trying to eliminate anthropogenic nitrogen. However, legacy nitrogen (nitrogen stored in groundwater in excess of a year) has become an emerging concern for water quality. It is not uncommon for springs in karst areas to be contaminated with high concentrations of nitrogen. These springs present a point source that can be treated by an emerging technology: bioreactors. Bioreactors are subterranean, woodchip filled basins that provide a location for microbes to exchange water soluble nitrogen for inert nitrogen gas. The consistency in nitrogen loading and constant flow provide stability relative to more traditional bioreactor installations. Most typically, bioreactors are installed downstream of agricultural drainage systems, and influent flow and nitrogen load depend wholly on precipitation/irrigation and nitrogen application. In this thesis, a novel spring fed bioreactor is studied. Removal rates of nitrogen are quantified using a regression driven by reaction kinetics. The analysis showed bioreactor efficiency was intimately related to hydraulic residence time, nitrogen loading, bioreactor bed temperature, and bioreactor age. The spring fed bioreactor is found to be advantageous because of its consistency, and disadvantages because springs are colder and thus less efficient than typical irrigated runoff.

Dedication

To my significant other, Darby Nikolai Throwback Frisk Houghton: your bottomless patience and unending kind spirit have been integral to the completion of this thesis. You are my #1.

Acknowledgements

It would be easy for me to write a thesis length acknowledgements section, but I will do my best to spare you. I want to thank my advisor, Zachary Easton. I have learned a lot under his guidance, and I appreciate the work he has put into me as a graduate student and a colleague. His work ethic is matched by few, and his passion for this field is contagious. Secondly, I want to thank my committee member Kurt Stephenson. He has always been kind and a believer in my work, and I will certainly miss our unscheduled calls to discuss methods and analysis. I would also like to thank my committee member Scotland Leman for being so welcoming to my enthusiasm of learning in his classes. My research was strongly formed by the classes I took under Dr. Leman. Next, I would like to thank Julie Shortridge for her support of my research. I look forward to paying your mentorship forward in my career.

I want to thank the wonderful people who have made up the “E-Lab” during my degree. Specifically, I want to thank Amy Collick for refining the first two chapters of this thesis. I have really enjoyed this collaboration. I would be remiss if I didn’t thank Dan Fuka for his fantastic research ideas and support throughout this dissertation. I would also like to thank Roja Kaveh Garna who has been all that anyone could ask for in a colleague. Her unending good spirits have gotten me through some of my worst days. Her willingness to help me with whatever I need has been vital, and I will always admire her work ethic. Next I would like to thank William Auchincloss for being a strong supporter of me and helping me with all my lab work. Lastly, I would like to thank Sabrina Mehzabin and Binyam Asfaw. I look forward to seeing what kind of impact you will have on this field.

I would also like to thank the BSE department as a whole. I have really enjoyed my time working as a GRA/GTA for this department and am proud to be associated with BSE. The administrators in this department are all such sweet people who are eager to help me in any way possible. Special thanks to Laura Leman who fielded all my questions no matter how outlandish. I would also like to affirm my appreciation for my funding resources: NSF [award no. 1740704, Collaborative Research: EarthCube Integration--Brokered Alignment of Long-Tail Observations (BALTO)], and USDA NRCS Conservation Innovation Grants Program [award no. 69-3A75-13-232].

I could not have done this without the amazing support of my family. I would like to thank my father, Scott Buell, who sent me care packages for my test weeks and was always ready to go to bat for me (even without being asked). For those of you who know my mother, Diane Buell, you may not be surprised to know that she’s always been a strong role model for my life. I will always remember her face when I told her in Cazenovia, NY in 2016 that I was thinking about getting a PhD. She didn’t even flinch, at the time I thought it was so outlandish but she thought it was an obvious next step. I would also like to thank my brothers: Brennan (M.S.), Colby (M.D.), and Reggie (hometown famous) Buell. The four of us are the goofiest group of overachievers, and I love you all.

Lastly, I would like to thank my amazing friends. The wonderful ladies at 608 Preston made graduate school manageable, and dare I say, fun. I love you all, and I will always think of fancy feasts, craft nights, and our fights with Townside fondly. My sincerest appreciation to the strong women and men of VT crew who knew my worth when I did not; I will never forget full moon rows on Claytor Lake. Thank you to my closest friends William Ferris, Lydia Perkins, and Greta Healy (heiress to the Heely’s Inc. fortune). I would also like to thank my dog, Stella, for her unconditional affection. From the bottom of my heart, I would like to thank my significant other, Darby. He has done more for me than I can articulate. Lastly, thank you to all the unnamed people who made this degree possible.

Table of contents

List of figures

List of tables

List of abbreviations

Abbreviation	**Shortened from**
as	arcsecond
ASTER	Advanced Spaceborne Thermal Emission and Reflection Radiometer
AR1	Autoregressive coeffcient of lag 1
ARIMA	AutoRegressive Integrated Moving Average
AWC	Availible water content
CA	Upslope contributing area
D8	D8 flow direction algorithm
DC	Dead Creek
DEM	Digital elevation model
Dinf	D-Infinity flow direction algorithm
DO	Dissolved oxygen
GDEM	Generalized Digital Environmental Model
GPS	Global positioning system
HRT	Hydraulic residence time
LiDAR	Light detecting and ranging
LOC	Little Otter Creek
m	meter
N	nitrogen
NED	National elevation database
NRC/NRCS	National resource council
ORP	Oxidative redox potential
SAR	Synthetic aperture radar
SCA	Specific upslope contributing area
SRTM	Shuttle radar topographic mission
SSURGO	USDA-NRCS Soil survey geographic
StREAM Lab	Stroubles research, education, and management lab
TI/TIV	Topographic wetness value
TIC	Topographic wetness class
USGS	United States geological survey

Chapter 1: Introduction

1.1 Problem Statement

1.1.1 Improving characterization of different environmental processes and environmental engineering solutions

The accurate characterization of environmental processes is of great interest to a myriad of constituents including policy makers, recreational users, and businesses. Specifically, knowing how inputs, such as nitrogen applications on farmland or climate scenarios, would affect the environmental goods and services, defined as common-pool resources that residents and companies rely heavily on, is critical for stakeholders' livelihoods. Services such as these are generally dwindling and several studies have evaluated the amount residents would pay to restore these services (Jordan and Elnagheeb 1993; Genius et al., 2008; Aguilar et al., 2018; Liu 2020). Hence, there is an economic incentive to understand environmental processes at a fundamental level and thus inform how these services work and how they can be restored via engineered solutions. The number of environmental processes and engineered solutions to address are vast; this thesis seeks to address a single environmental process (former) and a single engineered solution (latter): (1) soil characteristic distribution in a landscape, and (2) implementation of a bioreactor to treat groundwater contamination.

1.1.2 Soil characteristic representation

Soil characteristics, such as texture (sand, silt, and clay), directly affect multiple environmental sciences including hydrology, agronomy, and geotechnical engineering. For example, soil texture can affect crop growth, nutrient export, structural stability of hillslopes, and construction projects among many other applications. As such, efforts to categorize soils in the United States are extensive. Currently, the USDA has about 20,000 soil samples (pedons) used to inform its current soil maps (Nemecek 2020). There are several studies that indicate this current methodology, USDA-NRCS Soil Survey Geographic (SSURGO) method, is falling short in accurately representing soil characteristics (Collick et al., 2015; Fuka et al., 2016; Cole, 2017). SSURGO currently uses a combination of pedon information and landscape photographs to distribute soils. SSURGO distributed soil maps are prone to high error rates and the aforementioned studies have found a poor relationship between measured and SSURGO approximated soil properties.

Integration of digital elevation maps (DEMs - raster data that represents the landscape) to assist in soil characteristic distribution is a proposed alternative or enhancement to the current SSURGO maps. Several studies have considered using landscape as a predictor of soil characteristics (Moore et al., 1993; Collick et al., 2015; Fuka et al., 2016). This idea is physically based, as one would expect soil distribution to be linked to landscape characteristics. For example, water would preferentially take clay particles downhill over sand particles because sand is larger and thus harder to move. Multiple soil processes are linked to the landscape features that can be derived from DEMs such as landscape slope, catchment area (CA), and topographic wetness (TIV). CA is defined as the area of the landscape that can be expected to drain to a single raster location in the watershed; TIV is a proxy for landscape wetness and is calculated using slope and CA as inputs.

As DEMs become easier and less expensive to generate, these datasets are becoming abundant and present in a variety of resolution sizes and generation methods. However, little has been done to identify how successful specific DEMs would be at distributing soil characteristics relative to other DEMs. DEMs have been documented to show that different resolutions result in different derived spatial attributes and these spatial attributes can affect environmental process modeling (Wolock & Price 1994; Zhang & Montgomery 1994; Hancock et al., 2006; Sørensen et al., 2006; Schumann et al., 2008; Vaze et al., 2010; Buchanan et al., 2014; Gibson et al., 2021). The aforementioned papers largely address topographic wetness and hydraulic processes and we are interested in doing the same for soil physical properties.

1.1.3 Spring fed bioreactor

Extensive application of nutrients to assist in crop growth has resulted in high levels of groundwater contamination of nitrogen present in much of the eastern United States (Van Meter & Basu 2017; Van Meter et al., 2018; Easton et al., 2019; Stephenson et al., 2021). High levels of nitrogen can cause “blue baby syndrome” if consumed and has resulted in widespread eutrophication in surface waters. Eutrophication, defined as a process of unsustainable aquatic plant growth followed by widespread death resulting in hypoxic/anoxic conditions, is a severe detriment to the ecology, economy, and recreational use of surface waters (Dodds et al., 2009; Dorgham 2014). Typically, this is a result of high, often anthropogenic, nutrient loads entering water bodies. Because groundwater concentrations of nitrogen are difficult to estimate and nearly impossible to eliminate the source instantaneously, legacy nitrogen (defined as water that contains nitrogen and has been subsurface for more than a year) has been cited as one of the biggest issues plaguing initiatives to rehabilitate river networks in the eastern United States (NRCS 2011).

This presents an opportunity to treat groundwater using an emerging area of research: bioreactors. Bioreactors, in this context, refers to a basin of organic carbon material where water is diverted and fed slowly (relative to its bypass) through the organic media. Woodchips (which are most typically used) provide a surface and carbon source for denitrifying bacteria. Bioreactors are an emerging nutrient reduction technology and research indicates their capability of reducing nitrogen from artificially drained agricultural fields (Christianson et al., 2012; Christianson et. al., 2013; Christianson et al., 2017; Rosen & Christianson, 2017; Hassanpour et al., 2017; Bock et al., 2018; Coleman et al., 2019). These studies have found bioreactors to have a wide range of removal efficiencies that are often tied to influent concentration, bed temperature, and hydraulic residence time (amount of time water sits in the bioreactor) (HRT). Though all factors affecting bioreactor efficiency are of interest, it is particularly important to optimize the HRT because the amount of flow entering the bioreactor can be controlled by bioreactor designers and managers. Pairing bioreactors with springs provide a uniquely stable environment for microbial communities; the semi consistent loading and flow of spring water will likely benefit microbiological activity (Deng et al., 2012; Hassanpour et al., 2017; Lopez-Ponnada et al., 2017; Ali et al., 2021). This, paired with the presence of widespread legacy nitrogen present in the mid Atlantic provides an opportunity for pairing bioreactors to springs contaminated with high levels of nitrogen (Stephenson et al., 2021).

1.2 Research Objectives

The aim of this research described hereafter is to further our understanding regarding two environmental issues: soil characteristic distribution, and treating legacy nitrogen with bioreactors. Specifically, the objectives pursued are as follows:

1. Understand how spatially derived metrics such as slope, catchment area, and topographic wetness values differ spatially when a suite of flow direction algorithms and DEMs are compared
2. Propose and test a framework for distributing soil characteristics using multiple DEMs as predictors
3. Offer a physically based model that explains how bioreactor performance relates to bioreactor conditions
4. Recommend a method to help bioreactor managers maximize mass/time of nitrogen removed via denitrification

1.3 Organization of thesis

1.3.1 Chapter 1: Introduction

Chapter 1 provides a brief introduction to the problems this research intends to advance, outlines the research objectives, and concisely explains the organization of the thesis.

1.3.2 Chapter 2: Digital Elevation Model (DEM) assessment for landscape representation

Chapter 2 addresses research objectives (1) and (2) by investigating a small watershed in southwest Virginia using four different DEMs ranging from 0.75m to 30m in resolution. This manuscript was submitted to Georderma, the global journal of soil science, on July 20th, 2022. The dataset is published via zendo ebuell (2022b).

Attributions: I analyzed the data and led the writing of this chapter. Co-authors of the manuscript include Daniel R. Fuka, Amy S. Collick, Roja Kaveh, and Zachary M. Easton. Fuka and Easton contributed to the methods development and data interpretation. Fuka, Collick, Kaveh, and Easton contributed to manuscript preparation and review.

1.3.3 Chapter 3: Integrating multiple Digital Elevation Models into soil characteristic distribution

Chapter 3 further explores the general framework presented in chapter 2 and seeks to further address objectives (1) and (2) for two watersheds located in Vermont. Six DEMs were evaluated against 59 soil samples collected by the Vermont Association of Conservative Districts. The target manuscript submission date is late summer 2022. The dataset is published via zendo ebuell (2022a).

Attributions: I analyzed the data and led the writing of this chapter. Co-authors of the manuscript include Roja Kaveh, Sabrina Mehzabin, Binyam Asfaw, Louise Koepele, Daniel R. Fuka, Amy S. Collick, William Auchincloss, Zachary M. Easton. Kaveh, Fuka and Easton contributed to the methods development and data interpretation. Kaveh, Mehzabin, Asfaw, Koepele, and Auchincloss contributed to the writing of the introduction and the methods. Fuka, Collick, Kaveh, and Zachary M. Easton contributed to manuscript preparation and review.

1.3.4 Chapter 4: Characterization of Nitrate Removal in a Spring Fed Bioreactor

Chapter 4 seeks to address research objectives (3) and (4) using a spring fed bioreactor in northern Virginia. A year of daily data is used to train a physically based linear regression model and corresponding maximal nitrogen removal conditions are derived. The target manuscript submission date is fall 2022.

Attributions: I analyzed the data and led the writing of this chapter. Co-authors of the manuscript include Kurt Stephenson, Daniel R. Fuka, and Zachary M. Easton. Stephenson, Fuka, and Easton contributed to the methods development, data interpretation, manuscript preparation, and review.

1.3.5 Chapter 5: Conclusions

This chapter summarizes the findings presented in the research and reinforces impacts of each manuscript developed for this thesis.

References

Aguilar, F.X., Obeng, E.A., Cai, Z. 2018. “Water Quality Improvements Elicit Consistent Willingness-to-Pay for the Enhancement of Forested Watershed Ecosystem Services.” *Ecosystem Services* 30 (April): 158–71.

Ali, W., Takaijudin, H., Yusof, K.W., Osman, M., Abdurrasheed, A. S. 2021. The Common Approaches of Nitrogen Removal in Bioretention System. *Sustainability: Science Practice and Policy*, *13*(5), 2575. https://doi.org/10.3390/su13052575

Bock, E. M., Coleman, B. S. L., Easton, Z.M. 2018. Performance of an under-loaded denitrifying bioreactor with biochar amendment. *Journal of Environmental Management*, *217*, 447–455. https://doi.org/10.1016/j.jenvman.2018.03.111

Buchanan, B.P., Fleming, M., Schneider, R.L., Richards, B.K., Archibald, J., Qiu, Z., Walter, M.T., 2014. Evaluating topographic wetness indices across central New York agricultural landscapes. Hydrol Earth Syst Sci 18, 3279–3299.

Christianson, L, Bhandari, A., Helmers, M., Kult, K., Sutphin, T., Wolf, R. 2012. PERFORMANCE EVALUATION OF FOUR FIELD-SCALE AGRICULTURAL DRAINAGE DENITRIFICATION BIOREACTORS IN IOWA. *American Society of Agricultural and Biological Engineers*, *55*(6). https://vt.hosts.atlas-sys.com/illiad/illiad.dll?Action=10&Form=75&Value=1611795

Christianson, L., Helmers, M., Bhandari, A., Moorman, T. 2013. Internal hydraulics of an agricultural drainage denitrification bioreactor. *Ecological Engineering*, *52*, 298–307. https://doi.org/10.1016/j.ecoleng.2012.11.001

Christianson, L. E., Collick, A. S., Bryant, R. B., Rosen, T., Bock, E. M., Allen, A. L., Kleinman, P. J. A., May, E. B., Buda, A. R., Robinson, J., Folmar, G. J., Easton, Z. M. 2017. Enhanced denitrification bioreactors hold promise for mid-Atlantic ditch drainage. *Agricultural & Environmental Letters*, *2*(1), 170032. https://doi.org/10.2134/ael2017.09.0032

Cole, S.A. 2017. Comparing SSURGO data versus geospatial field measurements to estimate soil texture and infiltration rate classes in glaciated soils (PhD Thesis). Clemson University.

Coleman, B. S. L., Easton, Z. M., & Bock, E. M. (2019). Biochar fails to enhance nutrient removal in woodchip bioreactor columns following saturation. *Journal of Environmental Management*, *232*, 490–498. https://doi.org/10.1016/j.jenvman.2018.11.074

Collick, A.S., Fuka, D.R., Kleinman, P.J.A., Buda, A.R., Weld, J.L., White, M.J., Veith, T.L., Bryant, R.B., Bolster, C.H., Easton, Z.M. 2015. “Predicting Phosphorus Dynamics in Complex Terrains Using a Variable Source Area Hydrology Model: MODELLING P DYNAMICS IN COMPLEX TERRAINS.” *Hydrological Processes* 29 (4): 588–601.

Deng, Z., Sun, S., Gang, D. D. 2012. Modeling nitrate-nitrogen removal process in first-flush reactor for stormwater treatment. *Bioprocess and Biosystems Engineering*, *35*(6), 865–874. https://doi.org/10.1007/s00449-011-0671-3

Dodds, W. K., Bouska, W. W., Eitzmann, J. L., Pilger, T. J., Pitts, K. L., Riley, A. J., Schloesser, J. T., Thornbrugh, D. J. 2009. Eutrophication of U.S. Freshwaters: Analysis of Potential Economic Damages | Environmental Science & Technology. Environmental Science & Technology, 43(1), 12–19. https://doi.org/10.1021/es801217q

Dorgham, M. M. 2014. Effects of Eutrophication. In A. A. Ansari & S. S. Gill (Eds.), Eutrophication: Causes, Consequences and Control: Volume 2 (pp. 29–44). Springer Netherlands. https://doi.org/10.1007/978-94-007-7814-6_3

Easton, Z.M., Bock, E., Stephenson, K. 2019. "Feasibility of Using Woodchip Bioreactors to Treat Legacy Nitrogen to Meet Chesapeake Bay Water Quality Goals." *Environmental Science & Technology* 53 (21): 12291–99.

ebuell. (2022a). ebuell/-Assessing-DEM-resolution-for-accurate-representability-of-soils: version1 release of Assessing DEM resolution for accurate representability of soils (Version Version1). Zenodo. https://doi.org/10.5281/zenodo.6857407

ebuell. (2022b). ebuell/Evaluating-Digital-Elevation-Models-and-Topographic-Indices-for-Geomorphic-Landscape-Representaton: version1 (Version version1). Zenodo. https://doi.org/10.5281/zenodo.6791484

Fuka, D.R., Collick, A.S., Kleinman, P.J.A., Auerbach, D.A., Harmel, R.D., Easton, Z.M. 2016. "Improving the Spatial Representation of Soil Properties and Hydrology Using Topographically Derived Initialization Processes in the SWAT Model," November. https://doi.org/10.1002/hyp.10899.

Genius, M., Hatzaki, E., Kouromichelaki, E. M., Kouvakis, G., Nikiforaki, S., Tsagarakis, K. P. 2008. "Evaluating Consumers' Willingness to Pay for Improved Potable Water Quality and Quantity." *Water Resources Management* 22 (12): 1825–34.

Gibson, A.J., Hancock, G.R., Bretreger, D., Cox, T., Hughes, J., Kunkel, V., 2021. Assessing digital elevation model resolution for soil organic carbon prediction. Geoderma 398, 115106.

Hancock, G.R., Martinez, C., Evans, K.G., Moliere, D.R. 2006. A comparison of SRTM and high-resolution digital elevation models and their use in catchment geomorphology and hydrology: Australian examples. Earth Surf Process. Landf. 31, 1394–1412.

Hassanpour, B., Giri, S., Pluer, W. T., Steenhuis, T. S., Geohring, L. D. 2017. Seasonal performance of denitrifying bioreactors in the Northeastern United States: Field trials. *Journal of Environmental Management*, *202*(Pt 1), 242–253. https://doi.org/10.1016/j.jenvman.2017.06.054

Jordan, J.L., Abdelmoneim, H.E. 1993. "Willingness to Pay for Improvements in Drinking Water Quality." *Water Resources Research* 29 (2): 237–45.

Liu, Y. 2020. "The Willingness to Pay for Ecosystem Services on the Tibetan Plateau of China." *Geography and Sustainability* 1 (2): 141–51.

Lopez-Ponnada, E. V., Lynn, T. J., Peterson, M., Ergas, S. J., Mihelcic, J. R. 2017. Application of denitrifying wood chip bioreactors for management of residential non-point sources of nitrogen. *Journal of Biological Engineering*, *11*, 16. https://doi.org/10.1186/s13036-017-0057-4

Moore, I. D., Gessler, P. E., Nielsen, G.A., Peterson, G.A. 1993. "Soil Attribute Prediction Using Terrain Analysis." *Soil Science Society of America Journal*. https://doi.org/10.2136/sssaj1993.03615995005700020058x.

Nemecek, J. 2020. "National Cooperative Soil Survey (NCSS) Soil Characterization Database: The National Cooperative Soil Survey (NCSS) Soil Characterization Database Contains the Analytical Results from the Kellogg Soil Survey Laboratory (KSSL) at the NCSS." September 9, 2020. https://nrcs.maps.arcgis.com/home/item.html?id=65ffa754044548919781c0f0136aec88.

NRCS. 2011. *Achieving Nutrient and Sediment Reduction Goals in the Chesapeake Bay* (Committee on the Evaluation of Chesapeake Bay Program Implementation for Nutrient Reduction to

Improve Water Quality, Water Science and Technology Board, & Division on Earth and Life Studies (eds.)). The National Academies Press.

Rosen, T., & Christianson, L. 2017. Performance of Denitrifying Bioreactors at Reducing Agricultural Nitrogen Pollution in a Humid Subtropical Coastal Plain Climate. *WATER*, *9*(2), 112. https://doi.org/10.3390/w9020112

Schumann, G., Matgen, P., Cutler, M.E.J., Black, A., Hoffmann, L., Pfister, L. 2008. Comparison of remotely sensed water stages from LiDAR, topographic contours and SRTM. ISPRS J Photogramm Remote Sens 63, 283–296.

Sørensen, R., Zinko, U., Seibert, J., 2006. On the calculation of the topographic wetness index: evaluation of different methods based on field observations. Hydrol Earth Syst Sci 10, 101–112.

Stephenson, K., Easton, Z.M., Bock, E.M., Ferris, W. "Treatment of Legacy Nitrogen as a Compliance Option to Meet Chesapeake Bay TMDL Requirements." 2021. 302327. Southern Agricultural Economics Association. https://ideas.repec.org/p/ags/saea20/302327.html.

Vaze, J., Teng, J., Spencer, G. 2010. Impact of DEM accuracy and resolution on topographic indices. Environ. Model. Softw. 25, 1086–1098.

Van Meter, K.J., Basu, N.B. 2017. "Two Centuries of Nitrogen Dynamics: Legacy Sources and Sinks in the Mississippi and Susquehanna River Basins." *Global Biogeochemical Cycles*. https://doi.org/10.1002/2016GB005498.

Van Meter, K. J., Van Cappellen, P., Basu, N. B. 2018. "Legacy Nitrogen May Prevent Achievement of Water Quality Goals in the Gulf of Mexico." *Science* 360 (6387): 427–30.

Wolock, D.M., Price, C.V. 1994. Effects of digital elevation model map scale and data resolution on a topography-based watershed model. Water Resour Res 30, 3041–3052.

Zhang, W., Montgomery, D.R. 1994. Digital elevation model grid size, landscape representation, and hydrologic simulations. Water Resour. Res. 30, 1019–1028. https://doi.org/10.1029/93WR03553

Chapter 2: Evaluating Digital Elevation Models (DEMs) and Topographic Indices (TI) for Geomorphic Landscape Representation

Elyce Buell[a], Daniel R. Fuka[a], Amy S. Collick[b], Roja Kaveh[a], Zachary M. Easton[a]

[a]Department of Biological Systems Engineering, Virginia Tech, Blacksburg, VA
[b]Department of Agricultural Sciences, Morehead State University, Morehead, KY

Keywords: Soil properties, Digital elevation model, LiDAR, Soil mapping, Catchment area, Slope

Abstract

Currently, the SSURGO method of distributing soils is prone to high error rates. This study is conducted to propose a new method of distributing soils using multiple DEMs as inputs. Thirty-six soil samples are analyzed for clay content, organic matter, and horizon thickness for A and BA horizons in southwest Virginia. Four DEMs (USGS ⅓ and 1as; 2010 and 2018 aerial LiDAR) are analyzed for spatial differences between derived properties (slope, Specific Catchment Area (SCA), and TI). Using multivariate regression, these soil properties are predicted, and a framework for soil map distribution is proposed. The disagreement of TI across multiple DEMs was largely driven by the differences between SCAs, which varied widely because of the resolution differences. Fine resolution routes flow through much smaller rasters which carved out narrower flow paths when compared to those from coarser DEMs. When evaluating soil properties, coarse resolution DEMs showed promising results for relating soil properties for the BA horizon. A mixture of coarse and fine resolution DEMs are found to be advantageous when pairing a slope and SCA to predict the distribution of a soil characteristic. This proposed framework of integrating multiple DEMs into soil characteristic distribution has the potential to improve soil property mapping.

2.1 Introduction

Correct representation of the landscape is critical in a number of applications, including land-use planning, infrastructure siting, soil science, surface energy budgets, hydrologic studies, and flood inundation analysis and predictions (Moore *et al.*, 1993; Malczewski, 2004; Tovar-Pescador *et al.*, 2006; White *et al.*, 2011; Bove *et al.*, 2020; Muthusamy *et al.*, 2021). How landscapes have been measured has changed over time from measurements made from the surface, from the use of sextants to precision GPS surveying, and from remote sensing platforms using imagery, radar, GPS, and Light Detecting and Ranging (LiDAR) from satellites, aircraft, all the way down to just above the surface using unmanned aerial vehicles (UAVs) and robots (Rodr'ıguez *et al.*, 2006; Rock *et al.*, 2011; Tachikawa *et al.*, 2011; Fankhauser *et al.*, 2014).

Digital elevation models (DEMs) are a common way of storing and displaying land surface elevation (Mukherjee *et al.*, 2013). Raster (grid-based) DEMs are georeferenced representations of the earth and have been created in a variety of ways including digitizing ground survey contour lines, by synthetic aperture radar (SAR), and other photogrammetric stereo models including both aerial and satellite imagery (Kelly *et al.*, 1977; USGS, 1993). SAR-based measurements use multiple radar images of a landscape, while photogrammetric methods use images from at least two different vantage points of the same area to create a DEM (Mukherjee *et al.*, 2013). More recently, DEMs generated using LiDAR and differential GPS (typically ~0.3-1m) are becoming increasingly common (Resop *et al.*, 2019; Muhadi *et al.*, 2020). Differential GPS, often used in small ground campaigns, employs information from satellites to georeference points across a landscape (Wilson & Atkinson, 2005). LiDAR measures light reflected from the object (ground surface) to determine the elevation (US Department of Commerce, National Oceanic and Atmospheric Administration, 2021).

Typical DEM resolutions in the U.S. range from 30m grids, often a combination of digitized contour lines and methods, to <10 cm resolution for airborne LiDAR campaigns. Each of the methods also has the capability to provide varying resolutions with new campaigns, for instance, photogrammetric methods produce resolutions of 5m to 30m, and LiDAR produces even finer resolution DEMs, down to cm scales.

DEMs and their derived attributes (slope, aspect, drainage area, topographic wetness index, etc.) are important data for the assessment of any surface process using terrain analysis (Wolock & Price, 1994; Mukherjee *et al.*, 2013). In many cases, terrain influences the spatial distribution of hydrological, geomorphological, and biological properties such as the location of wetlands (Goldman *et al.*, 2020), soil moisture patterns (Western *et al.*, 1999), and soil chemistry (Dindaroglu *et al.*, 2021). Because of their widespread use, and relative ease of generation, terrain models are easy to find, oftentimes with multiple resolutions and generation techniques available for a single area of the landscape. Terrain characteristics are most typically represented using DEMs. Extraction and calculation of terrain attributes from DEMs provide essential information on the geomorphic variation of the landscape. Terrains are often described by their primary (slope, elevation, specific catchment area) or secondary (derived indices using combinations from primary attributes) characteristics (Oksanen and Sarjakoski, 2005; Sena *et al.*, 2020) such as the upslope and downslope topographic indexes (Hjerdt *et al.*, 2004; Lanni *et al.*, 2011).

For instance, Moore *et al.* (1993), Collick *et al.* (2015), and Fuka *et al.* (2016), demonstrate that elevation data and derived terrain metrics, including the topographic index, show characteristic correlations with soil properties, including organic matter, soil texture, horizon thickness, and spot measurements of elevation. Although several studies have demonstrated strong relationships between terrain attributes and various other properties (soil among them), there are no studies in the literature that evaluate how various DEM resolutions, DEM processing methods, and derived characteristics impact relationships between terrain characteristics and landscape properties.

This research assesses if and how varying DEM development methods, resolutions, and derivative indices can be combined to increase the knowledge of the spatial characteristics of the landscape. We specifically evaluate the influence of DEM resolution, DEM processing, and flow direction algorithms on correlations with landscape attributes, including soil properties, and derived terrain attributes including watershed boundaries, specific catchment area (SCA), slope, and the upslope topographic index (TI).

2.2 Materials and methods

2.2.1 Study Location/Watershed Description

This study was conducted at the Virginia Tech StREAM Lab (Stroubles Research, Education, and Management https://www.bse.vt.edu/research/facilities/StREAM_Lab.html) (figure 2-1), a watershed with an area of 26 km^2 containing a mixture of agricultural, forested, and urban land use, and that has been used extensively for ecohydrological research (Parece *et al.*, 2010; Thilakarathne *et al.*, 2018). Within the StREAM Lab, we selected a small subwatershed, Doc's branch, a tributary with a watershed area of 2 km^2 consisting of mixed agricultural (58%), developed (23%), and forested (19%) land use.

2.2.2 Digital Elevation Models

Four DEMs commonly used in hydrological studies were used for this study (table 2-1). These include USGS 1 arcsecond (arcsec) resolution (28m horizontal resolution), USGS ⅓ arcsec resolution (9m resolution) (USGS, 1993; Archuleta *et al.*, 2017), a DEM based on a 2010 LiDAR (1.5m resolution) (Benham, 2010; Resop *et al.*, 2019), and a DEM based on a more recent 2018 LiDAR (0.76m resolution) (Simpson, 2018; Drewberry, 2019). The USGS ⅓ arcsec and 1 arcsec DEMs were created using a number of different techniques, compiled, and stitched together by USGS to produce the USGS NED (Gesch *et al.*, 2002). The USGS DEMs for the Docs Branch watershed were developed using a combination of LiDAR and ISFAR. Both the 2010 and 2018 LiDAR datasets were created by the Virginia Information Technologies Agency (VITA). Metadata for the DEMs are summarized in table 2-1.

The DEMs used in this analysis represent the landscape over the range of years (~1960 to 2018) that they were developed. Over the time spanned by the DEMs, there is one notable alteration to the watershed elevations: the expansion of Highway 460 in 2016 (figure 2-1), though none of these alterations were within the contributing areas of sampling locations for this study.

Table 2-1: Summary of DEMs evaluated, where those marked "various" did not have metadata describing those details for the specific locations.

DEM abbreviation	Source	Data Acquisition Date	Data collection sensor	Vertical uncertainty		Horizontal Resolution
				non-vegetated	vegetated	
2018 LI	VGIN	1/7/2018	Leica ALS-50 LiDAR system	5.7 cm	10.8 cm	0.76 m
2010 LI	VGIN	3/30/2010	Riegl LMS-Q1560 and/or Riegl VQ1560i	19 cm	37 cm	1.5 m
1/3as	USGS	Between 1960&2016	Various	Various	Various	9 m
1as	USGS	Between 1960&2016	Various	Various	Various	28 m

2.2.3 Soil Sampling

Thirty six soil sampling locations were chosen to reflect a range of terrain, landuse, and geomorphic conditions throughout the watershed. Soil sampling locations were chosen such that the positions were distributed across the watershed, were accessible with sampling machinery, and represented the expected variability in watershed properties (Figure 2-1). Soil cores were taken in November of 2019 by the investigators using a #5-UV Model Hydraulic Soil Core Sampling machine (Giddings Machine Company) mounted on the back of a John Deere™ Gator Utility Vehicle. Soil cores were pressed until the full depth of the core contained a sample (core tubes are 126 cm in length) or until encountering a layer of material that couldn't be penetrated by the Giddings, with an approximate force of $6.6*10^5$ kg/m^2. Clay content, organic matter content, and horizon depth were measured in the A and BA horizons

2.2.4 Laboratory Analysis

Soil attributes analyzed include horizon thickness, soil organic matter content, and soil texture for each horizon. After collecting soil cores, horizons were identified. The soil horizons identified included A/Ap, BA, and Bt horizons. In four instances, the cores did not have BA horizons. Horizon thicknesses are measured to the middle of the boundary with an error of +/- 1 cm.

Organic matter was measured by loss on ignition tests for each horizon for all soil cores using Sparks *et al.* (2020). Samples ranging from 50g to 250g were incinerated at 425 ^{o}C for at least 4 hours. Gravel (as defined as particles larger than 2mm in their biggest dimension) was found by separating the gravel out using a 2-mm sieve and calculating the ratio of gravel weight to total sample weight (after loss on ignition test is done). Fractional sand, silt, and clay (defined as rough diameters between 2-0.06mm, 0.06mm-0.002mm, and 0.002-0mm, respectively) were determined using the hydrometer method (ASTM, 2014). After the hydrometer is read at the times indicated by the protocol, this data was fed into the “texture” function using the "envalysis" package in R to extract the fraction of clay and sand (Steinmetz, 2021). All laboratory analysis is conducted by the investigators of this project.

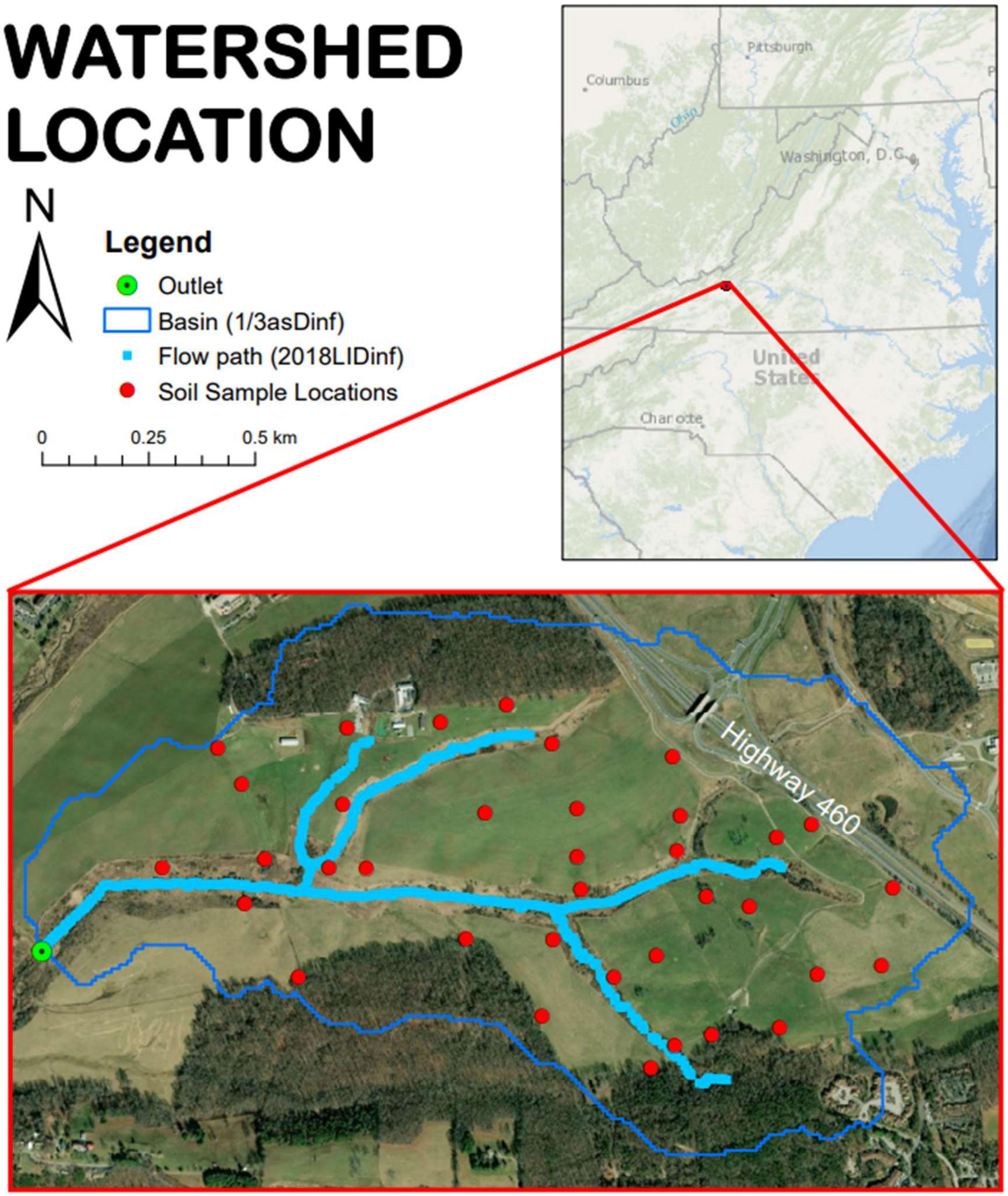

Figure 2-1 Doc's Branch Watershed as delineated by United States Geological Survey (USGS) ⅓ arcsec digital elevation model. The blue line in satellite view shows the watershed boundaries, red points show the locations for soil pedon samples, and the green point shows the basin pour point.

2.2.5 SSURGO Soils Data

For comparisons against measured soil properties, SSURGO soils properties were extracted for each sampling location from the USDA-NRCS Soil Survey Geographic (SSURGO) database using the soilDB R package (Beaudette *et al.*, 2019). The SSURGO database distributes soils based on measurements made at 20,000 pedons, spanning all American states and most territories (Nemecek, 2020). On average, this is a sampling density of roughly 1 pedon for every 350 to 500 km^2. Although much of the continental United States exceeds this density, realistic sampling densities are still fairly sparse (Gatzke *et al.*, 2011). For the study watershed there are three nearby pedons, approximately 15km southwest of the watershed (Nemecek, 2020).

The SSURGO soils were extracted from the database at each of the soil sampling locations. Horizon depth, clay, and organic matter were used to compare against the measured soil properties. SSURGO often presented two to three options for soil classifications, and a high, low and regular value for each. All were extracted and evaluated. The regular values are used in this study. This dataset is used to compare to the measured data and acts as a control to see how well using this popular method would represent the watershed soils.

2.2.6 Digital Elevation Model Processing

DEM-derived spatial characteristics used for this analysis include slope, upslope contributing area (SCA), topographic index value (TIV), and topographic index class (TIC) derived using two different flow algorithms (D8 and D-infinity, described below). The data generated by these raster manipulations were extracted from the distributed rasters by overlying the spatial locations of the 36 soil sampling locations and extracting the associated raster value. These numeric values are correlated against soil properties measured in the watershed. All DEM processing and data extraction were performed in R using the TauDEM (Tarboton, 2005), raster package (Karney, 2013), and shapefiles packages (Stabler, 2013).

2.2.6.1 Slope

To calculate slope at each raster, the steepest downslope descent is calculated and the value is assigned to that raster. For D8, slope is defined as the steepest drop over two adjacent cells, and for Dinf, the slope is calculated along the triangular facet of the plane with the steepest slope across adjacent cells. (Tarboton, 1997, 2014).

2.2.6.2 Flow Direction

Prior to calculating SCA, the flow direction routing between adjacent cells must be determined. Two methods of routing flow between neighboring DEM cells are evaluated: D8 and D-Infinity (Dinf). The D8 flow routing algorithm routes all flow to a single raster following the steepest down-slope gradient. The Dinf flow routing algorithm proportions flow to adjacent downslope cells based on the steepest downgradient slope from a triangular grid centered on each adjacent downslope cell, partitioning flow between all adjacent downslope cells. The differences between the D8 and Dinf methods and a more in-depth discussion can be found in Tarboton (1997).

2.2.6.3 Specific Catchment Area (SCA)

The catchment area of a particular point is the area that drains to that location (as specified by the input DEM in units of L^2). The SCA is the catchment area normalized by the length of the raster (or the resolution of the raster) yielding a value in units of L. Here we use SCA because it has shown better correlation with physical properties in previous studies (Moore et al., 1993; Collick et al., 2015; Fuka et al., 2016). The *SCA* is calculated as: *SCA = CA/raster length*. Where *CA* is the upslope contributing area per unit of contour line (m^2) and *raster length* is the width of the raster (m).

As discussed previously, D8 assumes that all flow is routed into one adjacent down slope raster (based on steepest descent), and thus determining the catchment area for this application is simply the sum of all upslope cells. Catchment area for Dinf differs in one key way; the Dinf algorithm assigns the next raster's catchment area proportional to the amount of flow the raster is receiving from the uphill raster, thus weights the resulting grid based on proportional contributing area (Tarboton, 1997).

2.2.6.4 Topographic Index Value (TIV) and Topographic Index Class (TIC)

The Topographic Index (*TIV*) is a grid created by combining *SCA* and slope raster as:

$$TIV = ln\left(\frac{SCA}{tan(slope)}\right)$$

where *slope* is topographic slope of the cell (expressed in radians), (Lyon *et al.*, 2004; Easton *et al.*, 2008). The Topographic Index Class (TIC) reclassifies the TIV into equal-area groups, and for this study, 10 TICs were selected per the methods of Easton *et al.* (2008), who showed that 10 classes generally provide sufficient detail to discriminate processes at a sub-field scale. TICs are created such that TIV above the 90th percentile are assigned a TIC of 10, TIV in the 80th-90th percentile are assigned a TIC of 9, and a TIV in the 0th-10th percentile are assigned a TIC of 1.

2.2.7 Correlation Analysis

All of the measured and generated data described above are subject to various correlation analysis. We correlate derived terrain characteristics among DEMs and DEM processing methods (e.g., watershed boundaries, slopes, TIV, etc. derived from the DEMs with like characteristics from the other DEMs) as in Figures 2-2 - 2-5, as well as with measured properties (e.g., soil physical measurements) and database extracted properties (e.g., SSURGO soils data) as in Figure 2-6.

2.2.8 Multivariate Regression to Predict Soil Properties

Regression analysis was used to predict soil properties. To constrain the analysis and to provide regressions that were both interpretable and not overfitted, we limited the number of predictors (derived data) to a single slope and a single SCA (two input parameters total) [eq 2-1].

$$Y = m_1 * slope + m_2 * ln(SCA) + b \qquad \text{eq. 2-1}$$

Where Y is soil property of interest (organic matter, horizon thickness, or clay content for the A or BA horizon), slope is a single input of slope selected from the eight slope options (four DEMs for both D8 and Dinf flow directions), SCA is a single input of SCA selected from the eight SCA, and m_1, m_2, and b are regression estimates. Note that the log of SCA is taken because a log transformation of SCA linearized the relationship between SCA and soil properties. The best pairing of slope and SCA was determined by forward step regression comparing all pairwise combinations and evaluating the resulting Akaike Information Criterion (AIC). Regressions yielding the lowest AIC were selected as the most appropriate model to predict a given soil property. AIC is selected over the Bayesian information criterion because Type II error is preferred over Type I error for this application (Friedman *et al.,* 2009).

2.2.9 Evaluating Prediction of Soil Characteristics

Using Markov chain Monte Carlo (MCMC) analysis, the prediction capability of a suite of spatial inputs is evaluated. The soil characteristic of interest is randomly split into a training and testing dataset of 18 samples each. A regression is trained on the training dataset and applied to the testing dataset to evaluate model robustness. This process is repeated 1,000 times; 1,000 repetitions is confirmed to be sufficient for result convergence. To create soil characteristic maps for visualization, the resulting MCMC regression coefficients are averaged and applied to the applicable spatial rasters.

2.3 Results

The data and results described in the DEM/soil analyses can be found at ebuell (2022).

2.3.1 DEM Differences

Elevation differences between DEMs are shown in supplemental materials, Figure 2-S1. As expected, the differences between the DEMs are greatest when comparing the higher resolution LiDAR to the coarser resolution ⅓ and 1 arcsec USGS sourced DEMs, with differences of +/-5-10m not uncommon. Figure 2-S1 also reveals differences between similarly processed DEM sources, such as the USGS 1 arcsec and the ⅓ arcsec, where differences of +/- 2.5m are widely present. Differences between the LiDAR DEMs were generally constrained to +/- 0.5 m. The elevation differences between DEMs was manifested in stream network and watershed boundary delineation differences although some of the difference in watershed boundary was attributable to the construction of the 460 interchange between pre 2018 acquisition missions (e.g., 2010 LiDAR, USGS ⅓, 1 arcsec) and the most current LiDAR (e.g., 2018 LiDAR). There are also differences present that cannot be attributed to construction where the 2010 LiDAR is substantially different from both of the USGS ⅓ and 1 arcsec DEMs, due primarily to DEM resolution. While there were some minor differences in flow paths, all DEMs approximated the same flow path extent.

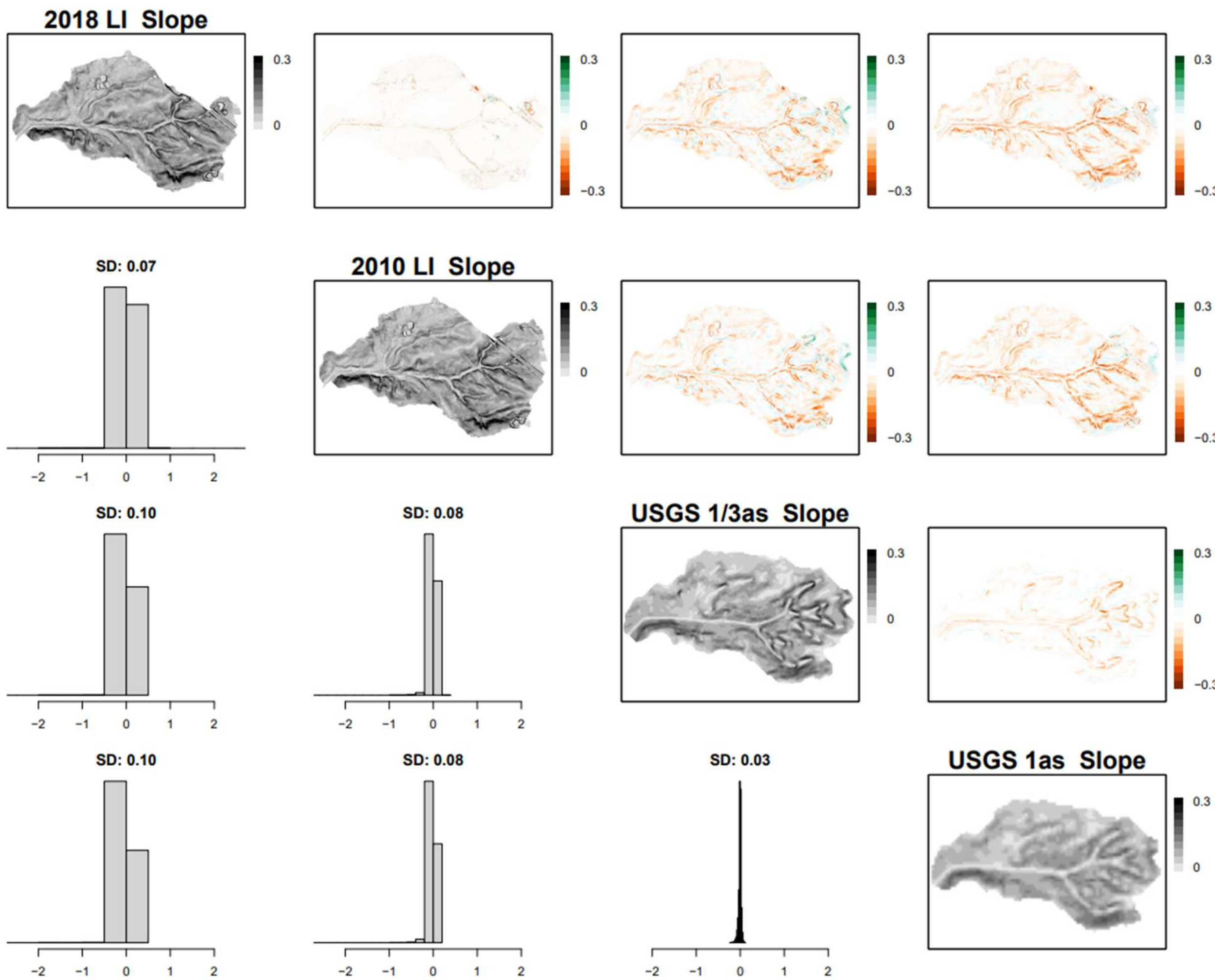

Figure 2-2 Spatial differences between slopes from various DEMs using the Dinf flow direction algorithm. These are calculated by the following equation: Coarser resolution - finer resolution (eg. 2010LIDAR - 2018LIDAR). Resulting watershed boundaries are found in the lower right corner. 2018LI - blue, 2010LI - green, 1/3as - purple, 1as - orange.

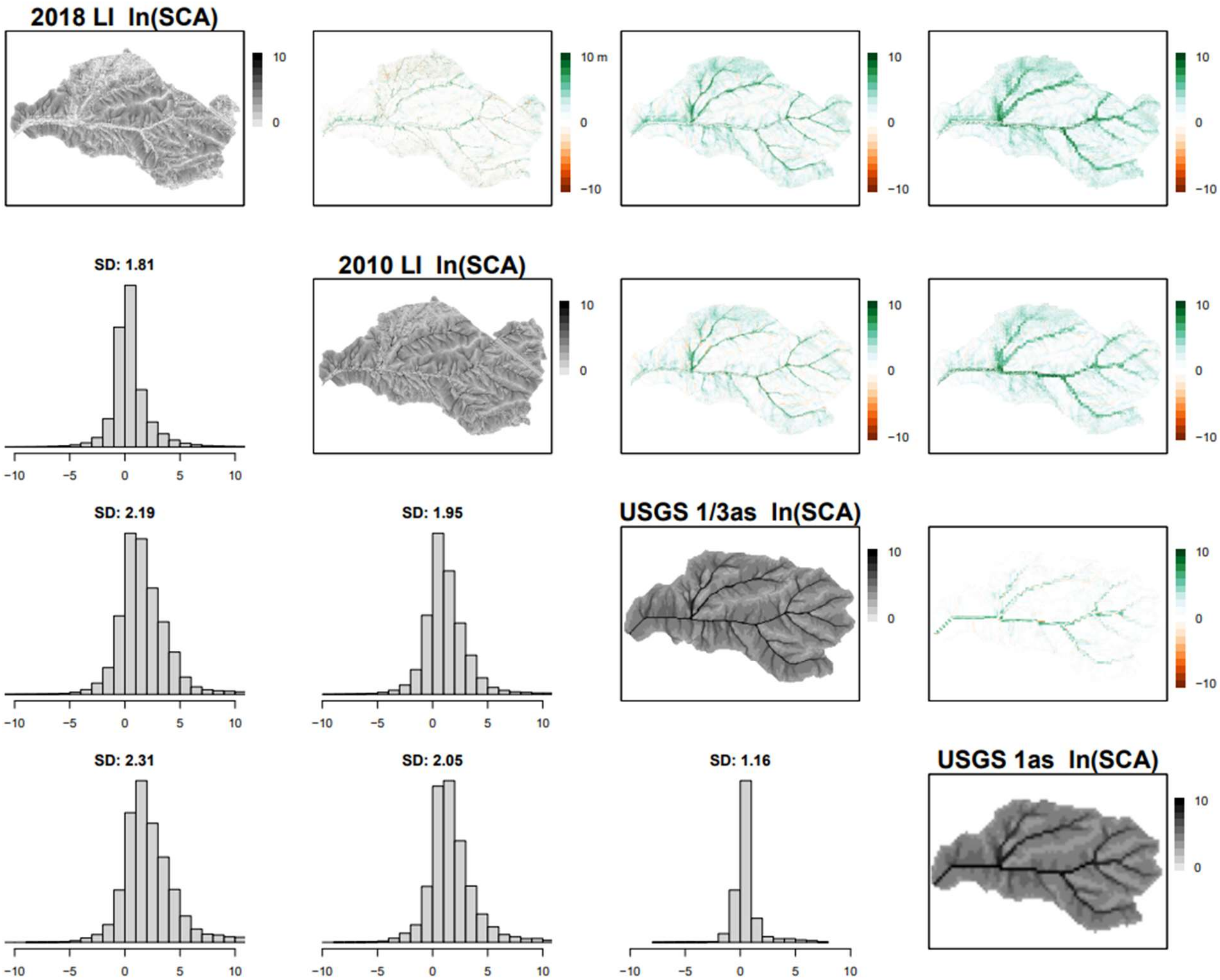

Figure 2-3 Spatial differences between ln(SCA) from various DEMs sources using the Dinf flow direction algorithm. These are calculated by the following equation: Coarser resolution - finer resolution (eg. 2010LIDAR - 2018LIDAR).

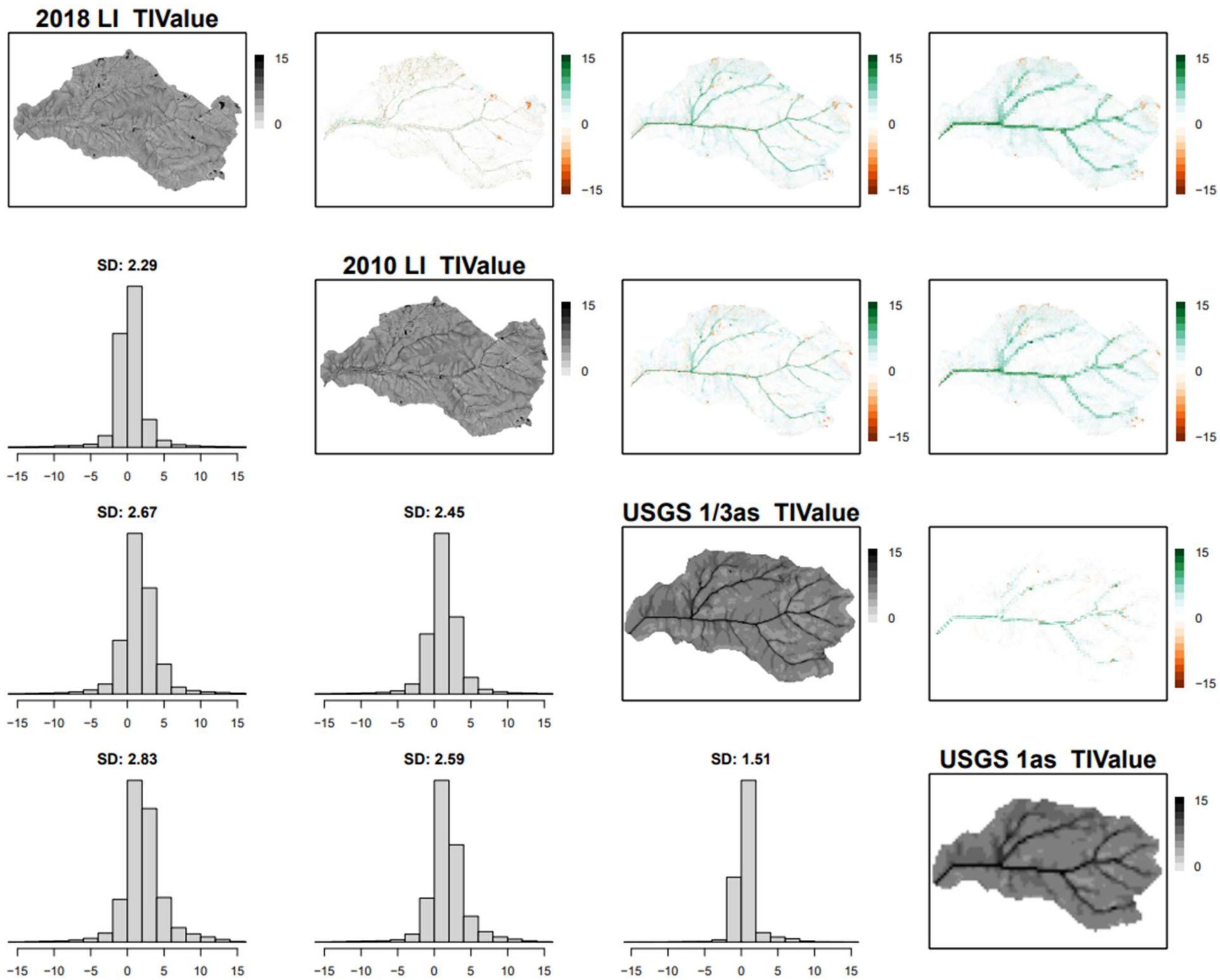

Figure 2-4 Spatial differences between TIV from various DEMs sources using the Dinf flow direction algorithm. These are calculated by the following equation: Coarser resolution - finer resolution (eg. 2010LIDAR - 2018LIDAR).

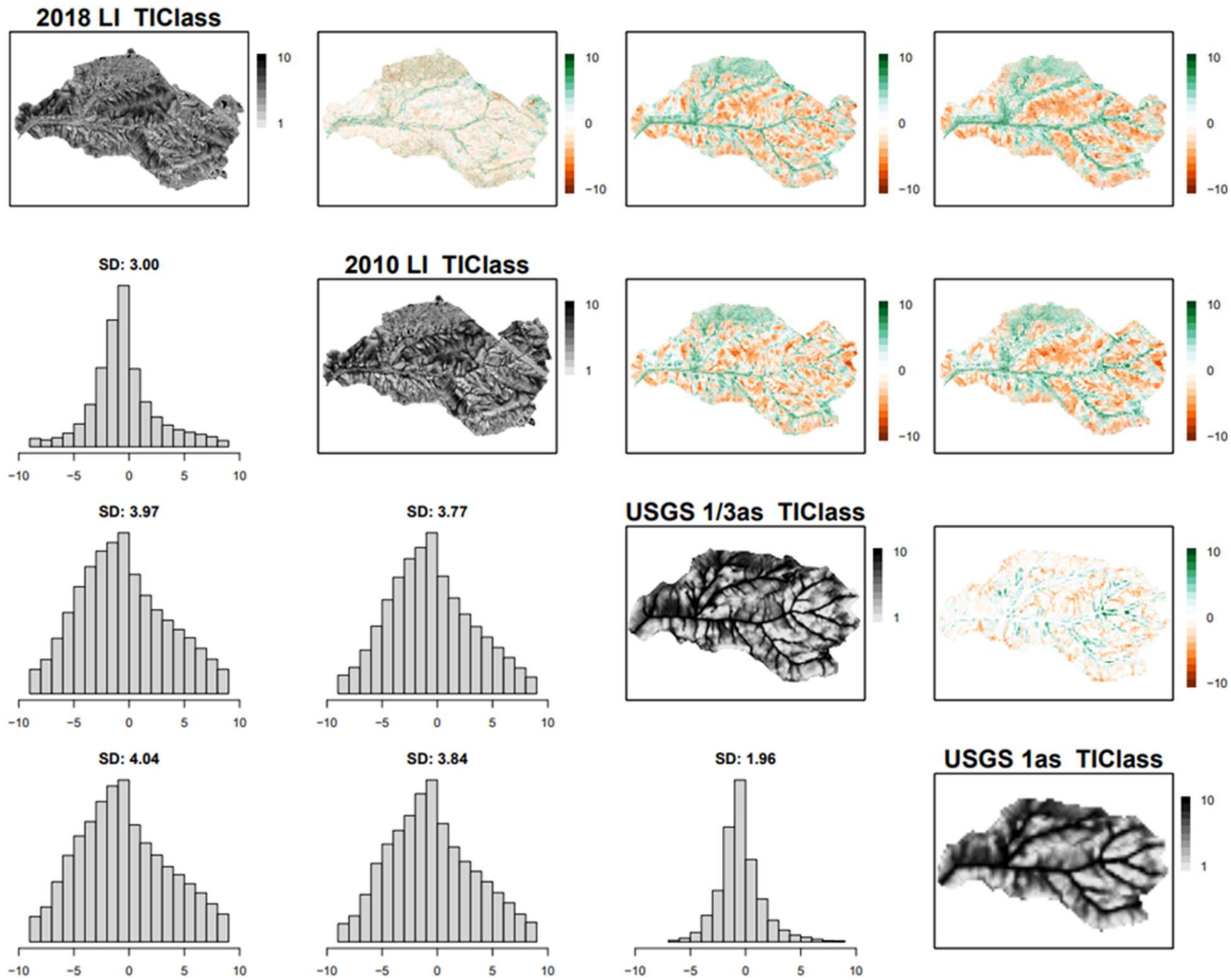

Figure 2-5 Spatial differences between TIC from various DEMs sources using the Dinf flow direction algorithm. These are calculated by the following equation: Coarser resolution - finer resolution (eg. 2010LIDAR - 2018LIDAR).

2.3.1.1 Slope

Figure 2-2 displays the correlations among DEM derived slopes using the Dinf flow direction algorithm (DEM derived slopes using the D8 algorithm in Figure 2-S2 for reference). A comparison of figures 2-2 & 2-S2 reveals few differences, spatially or in magnitude, between choice of flow direction algorithm. Indeed, the correlation coefficients between the slopes derived by the two algorithms is 0.99 (data not shown). There are however differences among slopes from various DEMs. Positive values (green) show areas where the slope in the coarser resolution is calculated to be higher than the finer resolution. Negative values (orange) show areas where slope in the finer resolution is greater than the slope in the coarser resolution. Both LiDAR based DEMs yield more frequent high slopes when compared to both the ⅓ and 1 arcsec DEMs. As the DEM resolution becomes finer, each grid integrates a smaller fraction of the landscape, and can thus capture smaller landscape features, such as short steep banks in the near stream region and the steep hill slope in the south-eastern area of the watershed. Interestingly, while both LiDAR DEMs show steeper slopes on the face of that hill slope, they also show shallower slopes at the top of the hill slope (area in green near the watershed boundary). There are fewer, although still interesting differences, between the LiDAR DEMs slope values. Although there was no clear bias towards over or under estimating slope (e.g., there are an equal number of orange and green pixels), slope differences between the LiDAR DEMs do tend to be of greatest magnitude in the near stream areas (figure 2-2). Similar results are seen for the slope comparison between the coarser ⅓ and 1 arcsec DEMs (figure 2-2).

2.3.1.2 SCA

Similar to slope, there are few differences in SCA between the two flow direction algorithms, except perhaps a slight bias towards higher estimated SCA using the D8 algorithm (e.g., more positive values in Figure 2-S3 than in Figure 2-3). This is perhaps not surprising given that D8 routes flow to only one adjacent downslope neighbor, thus accumulating SCA faster. The spatial differences and their magnitudes between the two flow direction algorithms are not significant: the correlation coefficient between SCAs derived by the two flow direction algorithms is 0.99, indicating minimal differences between algorithms.

The largest differences tend to be found between the higher resolution LiDAR based DEMs and the coarser resolution ⅓ and 1 arcsec DEMs, with the ⅓ and 1 arcsec DEMs showing greater SCA in the flow paths than the LiDAR DEMs. Indeed both the preponderance of positive (green) values and the distributions with positive central tendencies in Figure 2-3 indicate a positive bias by the coarser DEMs. This is due to SCAs derived from LiDAR routing flow through smaller grid cells than the coarser USGS resolutions. However, there are also some substantial differences in non-flow path areas, such as the northern region of the study area, where the coarser ⅓ and 1 arcsec DEMs have substantially greater SCA values. There are some smaller differences between the LiDAR DEM SCA values, but the differences do not have a systematic directional bias (figure 2-3), but are greatest in magnitude in the near-stream areas. Differences between the ⅓ and 1 arcsec DEMs are similarly minor although there is a slight bias for the coarser 1 arcsec DEM showing larger SCA values, particularly in near-stream flow paths (figure 2-3).

2.3.1.3 TIV

Figure 2-4 shows the differences in TIVs for the Dinf algorithm (figure 2-S4 shows the D8 TIV comparisons). Unlike Slope and SCA, there are some differences between the TIV as calculated by the two flow direction algorithms. The coarser ⅓ and 1 arcsec DEMs had higher correlations between D8 and Dinf (0.93-0.98), indicating more similarity, while the higher resolution LiDAR DEMs were less similar, with coefficients of 0.85-0.87. Differences attributable to the DEMs is also apparent, although they tended to be propagations of the patterns and differences seen in the SCAs, with the positive (green) values and the distributions with positive central tendencies in figure 2-4 indicating a positive bias by the coarser DEMs. While the bias is greater in the near stream flow paths, there is also the tendency towards positive bias across the entire spatial domain.

2.3.1.4 TIC

Figure 2-5 displays the results for TI Class (TIC) using the Dinf flow direction algorithm. Figure 2-S5 shows the spatial differences for TIC for the D8 flow direction algorithm. Both flow direction algorithms produced approximately similar distributions, with both showing a positive (green) bias in the near stream flow paths and a negative bias (orange) on the contributing hillslopes for the coarser DEMs. The largest differences in figure 2-5 are clearly due to resolution scales, with the largest differences between TICs between higher resolution LiDAR DEMS and the coarser resolution USGS ⅓ and 1 arcsec DEMs with +/- 1 standard deviation around the mean encompassing up to 8 TICs. There were less differences between the LiDAR DEMs, with 1 standard deviation encompassing 6 TICs (Figure 2-5). The smallest differences between DEMs was between the ⅓ and 1 arcsec products, with +/- 1 standard deviation around the mean encompassing 4 TICs (figure 2-5).

2.3.2 Relating spatial data to soil physical properties

We have shown that various source DEMs result in different landscape representations, as expressed in the estimates of slope, SCA, TIV, and TIC. Next we use simple correlation and multivariate regression to determine how well the various DEM attributes relate to, and can be used to predict, soil properties in the watershed.

As figure 2-6 shows, there is little evidence that any single DEM results in better correlations (using simple 1:1 comparisons) with soil properties in the watershed. Likewise no single derived DEM product (Slope, SCA, TIC, TIV) is clearly better at capturing the variation in soil properties. There are mixed positive and negative correlations, and soil properties are not always most correlated with the highest resolution DEM products, although LiDAR based DEMs tended to be more strongly correlated with specific soil properties such as horizon thickness, and lower resolution with organic matter and a-horizon clay content (figure 2-6). LiDAR derived Dinf SCA and TIV tended to be more highly correlated with soil properties than D8 SCA and TIV, while for lower resolution 1 and ⅓ arcsec DEMs there is not a considerable difference between flow routing algorithms.

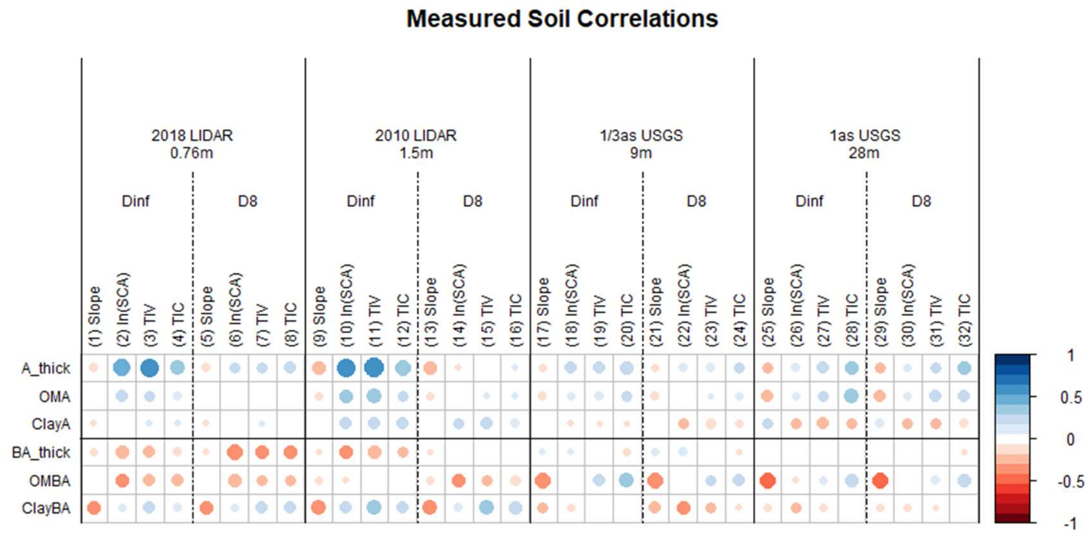

Figure 2-6 Correlations between measured soil properties and derived spatial data as expressed by the coefficient of correlation, R

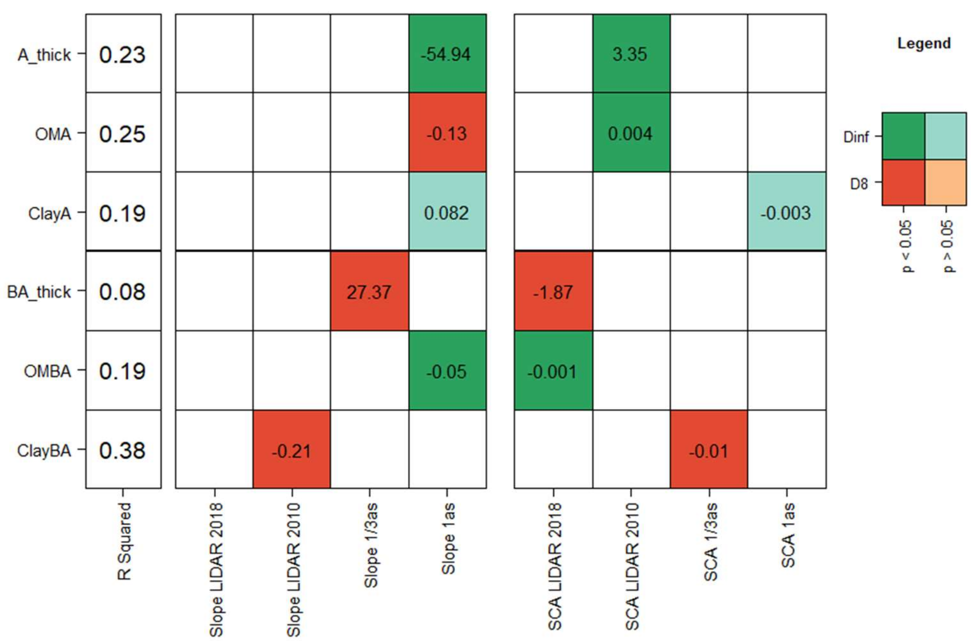

Figure 2-7 Summary of multivariate TIV regressions predicting soil properties. Left column shows the R^2 of the resulting paired multivariate regression. The remaining columns show the paired inputs for the regression and regression coefficients.

2.3.2.1 Multiple Regressions of Varying Input Resolutions

Using the forward step selection algorithm to select predictors (one slope and one SCA each with four resolutions and two flow direction routing algorithms), optimal regressions and their corresponding correlation are displayed in figure 2-7. This analysis reveals several interesting findings, first, combining information from multiple DEMs provides more information about the soils distribution in the watershed than using information from a single DEM (compare figures 2-6 & 2-7). Second, the highest resolution DEMs were selected as regression predictors only 5 out of 12 times, indicating that there is as much if not more information in lower resolution DEMs, at least for slope estimates (e.g., only one LiDAR based slope was selected). However, higher resolution LiDAR SCAs appear to provide more information than lower resolution SCAs (LiDAR selected 4 out of 6 times). It is interesting to note that lower resolution slopes and higher resolution SCAs were often paired as the selected predictors. This is because increasing the resolution quickly inflates the slope estimates (Sadeghi et al., 2011). Additionally the magnitude of the regression coefficients are substantially larger for the slope predictors (several orders of magnitude in some cases), indicating that the slope predictor is having a much larger effect on the dependent (soil) variables than the SCA predictor.

We compare the topographically distributed soil properties and SSURGO-derived soil data to the measured data at 36 locations in the StREAM lab watershed that were well distributed across the TI classes. Figure 2-8 shows the results of the multivariate regression and SSURGO vs measured soil properties. For all three soil properties and both soil horizons the multivariate regression method provides much better estimates of measured values than SSURGO, the U.S. finest resolution soils data.Cleary including terrain attributes results in significant improvements of soil characterization. Indeed previous studies of Moore et al. (1993) and Fuka et al. (2016) both showed significant correlations between terrain adjusted soil properties and measured pedon data. As is evident in Figure 2-8 the multivariate regression resulted in predicted soil properties more closely following the 1:1 line and all with positive regression R^2 values (0.10-0.38), while the SSURGO estimates often fall far from the 1:1, and have negative regression R^2 values. R^2 is calculated using the following equation: R^2 = 1-sum of squared error/sum of squared total. From this equation we can see that once R^2 go negative they can get quite large in magnitude quite quickly. As such, the interpretation of these results puts little emphasis of the magnitude of negative R^2s. That considering terrain characteristics improves soil property prediction is perhaps not surprising, as others have postulated that relationships between terrain and soil characteristics in saturation excess-dominated soils (Ciolkosz & Waltman, 2000; Buchanan et al., 2014; Collick et al., 2015) which these results support, and can be used to create spatially distributed soil maps.

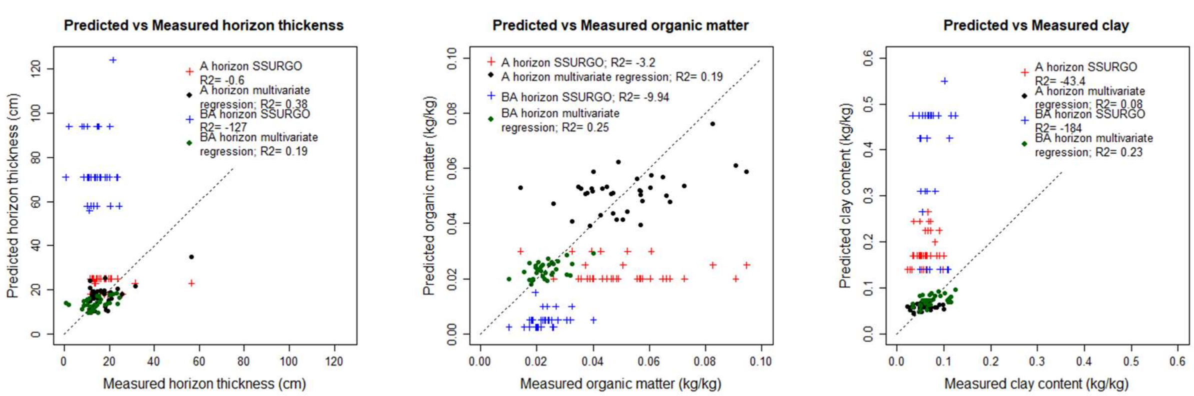

Figure 2-8 SSURGO and multivariate regression distributed soil property compared to measured property for the A and BA horizons

2.3.2.2 Soil Property Mapping

The multivariate TIV regression analysis discussed in the methods and in the previous section can be used to improve soil property distribution mapping. Applying the multivariate regressions spatially across the StREAM lab results in soil property distribution maps for the A horizon, shown in figure 2-9 and for the B horizon, shown in Figure 2-10. For all three soil properties (A or BA horizon thickness, organic matter, and clay content) the multivariate regression provides better predictions as shown in figures 2-9 and 2-10 A1-A3, where the verification data R^2 used to test the multivariate regression shows a distribution centered well above 0, while the individual correlations are centered around an R^2 of 0. The spatial maps for the multivariate regressions provide further corroboration that the use of topographic data to infer spatial variability in soil properties can be used to generate high-resolution soils data, even when using lower resolution data (figures 2-9 and 2-10 B1-B3).

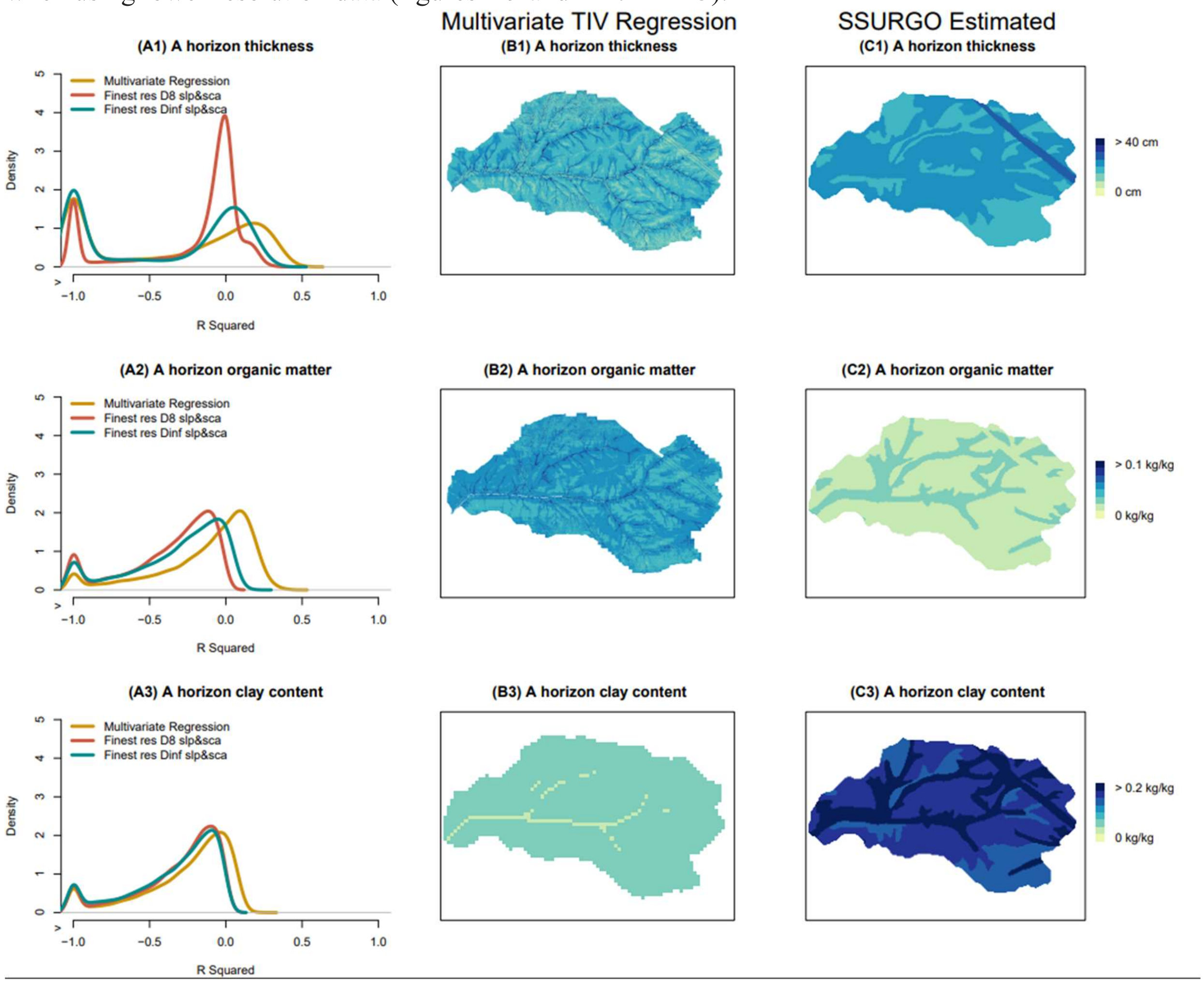

Figure 2-9 Probability density plots of the Monte Carlo test data for individual correlations shown in Figure 2-6 and multivariate regressions in Figure 2-7 for A horizon thickness (A1), A horizon organic matter (A2), and A horizon clay content (A3); A horizon thickness (B1), A horizon organic matter (B2), and A horizon clay content (B3 map from the multivariate regression; and A horizon thickness (C1), A horizon organic matter (C2), and A horizon clay content (C3) maps from SSURGO

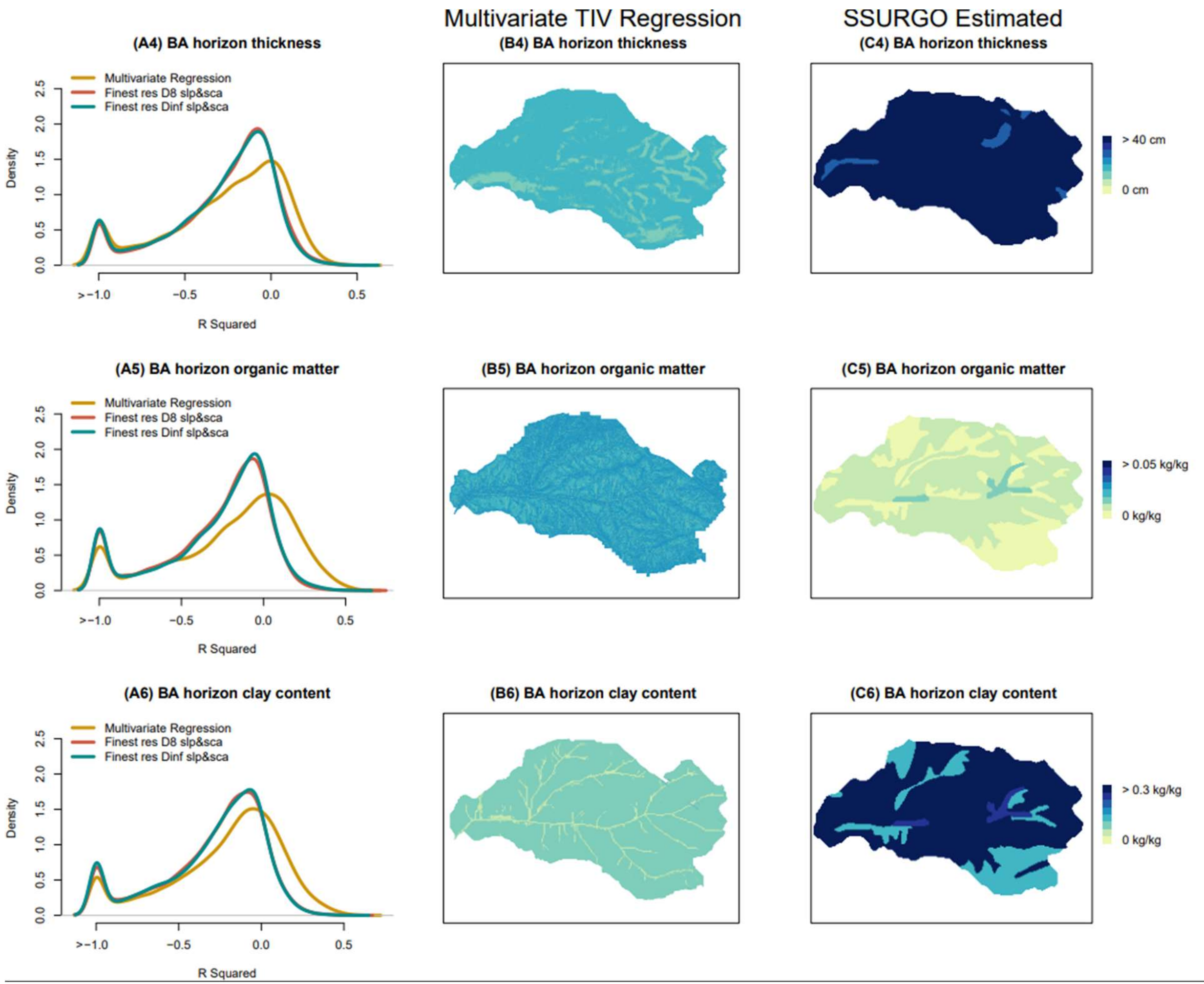

Figure 2-10 Probability density plots of the Monte Carlo test data for individual correlations shown in Figure 2-6 and multivariate regressions in Figure 2-7 for BA horizon thickness (A1), BA horizon organic matter (A2), and BA horizon clay content (A3); B horizon thickness (B1), BA horizon organic matter (B2), and BA horizon clay content (B3 map from the multivariate regression; and BA horizon thickness (C1), BA horizon organic matter (C2), and BA horizon clay content (C3) maps from SSURGO

2.4 Discussion

Accurate classifications of soils are integral to a wide variety of applications including achieving sustainability goals (Keesstra *et al.*, 2016), watershed modeling (Anderson *et al.*, 2014), erosion rates (Lal *et al.*, 2018), and containment transport (Yu *et al.*, 2018). Many of these processes have direct ramifications on public health, water quality, infrastructure and management. Although it is apparent that soils affect a broad range of environmental processes at a fundamental level, attempts to classify them have fallen short (Cole, 2017), and environmental science as a whole stands to gain better insight if soils are represented with increasing accuracy (Zhuo and Han, 2016). In the United States, the finest resolution nationally available soil is the SSURGO database.The SSURGO database distributes soils based on a collection of roughly 20,000 pedons that spans all American states and most territories (Nemecek, 2020). On average, this is a sampling density of roughly 1 pedon for every 350 to 500 km^2. Though much of the continental United States exceeds this density, realistic sampling densities are still fairly sparse. Thus, methods that can spatially downscale or improve finer resolution (sub field) estimates of soil properties are useful for any number of scientific disciplines. Indeed, Figure 2-8 shows that using terrain information in DEMs improves soil property characterization. Figures 2-9 and 10 corroborate this spatially, where using terrain properties provides a better estimate of the spatial distribution of soil properties than SSURGO.

We also show that the highest resolution DEMs do not always provide the greatest information content as related to soils, especially in deeper horizons. Thus, even though DEM resolutions continue to trend towards higher resolution, it is clear there is information in lower resolution products that is valuable in characterizing landscapes (Stolt et al., 1993; Wolock & Price, 1994; Sørensen and Seibert, 2007; Li et al., 2008).

In many instances, correlations between soil characteristics and slope or SCA were stronger for lower resolutions, particularly in the deeper BA horizon. Furthermore, the D8 flow direction algorithm indicates stronger correlations of slope in the BA horizons of lower resolution DEMs likely due to D8 being limited to a single flow direction, which may better represent the more static topography of deeper soils. Whereas soil characteristics in the shallower A horizon correlated better with the finer resolution spatial characteristics (Figure 2-6) and the more diverse flow routing partitioning in Dinf. In the case of the two LiDAR datasets, flow directed to a single downslope cell (D8) may diverge from its neighboring cells because of localized surface changes exposed due to higher sample density of LiDAR compared to the USGS datasets while Dinf will partition across more downslope cells. However, Figure 2-7 suggests that there may be a point in which obtaining higher resolution LiDAR data has little to no benefit in increasing our knowledge about soil morphological processes. Or any benefit is limited to localized surface changes or transformations, which are exposed at these higher sampling densities (Thomas et al., 2017), such as the development of fine-scale flow paths and erosion networks, and not to processes at deeper, more stable horizons.

For the multivariate regressions, both surface and subsurface horizon thickness were best captured with lower resolution DEMs (28m and 9m, respectively). Similar results were seen by Zhang & Montgomery (1994) who found that 10 m was the optimal resolution to explain several hydrologic features, and more recently Buchanan et al. (2014) suggest the optimal resolution for TIV-soil moisture correlation was 3m. Our results, from both the individual correlation analysis and the multivariate TIV regressions, corroborate these studies, with the optimal resolution generally falling between 1 to 10m. Furthermore, our findings suggest that there may be a point in which the benefits to obtaining higher resolution data provides little additional information on soil morphology. For example, coefficients in the multivariate regressions between soil characteristics in the BA horizon and SCA in the highest resolution LiDAR were relatively low in magnitude (e.g, slope coefficients were often an order of magnitude greater) indicating SCA has a more limited effect on regression model predictions.

Using the multivariate TIV regressions to predict soil properties improves the estimates of spatially distributed properties. This has important implications in many fields outside of soil science, where the focus has often been on vertical relationships between soil properties, and less on how soils are distributed spatially (Buol et al., 1989). For instance, knowledge of the spatial distribution of soil properties provides insight into how water moves in and across landscapes, important for water resource management and modeling (Lin, 2012), and topography is one of the key controls on soil development, which is important for many forms of soil and water resource management. Furthermore, as is evident in Figures 2-9 and 2-10 C1-C3, SSURGO and other soils databases are subject to uncertainties related to the boundaries of landscape units (i.e. the distinct brakes between SSURGO soils), the extrapolation of pedon point observations to soil-type polygons, and the variable intensity of sampling (Fuka *et al.*, 2016), which are reduced in the multivariate TIV regression modeling approach.

2.5 Conclusions

Results presented here indicate that even though resolutions are increasing, there is information in lower resolution products that should be maintained and included in landscape characterization. We identified some notable differences among different DEM resolutions and formulations of DEM derived products (Slope, SCA, TIV) and their correlation to spatial patterns of soil properties. Most importantly, we found that some TIV forms correlate relatively well with soil properties, and can be used to predict soil properties. Our principal findings include:

– There are not many scale-dependent differences between D8 and Dinf flow direction routines

–Coarse resolution DEMs showed greater promise on predicting surface horizon characteristics while both high and low resolutions provide insight on deeper horizon properties (i.e., BA horizon).

– Mixed resolution TIVs achieved good predictions of soil properties in agricultural fields.

Future studies should seek to understand how differences in DEMs and or DEM derived products can translate into differences in model outputs. Evaluating other indexes and or spatial mapping techniques such as the Downslope Topographic Index (which may be more appropriate for capturing deeper soil and hydrologic processes), or how various filtering approaches can be employed to smooth discrete soil property boundaries (Buchanan *et al.*, 2014).

Acknowledgments

We would like to acknowledge the help of Benjamin Smith, William Auchincloss, Jonathan Resop, Laura Lehmann, and computational support from the Advanced Research Computing at Virginia Tech, providing computational resources and technical support that have contributed to the results reported within this paper. URL: https://arc.vt.edu/.

Funding

This work was supported by NSF [award no. 1740704, Collaborative Research: EarthCube Integration--Brokered Alignment of Long-Tail Observations (BALTO)], USDA NRCS Conservation Innovation Grants Program [award no. 69-3A75-13-232]

References

Anderson TR, Groffman PM, Kaushal SS, Walter MT. 2014. Shallow groundwater denitrification in riparian zones of a headwater agricultural landscape. *Journal of environmental quality* 43 (2): 732–744 DOI: 10.2134/jeq2013.07.030

Archuleta C-AM, Constance EW, Arundel ST, Lowe AJ, Mantey KS, Phillips LA. 2017. The National Map seamless digital elevation model specifications. 11-B9. USGS, Reston, VA. DOI: 10.3133/tm11B9

ASTM. 2014. Standard Test Method for Particle-Size Analysis of Soils (Withdrawn 2016). D422-63. ASTM International. Available at: https://www.astm.org/Standards/D422 [Accessed 12 January 2021]

Beaudette D, Skovlin J, Roecker S. 2019. soilDB: Soil Database Interface Available at: https://CRAN.R-project.org/package=soilDB

Benham S. 2010. LiDAR Campaign (Blacksburg, VA) Report of Survey. VGIN, 1935 Jamboree Dr. Suite 100 Colorado Springs Co 80920. Available at: https://www.vita.virginia.gov/integrated-services/vgin-geospatial-services/elevation---lidar/ [Accessed 19 October 2020]

Bove G, Becker A, Sweeney B, Vousdoukas M, Kulp S. 2020. A method for regional estimation of climate change exposure of coastal infrastructure: Case of USVI and the influence of digital elevation models on assessments. *The Science of the total environment* **710**: 136162 DOI: 10.1016/j.scitotenv.2019.136162

Buchanan BP, Fleming M, Schneider RL, Richards BK, Archibald J, Qiu Z, Walter MT. 2014. Evaluating topographic wetness indices across central New York agricultural landscapes. *Hydrology and Earth System Sciences* **18** (8): 3279–3299 DOI: 10.5194/hess-18-3279-2014

Buol SW, Hole FD, McCracken RJ. 1989. Soil genesis and classification. *Iowa State University Press: Ames, Iowa*

Ciolkosz EJ, Waltman WJ. 2000. Pennsylvania's Fragipans by Available at: https://files.knowyourh2o.com/Waterlibrary/Stormwater/fragipan.pdf [Accessed 2 July 2022]

Cole SA. 2017. Comparing SSURGO data versus geospatial field measurements to estimate soil texture and infiltration rate classes in glaciated soils.Master of Science, Clemson University. Available at: https://core.ac.uk/download/pdf/268656509.pdf [Accessed 24 March 2021]

Collick AS, Fuka DR, Kleinman PJA, Buda AR, Weld JL, White MJ, Veith TL, Bryant RB, Bolster CH, Easton ZM. 2015. Predicting phosphorus dynamics in complex terrains using a variable source area hydrology model: MODELLING P DYNAMICS IN COMPLEX TERRAINS. *Hydrological processes* **29** (4): 588–601 DOI: 10.1002/hyp.10178

Dindaroglu T, Tunguz V, Babur E, Menshov O, Battaglia ML. 2021. Determination of the relationship among compound Topographic Index (CTI), soil properties and land-use in karst ecosystems. *Physical Geography*: 1–23 DOI: 10.1080/02723646.2021.1961361

Drewberry. 2019. Virginia FEMA NRCS South Central Lidar Project. U.S. Geological Survey, 1000 North Ashley Drive Suite 801 Tampa, FL 33602.

Easton ZM, Fuka DR, Walter MT, Cowan DM. 2008. Re-conceptualizing the soil and water assessment tool (SWAT) model to predict runoff from variable source areas. *Journal of* Available at: https://www.sciencedirect.com/science/article/pii/S0022169407005756

Fankhauser P, Bloesch M, Gehring C, Hutter M, Siegwart R. 2014. ROBOT-CENTRIC ELEVATION MAPPING WITH UNCERTAINTY ESTIMATES. In *Mobile Service Robotics*WORLD SCIENTIFIC; 433–440. DOI: 10.1142/9789814623353_0051

Friedman J, Hastie T, Tibshirani R. 2009. The Elements of Statistical Learning: Data Mining, Inference, and Prediction: 57–60

Fuka DR, Collick AS, Kleinman PJA, Auerbach DA, Harmel RD, Easton ZM. 2016. Improving the spatial representation of soil properties and hydrology using topographically derived initialization processes in the SWAT model DOI: 10.1002/hyp.10899

Gatzke SE, Beaudette DE, Ficklin DL, Luo Y, O'Geen AT, Zhang M. 2011. Aggregation strategies for SSURGO data: Effects on SWAT soil inputs and hydrologic outputs. *Soil Science Society of America journal. Soil Science Society of America* **75** (5): 1908–1921 DOI: 10.2136/sssaj2010.0418

Gesch D, Oimoen M, Greenlee S, Nelson C, Steuck M, Tyler D. 2002. The national elevation dataset. *Photogrammetric Engineering and Remote Sensing* **68** (1): 5–32 Available at: https://www.researchgate.net/profile/Dean_Gesch/publication/264158880_The_National_Elevation_Dataset/links/53d02e730cf2f7e53cfb703a.pdf

Giddings Machine Company. Hydraulic Soil Sampling, Coring and Drilling Machine: #5-UV / Model MGSRPSUV Available at: https://www.soilsample.com/5-uv-model-mgsrpsuv [Accessed 28 April 2021]

Goldman MA, Needelman BA, Rabenhorst MC, Lang MW, McCarty GW, King P. 2020. Digital soil mapping in a low-relief landscape to support wetland restoration decisions. *Geoderma* **373**: 114420 DOI: 10.1016/j.geoderma.2020.114420

Hjerdt KN, McDonnell JJ, Seibert J, Rodhe A. 2004. A new topographic index to quantify downslope controls on local drainage: TECHNICAL NOTE. *Water resources research* **40** (5): 2135 DOI: 10.1029/2004WR003130

Karney, CFF. 2013. Algorithms for geodesics. *Journal of Geodesy* **87** (1): 43–55 DOI: 10.1007/s00190-012-0578-z

Keesstra SD, Bouma J, Wallinga J, Tittonell P, Smith P, Cerdà A, Montanarella L, Quinton JN, Pachepsky Y, van der Putten, WH. 2016. The significance of soils and soil science towards realization of the United Nations Sustainable Development Goals. *SOIL* **2** (2): 111–128 DOI: 10.5194/soil-2-111-2016

Kelly RE, McConnell PRH, Mildenberger SJ. 1977. The Gestalt Photomapping System. *Photogrammetric Engineering and Remote Sensing* **43**: 1407 Available at: https://ui.adsabs.harvard.edu/abs/1977PgERS..43.1407K

Lal R, Mokma D, Lowery B. 2018. Relation between soil quality and erosion. In *Soil Quality and Soil Erosion*CRC Press; 237–258. Available at: https://www.taylorfrancis.com/chapters/edit/10.1201/9780203739266-14/relation-soil-quality-erosion-lal-mokma-lowery

Lanni C, McDonnell JJ, Rigon R. 2011. On the relative role of upslope and downslope topography for describing water flow path and storage dynamics: a theoretical analysis. *Hydrological processes* **25** (25): 3909–3923 DOI: 10.1002/hyp.8263

Li Z, Liu WZ, Wang QX. 2008. Effects of land use type and slope position on soil physical properties in loess tableland area. *Chinese Journal of Applied Ecology* **19** (06): 1303 Available at: http://www.cjae.net/EN/ [Accessed 25 January 2021]

Lin H. 2012. Chapter 1 - Hydropedology: Addressing Fundamentals and Building Bridges to Understand Complex Pedologic and Hydrologic Interactions. In *Hydropedology*, Lin H (ed.).Academic Press: Boston; 3–39. DOI: 10.1016/B978-0-12-386941-8.00001-0

Lyon SW, Walter TM, Gérard-Marchant P, Steenhuis TS. 2004. Using a Topographic Index to Distribute Variable Source Area Runoff Predicted With the SCS-Curve Number Equation. *Hydrological processes* **18** (15): 2757–2771 DOI: 10.1002/hyp.1494

Malczewski J. 2004. GIS-based land-use suitability analysis: a critical overview. *Progress in planning* **62** (1): 3–65 DOI: 10.1016/j.progress.2003.09.002

Moore ID, Gessler PE, Nielsen GA, Peterson GA. 1993. Soil Attribute Prediction Using Terrain Analysis. *Soil Science Society of America Journal* **57** (2): NP–NP DOI: 10.2136/sssaj1993.03615995005700020058x

Muhadi NA, Abdullah AF, Bejo SK, Mahadi MR, Mijic A. 2020. The Use of LiDAR-Derived DEM in Flood Applications: A Review. *Remote Sensing* **12** (14): 2308 DOI: 10.3390/rs12142308

Mukherjee S, Joshi PK, Mukherjee S, Ghosh A, Garg RD, Mukhopadhyay A. 2013. Evaluation of vertical accuracy of open source Digital Elevation Model (DEM). *International Journal of Applied Earth Observation and Geoinformation* **21**: 205–217 DOI: 10.1016/j.jag.2012.09.004

Muthusamy M, Casado MR, Butler D, Leinster P. 2021. Understanding the effects of Digital Elevation Model resolution in urban fluvial flood modelling. *Journal of Hydrology* **596**: 126088 DOI: 10.1016/j.jhydrol.2021.126088

Nemecek J. 2020. National Cooperative Soil Survey (NCSS) Soil Characterization database: The National Cooperative Soil Survey (NCSS) Soil Characterization Database contains the analytical results from the Kellogg Soil Survey Laboratory (KSSL) at the NCSS Available at: https://nrcs.maps.arcgis.com/home/item.html?id=65ffa754044548919781c0f0136aec88

Oksanen J, Sarjakoski T. 2005. Error propagation of DEM-based surface derivatives. *Computers & geosciences* **31** (8): 1015–1027 DOI: 10.1016/j.cageo.2005.02.014

Parece TE, DiBetitto S, Sprague T, Younos TM. 2010. The Stroubles Creek watershed: History of development and chronicles of research Available at: https://vtechworks.lib.vt.edu/bitstream/handle/10919/49495/VWRRC_sr201048.pdf

Resop JP, Lehmann L, Hession WC. 2019. Drone Laser Scanning for Modeling Riverscape Topography and Vegetation: Comparison with Traditional Aerial Lidar. *Drones* **3** (2): 35 DOI: 10.3390/drones3020035

Rock G, Ries JB, Udelhoven T. 2011. Sensitivity analysis of UAV-photogrammetry for creating digital elevation models (DEM). In *Proceedings of the Conference on Unmanned Aerial Vehicle in Geomatics, Zurich, Switzerland*mecinca.net. Available at: http://mecinca.net/papers/DRONES_IMU/UAV_analisis_ASPRS.pdf

Rodr'ıguez E, Morris CS, Belz JE. 2006. A Global Assessment of the SRTM Performance. *Photogrammetric Engineering & Remote Sensing* **72** (3): 249–260 DOI: 10.14358/PERS.72.3.249

Sadeghi A, Beeson P, Lang M, Tomer M. 2011. The Effect of DEM Resolution on Slope Estimation and Sediment Predictions. *2011 International* Available at: https://swat.tamu.edu/media/40684/sadeghi.pdf

Sena NC, Veloso GV, Fernandes-Filho EI, Francelino MR, Schaefer CEGR. 2020. Analysis of terrain attributes in different spatial resolutions for digital soil mapping application in southeastern Brazil. *Geoderma Regional* **21**: e00268 DOI: 10.1016/j.geodrs.2020.e00268

Simpson GD. 2018. Check Point Survey Report VA FEMA NRCS South-Central QL2 Virginia/West Virginia LiDAR Mapping Project. U.S. Geological Survey, 4601 Forbes Boulevard, Suite 300 Lanham, Maryland, 20706 .

Sørensen R, Seibert J. 2007. Effects of DEM resolution on the calculation of topographical indices: TWI and its components. *Journal of Hydrology* **347** (1): 79–89 DOI: 10.1016/j.jhydrol.2007.09.001

Sparks DL, Page AL, Helmke PA, Loeppert RH. 2020. *Methods of Soil Analysis, Part 3: Chemical Methods*. John Wiley & Sons. Available at: https://play.google.com/store/books/details?id=_oDWDwAAQBAJ

Stabler B. 2013. *shapefiles*. Available at: https://cran.r-project.org/web/packages/shapefiles/shapefiles.pdf

Steinmetz Z. 2021. Package 'envalysis': Miscellaneous Functions for Environmental Analyses. Github. DOI: 10.1016/0016-7061(93)90103-R

Stolt MH, Baker JC, Simpson TW. 1993. Soil-Landscape Relationships in Virginia: II. Reconstruction Analysis and Soil Genesis. *Soil Science Society of America journal. Soil Science Society of America* **57** (2): 422–428 DOI: 10.2136/sssaj1993.03615995005700020023x

Tachikawa T, Hato M, Kaku M, Iwasaki A. 2011. Characteristics of ASTER GDEM version 2. In *2011 IEEE International Geoscience and Remote Sensing Symposium*ieeexplore.ieee.org; 3657–3660. DOI: 10.1109/IGARSS.2011.6050017

Tarboton DG. 1997. A new method for the determination of flow directions and upslope areas in grid digital elevation models. *Water resources research* **33** (2): 309–319 DOI: 10.1029/96WR03137

Tarboton DG. 2005. Terrain analysis using digital elevation models (TauDEM). *Utah State University, Logan* **3012**: 2018 Available at: https://hydrology.usu.edu/taudem/taudem3.1/

Tarboton DG. 2014. TauDEM. Github. Available at: https://github.com/dtarb/TauDEM [Accessed 25 January 2021]

Thilakarathne M, Sridhar V, Karthikeyan R. 2018. Spatially explicit pollutant load-integrated in-stream E. coli concentration modeling in a mixed land-use catchment. *Water research* **144**: 87–103 DOI: 10.1016/j.watres.2018.07.021

Thomas IA, Jordan P, Shine O, Fenton O, Mellander P-E, Dunlop P, Murphy PNC. 2017. Defining optimal DEM resolutions and point densities for modelling hydrologically sensitive areas in agricultural catchments dominated by microtopography. *International Journal of Applied Earth Observation and Geoinformation* **54**: 38–52 DOI: 10.1016/j.jag.2016.08.012

Tovar-Pescador J, Pozo-Vázquez D, Ruiz-Arias JA, Batlles J, López G, Bosch JL. 2006. On the use of the digital elevation model to estimate the solar radiation in areas of complex topography. *Meteorological Applications* **13** (3): 279–287 DOI: 10.1017/S1350482706002258

US Department of Commerce, National Oceanic, Atmospheric Administration. 2021. What is LIDAR. *What is LIDAR* Available at: https://oceanservice.noaa.gov/facts/lidar.html [Accessed 1 December 2021]

USGS. 1993. Digital Elevation Models: Data Users Guide. U.S. Geological Survey, 507 National Center Reston, Virginia 22092 . Available at: https://pubs.usgs.gov/dug/0005/dug0005.pdf

Western AW, Grayson RB, Blöschl G, Willgoose GR, McMahon TA. 1999. Observed spatial organization of soil moisture and its relation to terrain indices. *Water resources research* **35** (3): 797–810 DOI: 10.1029/1998wr900065

White ED, Easton ZM, Fuka DR, Collick AS, Adgo E, McCartney M, Awulachew SB, Selassie YG, Steenhuis TS. 2011. Development and application of a physically based landscape water balance in the SWAT model. *Hydrological processes* **25** (6): 915–925 DOI: 10.1002/hyp.7876

Wilson M, Atkinson PM. 2005. The use of elevation data in flood inundation modeling: A comparison of ERS interferometric SAR and combined contour and differential GPS data. *International Journal of River Basin Management* **3** (1): 3–20 DOI: 10.1080/15715124.2005.9635241

Wolock DM, Price CV. 1994. Effects of digital elevation model map scale and data resolution on a topography-based watershed model. *Water resources research* **30** (11): 3041–3052 DOI: 10.1029/94wr01971

Yu C, Liu J, Ma J, Yu X. 2018. Study on transport and transformation of contaminant through layered soil with large deformation. *Environmental science and pollution research international* **25** (13): 12764–12779 DOI: 10.1007/s11356-018-1325-7

Zhang W, Montgomery DR. 1994. Digital elevation model grid size, landscape representation, and hydrologic simulations. *Water resources research* **30** (4): 1019–1028 DOI: 10.1029/93wr03553

Zhuo L, Han D. 2016. Misrepresentation and amendment of soil moisture in conceptual hydrological modelling. *Journal of Hydrology* **535**: 637–651 DOI: 10.1016/j.jhydrol.2016.02.033

Supplemental Materials

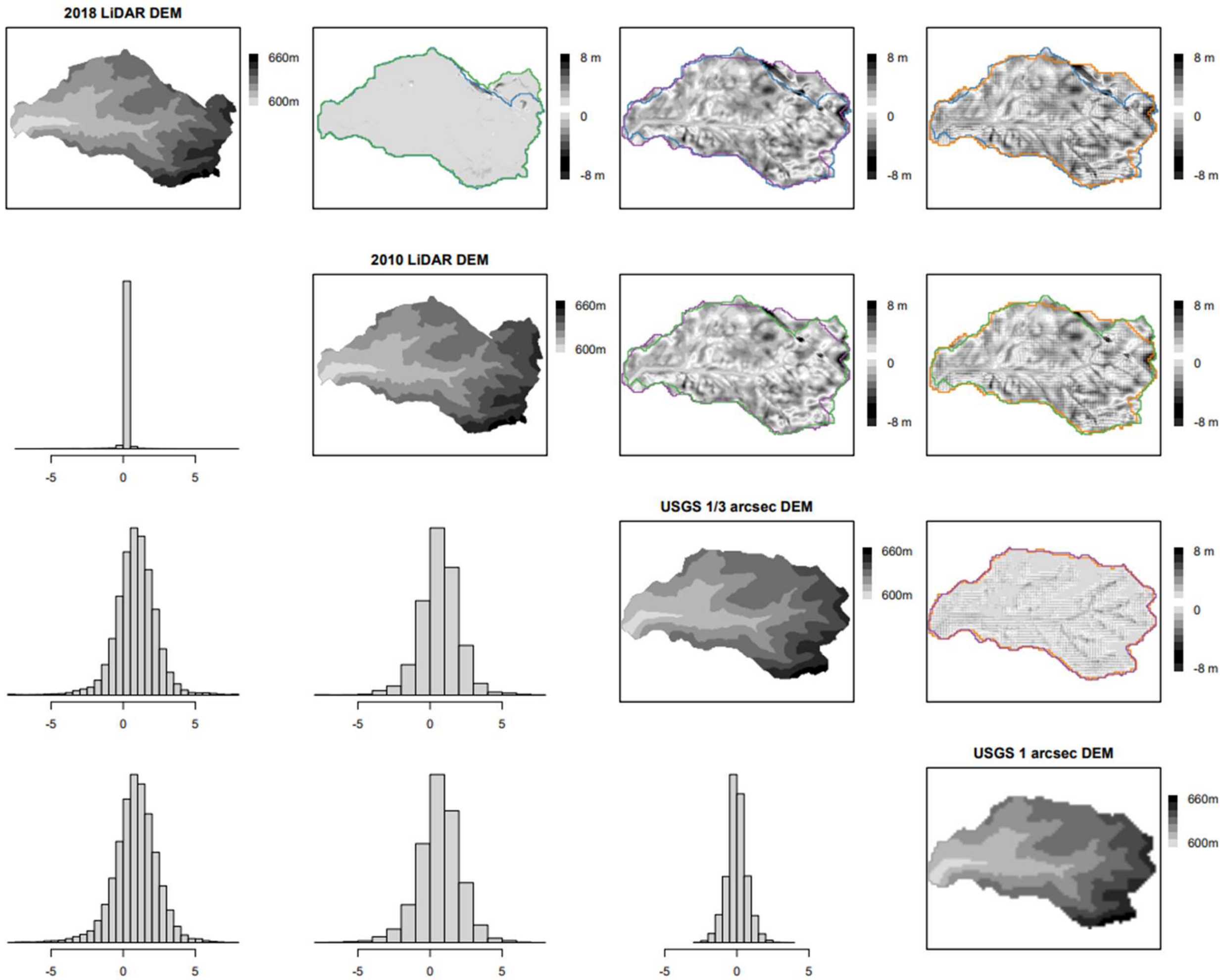

Figure 2-S1 Numerical differences between DEMs (Coarser resolution-Finer resolution). Watershed boundaries and stream networks: 2018 LI - blue, 2010 LI - green, ⅓ as - purple, 1 orange - red

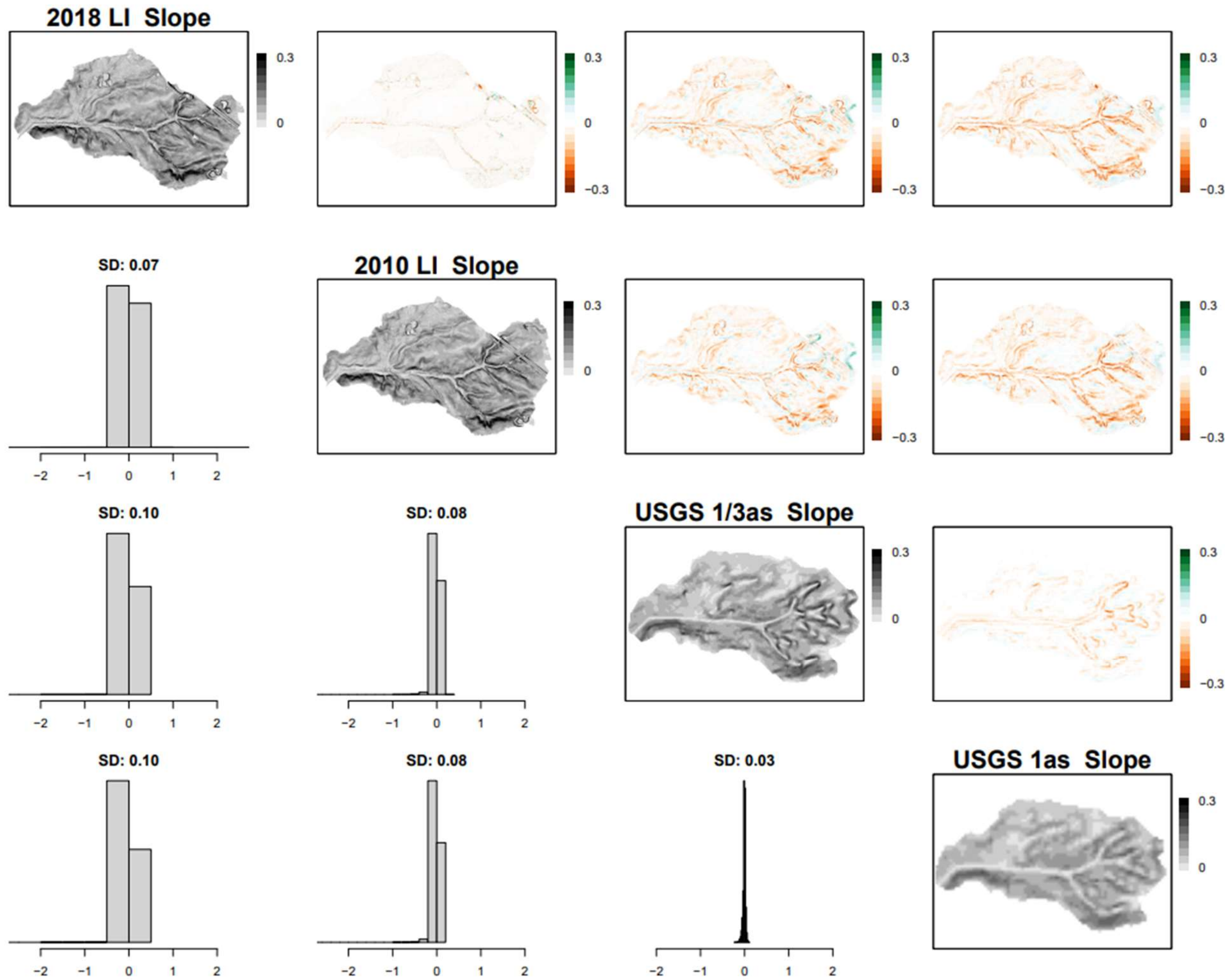

Figure 2-S2 Spatial differences between slopes from the source DEMs using the D8 flow direction algorithm. These are calculated by the following equation: Coarser resolution - finer resolution (eg. 2010LIDAR - 2018LIDAR). Resulting watershed boundaries are found in the lower right corner. 2018LI - blue, 2010LI - green, 1/3as - purple, 1as - orange.

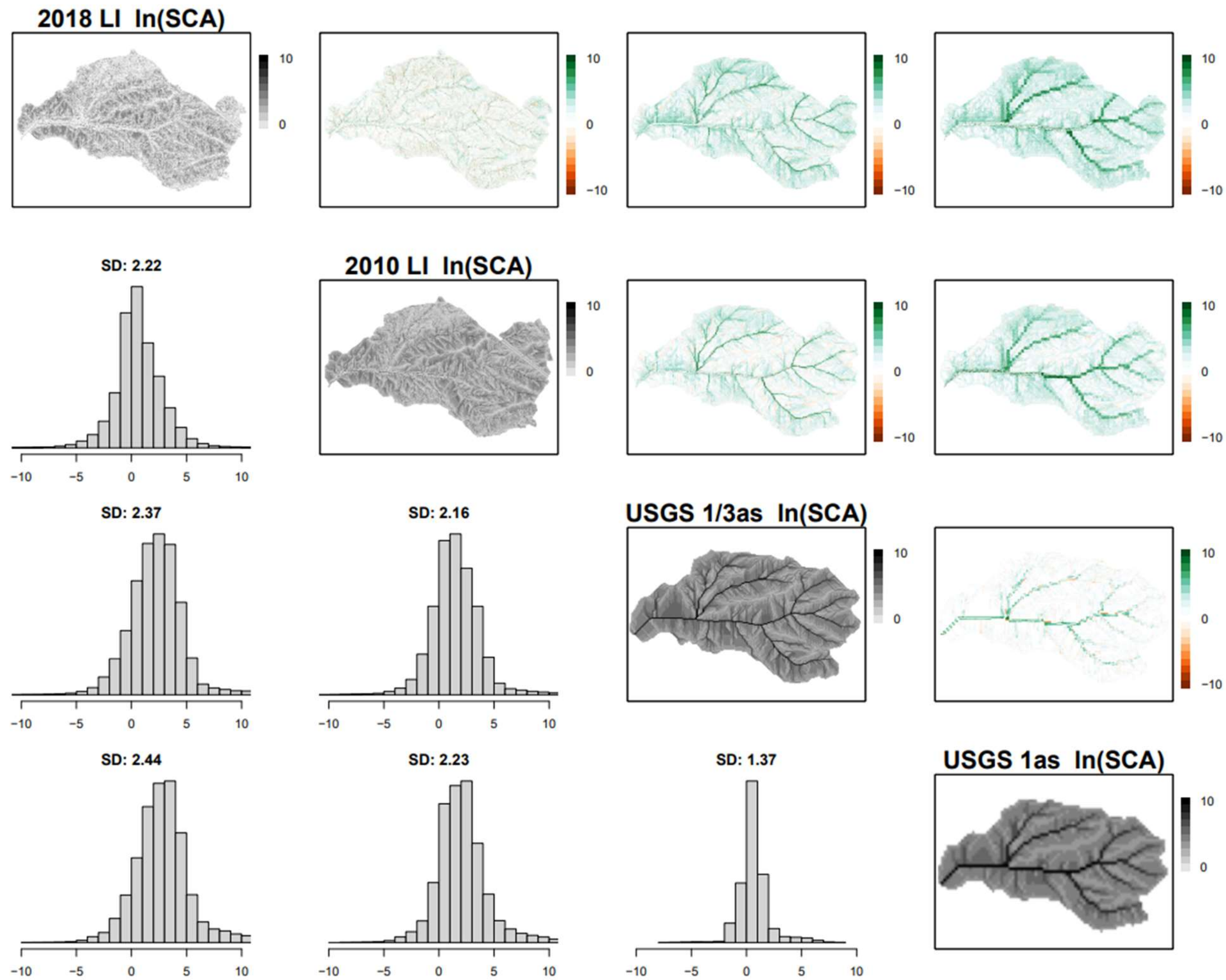

Figure 2-S3 Spatial differences between ln(SCA) from source DEMs using the D8 flow direction algorithm. These are calculated by the following equation: Coarser resolution - finer resolution.

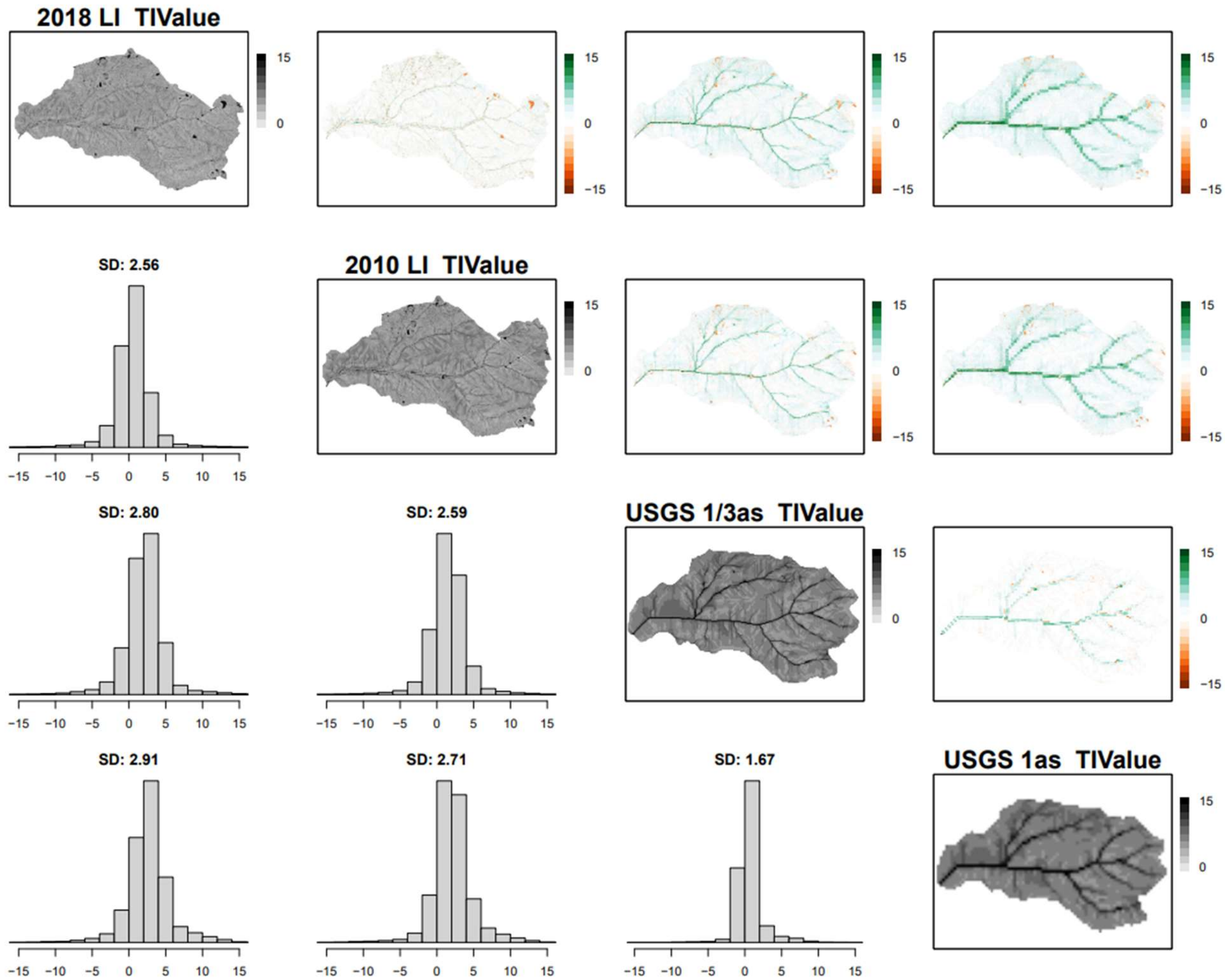

Figure 2-S4 Spatial differences between TIV from source DEMs using the D8 flow direction algorithm. These are calculated by the following equation: Coarser resolution - finer resolution.

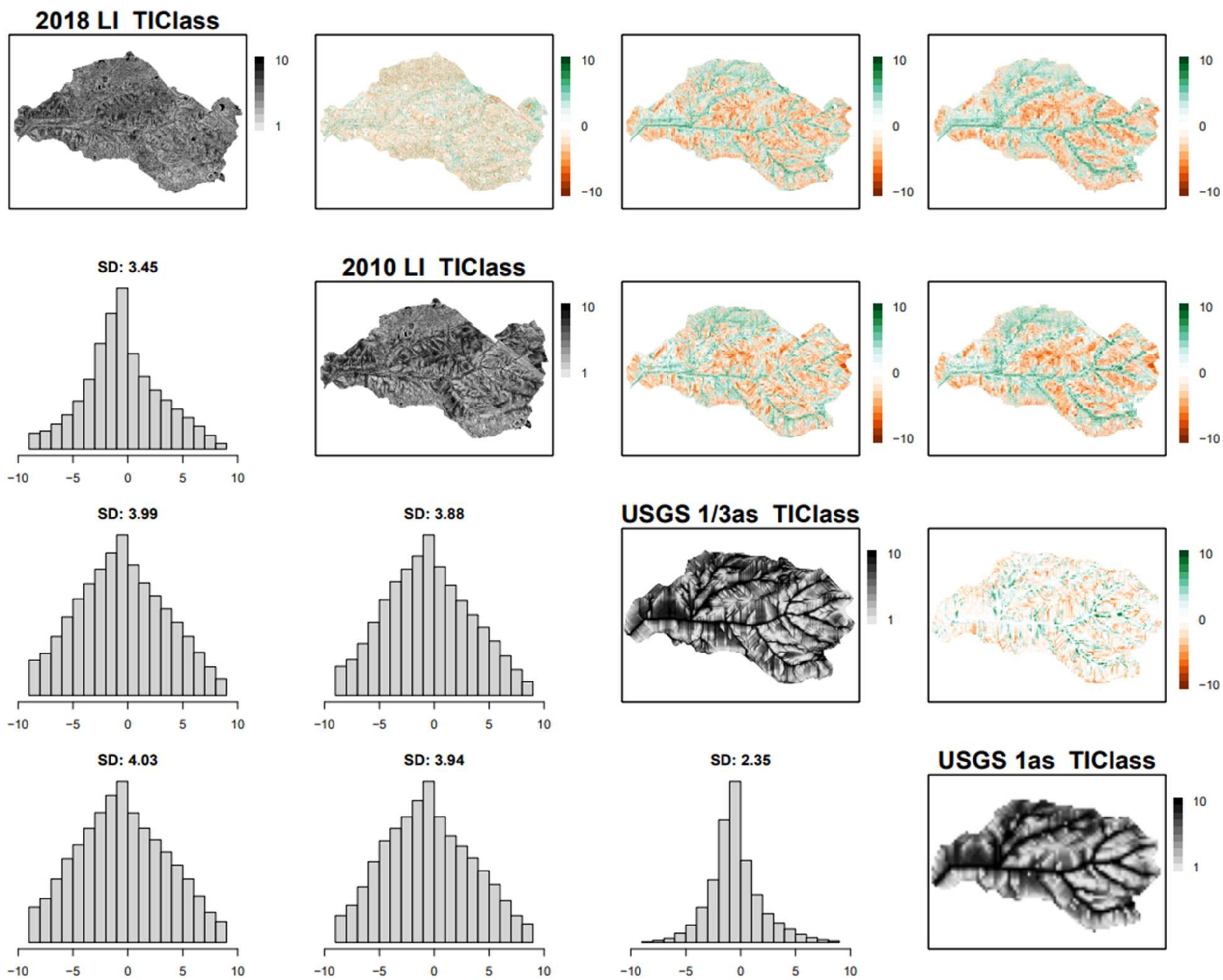

Figure 2-S5 Spatial differences between TIC from source DEMs using the D8Dinf flow direction algorithm. These are calculated by the following equation: Coarser resolution - finer resolution.

Chapter 3: Integrating multiple Digital Elevation Models into soil characteristic distribution

Elyce Buell[a], Roja Kaveh[a], Sabrina Mehzabin[a], Binyam Asfaw[a], Louise Koepele[a], Daniel R. Fuka[a], Amy S. Collick[b], William Auchincloss[a], Zachary M. Easton[a]

[a]Department of Biological Systems Engineering, Virginia Tech, Blacksburg, VA
[b]Department of Agricultural Sciences, Morehead State University, Morehead, KY

Keywords: Soil properties, Digital elevation model, LiDAR, Soil mapping, Catchment area, Slope

Abstract
SSURGO method for distributing soil properties is prone to error. This research proposes a novel method to distribute soils using multiple DEMs. The Vermont Association of Conservative Districts analyzed 59 soil samples located in western Vermont. Derived properties including slope and catchment area are calculated from six DEMs (USGS 1m, ⅓ as, and 1as, aerial LiDAR, SRTM, and GDEM). The general relationship between soils and DEM derived slopes and catchment areas are explored. Small resolution rasters are recursively coarsened and evaluated for soil characteristic representability to isolate effects of resolution from generation method or reported error. Slopes derived from fine resolutions were largely uninformative because of their high instances of zeros. Soil maps are then generated using a multivariate regression that uses a single slope and catchment area as inputs; resulting maps outperformed SSURGO distributed soil maps. In all cases, these regressions resulted in inputs that were from two DEMs meaning multiple DEMs have the opportunity to better soil maps.

3.1 Introduction

Digital elevation models (DEMs) represent the earth's surface using a georeferenced grid, where each square has an assigned elevation and resolution (Guth et al., 2021). DEMs are used broadly in multiple applications including geology, hydrology, ecology, meteorology, and floodplain mapping (Azizian & Brocca, 2020; Han et al., 2020; Steger et al., 2020; Zhang et al., 2020; Celis et al., 2021). Historically DEMs were produced using ground surveying, and manual photogrammetry of aerial images (Miller, 1958). During the 1980s, remote sensing-based DEMs began emerging using methods such as stereoscopic imaging (typical space-borne resolutions: 30m to 90m), synthetic aperture radar (InSAR - typically 30m), laser imaging and scanning, and light detection and ranging (LiDAR) (typical resolutions ranging from 0.3m-2m) (Hutsul & Smirnov, 2017; Zhang et al., 2019; Goyal et al., 2021). Most are produced using aircrafts (most typically for generating LiDAR or stereoscopic imaging) or satellites (most typically used for stereoscopic imaging) (Farr et al., 2007; Stoker et al., 2008; Tachikawa et al., 2011).

DEMs are primary data sources for analyzing the natural processes occurring in a landscape from which spatial attributes such as upslope area (the area of a landscape that contributes flow to a location of interest), slope, and topographic wetness can be extracted. These attributes affect soil characteristics, soil water distribution and abundance, susceptibility of landscapes to erosion, soil-moisture content and the distribution of flora and fauna (Wilson & Gallant, 2000; Nabiollahi et al., 2018; Raduła et al., 2018; Kopecký et al., 2021; Telak et al., 2021). DEM derivatives can be integral in our understanding of the landscape. For example, upslope area can be used to calculate theoretical flow accumulation, steady-state area contour runoff rate, soil characteristics, and soil-water content. Similarly, slope is integral to landscape morphology as it is used in determining overland and subsurface flow velocity, vegetation, cattle grazing density, susceptibility to erosion, soil water content, and land capability class (Moore, 1991; Wu et al., 2008; Paz-Kagan et al., 2016). Topographic wetness is used to describe the spatial distribution of soil-water content. This attribute helps identify locations that have a high probability of transporting nutrients (commonly referred to as critical source areas) (Collick et al., 2015). Identifying these critical areas can help keep livestock away from the pollutant concentration areas, making landscape wetness an important attribute with respect to management and policy applications. Thus DEMs and derived spatial characteristics have the opportunity to help us fundamentally understand landscape processes.

Landscape spatial characteristics are also integral in soil connectivity pattern and soil distribution in the landscape (Odeh et al., 1991; Thomas et al., 2016; Jancewicz et al., 2019). A physically-based relation between spatial attributes and measured soil properties can improve the accuracy of prediction of soil variables at unsampled locations (Moore et al., 1993; Odeha et al., 1994; Collick et al., 2015; Fuka et al., 2016). Spatial attributes derived from DEMs have been shown to distribute specific soil properties, including A-horizon thickness, organic matter content, extractable P, pH, and sand and clay content more accurately than traditional soil databases (Moore et al., 1993). Previous studies show strong relationships between a myriad of DEM-derived spatial characteristics and soil properties.

Many types of DEMs are available with differing resolutions and generation methods. When comparing one DEM to another, these DEMs often differ in spatially derived datasets such as slope and catchment area. Many studies have found coarse DEM datasets to be irrelevant (Muthusamy et al., 2021) and thus the prevailing narrative often is researchers assume the finest resolution dataset is best and should be used as a default. However, it is important to consider that landscapes and their soils are formed over long periods of time. It is likely that a small resolution raster alone will be insufficient to describe soil distribution due to a small raster being far outsized by the landscape features driving the soils distribution. There is an opportunity to distribute soils with increasing accuracy if spatial characteristics from several DEMs of differing resolution and age are considered.

This study evaluated the relationship between DEM derived characteristics, including slope, upslope contributing area and measured soil properties. Six DEMs, which differ in generation method and resolution, were used to evaluate the effects of scale on representing soil properties. Additionally, by using multiple well-informed spatial datasets, we can distribute soil properties better than that of SSURGO or traditional choices of finest resolution DEMs.

3.2 Materials and methods

3.2.1 Study Area

The study was conducted in the Little Otter Creek (LOC) and Dead Creek (DC) watersheds, in the Lake Champlain Basin located in Addison County, Vermont (figure 3-1). The LOC and DC watershed sizes are 160 km2 and 100 km2, respectively. Both watershed land uses include predominately agricultural land in the Lake Champlain basin with rolling topography and elevations ranging from 48 m to 113 m. Land use in both LOC and DC watersheds is dominated by dairy cropping systems with 44% of LOC and 65% of DC areas in hay production and 5% and 10% of LOC and DC in row crop agriculture, respectively. The majority of the remaining area is forested (36% for LOC and 14% for DC) and wetlands (10% for LOC and 5% for DC) with small areas of residential and industrial land (<6%) (Homer et al., 2004; USGS, 1994). Soils in the watersheds include Vergennes clay (27% LOC, 64% Dead Creek), and Covington and Panton silty clays (10% LOC, 22% Dead Creek). Rock land occupies 12% of the area in LOC. The climate in the area is humid continental with mean annual precipitation of 1100 mm and mean annual temperature of approximately 7.5 C.

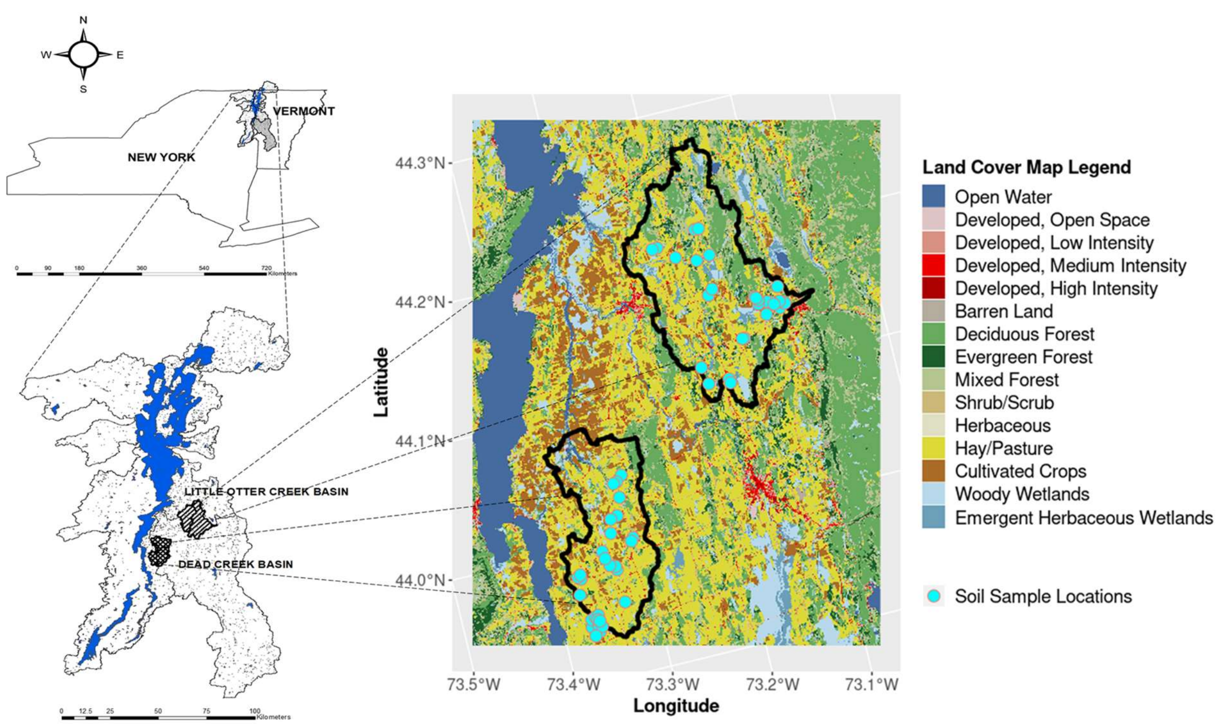

Figure 3-1 Study area map, location of the LOC and DC watersheds in the Lake Champlain watershed, VT, and a land use map of the watersheds

3.2.2 Soil Data

Soils samples were collected at fifty-nine locations (figure 3-1) and analyzed following the Cornell Soil Health protocol (Moebius-Clune et al., 2016) as collected by the Vermont Association of Conservative Districts (USDA NRCS, 2019). Six-inch soil cores were collected in agricultural fields between Fall 2020 and Fall 2021. Twenty-seven sites were located in the LOC watershed and thirty-two sites were located in the DC watershed (figure 3-1). Soil data of interest from the report include texture, water capacity, soil organic matter.

Table 3-1: Summary of DEM metadata

DEM Abbreviation	Source	Relevant Citations (data, metadata, and reported uncertainty)	Data Acquisition Date	Data Collection Sensor	Vertical Uncertainty (1 sd)	Resolution
LOC LiDAR	VCGI	Quantum Spatial, 2018; VCGI et al., 2018	Nov. 2017	Leica ALS 70 and Riegl LMS Q1560	0.1 m	0.7 m
DC LiDAR	VCGI	Quantum Spatial, 2016; VCGI et al., 2016	2013-2015	Leica ALS 70 and Optech Gemini LiDAR sensor	0.1 m	0.7 m
1m	USGS	Arundel et al., 2015; USGS, 2019	Unknown	Various	0.1 m	1.0 m
1/3as	USGS	USGS, 2019	1960-2016	Various	2.4 m [1]	10.3 m
1as	USGS	USGS, 2019	1960-2016	Various	4.1 m [2]	30.9 m
SRTM	USGS	Farr & Kobrick, 2000	Between 2000 and 2014	Spaceborne Imaging Radar-C	9.7 m	30.9 m
GDEM	NASA	NASA et al., 2019	2000-2013	ASTER	12.1 m [3]	30.9 m

[1,2,3] Uncertainty evaluated by a third party study: (1) Haneberg, 2006**;** (2) Holmes et al., 2000; (3) Abrams et al., 2019

3.2.3 Digital elevation models (DEMs)

DEMs were selected in a variety of scale/resolution and acquisition methods, including aerial LiDAR, historical USGS surveys, and the global SRTM and ASTER GDEM missions (Farr and Kobrick, 2000; Reuter et al., 2009; NASA et al., 2019). LiDAR utilizes visible or near infrared pulses to calculate distance/elevation. The USGS national DEM database uses a suite of historical surveys and contemporary resources (most typically LiDAR) to create national standardized (in resolution) DEMs (USGS, 1993). The Shuttle Radar Topography Mission (SRTM) produces DEMs of the earth utilizing phase-difference between two radar images using a technique called interferometric synthetic aperture radar (InSAR) (Farr et al., 2007). The Terra Advanced Spaceborne Thermal Emission and Reflection Radiometer (ASTER), utilized space borne stereoscopic imaging using space borne infrared cameras to create global DEM between 830 N and 830 S (Tachikawa et al., 2011). A summary of different types of DEMs is given in table 3-1.

3.2.4 Spatial Data Processing

Each DEM described above was subject to a series of spatial operations, slope, specific catchment area (SCA), topographic index value (TIV), and topographic index class (TIC). These operations are conducted for two flow direction algorithms. Flow direction algorithms define flow parsing between rasters and as is such, flow direction algorithm choice affects the calculated slope and SCA (and therefore TIV and TIC).

The flow direction algorithms investigated are D8 and D-infinity (Dinf). These are two methods of routing flow between neighboring DEM cells that differ in their routing algorithms. D8 selects a single downslope raster (using steepest descent) to which all upslope accumulated flow is routed. Dinf proportions flow to adjacent downslope cells based on the steepest downgradient slope from a triangular grid centered on each adjacent downslope cell. The differences between the D8 and Dinf methods and a more in-depth discussion can be found in Tarboton, 1997.

To calculate slope, at each raster the steepest downslope descent is calculated and the value is assigned to that raster. For D8 slope is defined as the steepest drop over two adjacent cells, and for Dinf, the slope is calculated along the triangular facet of the plane with the steepest slope across adjacent cells (Tarboton, 1997, 2014).

The catchment area of a particular point is the area that drains to that location (as specified by the input DEM in units of L^2. The SCA is the catchment area normalized by the length of the raster (or the resolution of the raster) yielding a value in units of L. Here we use SCA because it has shown better correlation with physical properties in previous studies (Moore et al., 1993; Collick et al., 2015; Fuka et al., 2016). The SCA is calculated as:

SCA = CA/(Raster Length)

Where CA is the upslope contributing area per unit of contour line (L^2) and raster length is the width of the raster (L). The Topographic Index (TIV) is a grid created by combining SCA and slope raster as:

$$TIV = \ln (SCA/\tan(slope))$$

where slope is topographic slope of the cell (expressed in radians), (Lyon et al., 2004; Easton et al., 2008). The Topographic Index Class (TIC) reclassifies the TIV into equal-area groups, for this study 10 TICs were selected per the methods of Easton et al., (2008), who showed that 10 classes generally provide sufficient detail to discriminate processes at a sub-field scale. TICs are created such that TIV above the

90th percentile are assigned a TIC of 10, TIV in the 80th-90th percentile are assigned a TIC of 9, and TIV in the 0th-10th percentile are assigned a TIC of 1.

All of the measured and generated data described above were subject to correlation analysis. We correlate derived terrain characteristics among DEMs and DEM processing methods (e.g., slopes, TIV, etc derived from the DEMs) with with measured properties (e.g., soil physical measurements) and database extracted properties (e.g., SSURGO soils data).

The first iteration of this investigation included TIVs and TICs as potential informants on soil distribution. As TICs are watershed specific, a single watershed is considered for section 3.2.3.1. LOC is selected over the DC watershed because initially, the researchers believed that streamflow simulation using a hydrological model would become relevant to this project. Flow simulation and calibration of watersheds within a short period of time are challenging for hydrologists. Thus, LOC watershed, instrumented with daily flow data for the past 30 years, was selected over DC with 2 years of flow data.

3.2.5 Multiple Regression

Multiple regression analysis was used to evaluate how well the derived data for slope and SCA represent measured soils [eq 3-1].

$$Y = m_1 * slope + m_2 * \ln(SCA) + b \qquad \text{eq. 3-1}$$

Where Y is soil property of interest (organic matter, predicted AWC, sand, or clay), slope is a single input of slope selected from the twelve slope options (six DEMs for both D8 and Dinf flow directions), SCA is a single input of SCA selected from the twelve SCA, and m_1, m_2, and b are regression estimates. Note that the log of SCA is taken because a log transformation of SCA linearized the relationship between SCA and soil properties. Constraining the regression inputs to a single slope and SCA is attractive because these two inputs together result in an established method for prediction of soil wetness: TIV and TIC. Currently, TIVs are calculated using a single DEM for both slope and SCA. Of particular interest is exploring how different resolutions may be combined to distribute soils. Information on slope and SCA from each individual DEM were extracted from the rasters for each sample location in Figure 3-1 and regressed against the various soil parameters described previously. Forward stepwise regression is utilized to choose the two best inputs that result in the lowest Akaike Information Criterion (AIC) and have a single input from both the slope and SCA category. The regression with the lowest AIC is selected (Portet, 2020).

3.2.6 LiDAR Aggregation and Evaluation

LiDAR aggregation seeks to discern if the patterns we are seeing are the result of different collection methods and errors or if they are the result of resolution size differences. To do this, much of the same steps described above is applied to a single raster at several different coarseness. The raster package in R (Karney, 2013) is used to combine the 0.7m LiDAR, 1m USGS, and ⅓ as USGS data into coarser resolution DEMs for evaluation. The “aggregate” function creates coarser rasters and can then assign mean values to the coarsened rasters. After the LiDAR data is aggregated, correlation can be evaluated. The aggregated data was compared to the evaluated physical soil data on SCA and watershed slope from all 59 soil sampling locations. Correlation between the DEM aggregate data and physical data was evaluated to determine if the data has higher correlation due to resolution size instead of randomness or collection method.

3.2.7 Cross validation

The cross validation analysis is conducted in order to compare the finest resolution slope and SCA for both flow direction algorithms (using eq. 3-1 but for LiDAR slope and SCA) to our trained multiple regressions results discussed in section 3.2.5. This analysis is conducted in order to depict how robust the regressions are to cross validation. Linear regressions for all three regression cases (LiDAR D8, LiDAR Dinf, and informed regression hereafter referred to as multiDEM/multivariate regression) trained on 30 randomly selected soil samples for each measured soil property. Following this, the remaining 29 samples are used to test the regression. Relevant statistics are saved and the process is repeated until convergence in results is found.

3.3 Results

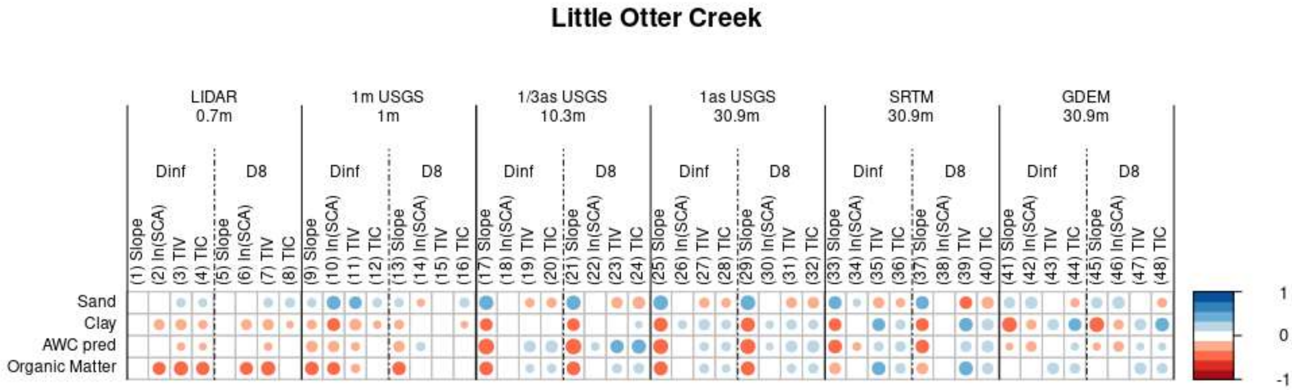

Figure 3-2 Correlations between spatially extracted characteristics and measured soil properties

3.3.1 Slope, SCA, TIC and TIV relationships

Slope, SCA, and topographic wetness values (TIV and TIC) are correlated with soil characteristics for the 28 soil samples in the LOC watershed. Topographic wetness classes can only appropriately be applied within watershed, hence, a single watershed is considered for section 3.3.1. Figure 3-2 compares all measured soil properties (sand, clay, predicted AWC [available water content], and organic matter) to all combinations of spatial characteristics (slope, SCA, TIV, and TIC), DEMs (LIDAR, 1m USGS, ⅓ as USGS, 1 as USGS, SRTM, and GDEM), and both flow direction algorithms considered (Dinf and D8).

As is evident in figure 3-2, the strongest correlations (both negative and positive) were associated with the slope estimates derived from nearly all of the DEMs, with the exception of the LiDAR DEM and GDEM. Calculating TIVs and TICs do not enhance correlations with soil properties (figure 3-2). Consider columns 9-12 in figure 3-2: the strength of the correlations observed in these columns are not strongest in the topographic wetness columns (11 and 12) and slope and SCA (columns 9 and 10) are as strong or stronger than topographic wetness. This is consistently observed in ~90% of correlations (64 of 72 comparisons). In theory, TIVs convey more information than its individual inputs (SCA and slope) and as a result, it is reasonable to expect them to correlate stronger than its individual inputs. However, this is seldom the case. For the TIV correlations to be stronger than their individual inputs, the correlations for SCA and slope would need to be opposite (i.e. one correlation positive, the other negative). This occurs very rarely (8 of 72 comparisons) in this set of data. In the rare case when topographic wetness is more informative than its individual inputs, TIVs and TICs are weakly correlated and thus not overly informative.

From this data, it is clear that the conventional calculation of topographic wetness is not enhancing representation of soils. The available soil data spans two watersheds; as a result, eliminating topographic wetness would yield additional power for the remaining analysis. Therefore, the remaining analysis will no longer explore TIV and TIC, and an additional 32 soil samples from the DC watershed can be included.

3.3.2 Slope

DEM derived slopes are correlated against six measured soil properties for 59 soil samples in LOC and DC basins. The relationships between measured soil properties and resolution and flow direction algorithm choice are examined for the application of soil distribution.

3.3.2.1 Flow direction algorithms

Choice of flow direction algorithm did not considerably impact the slope results (maximum pairwise difference between Dinf and D8 correlations is 0.02 with most pairwise differences below 0.01) as can be viewed Figure 3-S1. As Chapter 2 of this thesis shows, extracted slope calculations can be expected to not vary between D8 and Dinf. The key difference between Dinf and D8 presents itself strongly when considering flow routing schemes at a large scale (larger than individual rasters). However, the difference between the algorithms when considering a single raster are subtle. When referring to Tarboton, 1997, we see that the greatest difference between flow direction is 45 degrees. The extracted slopes for this slight difference in direction result in very similar slope values between the two flow direction algorithms. As a result of this finding, the remaining 3.3.2 sections will consider slopes derived from Dinf, though all findings described can be applied to the D8 collection of slopes.

3.3.2.2 Digital Elevation models

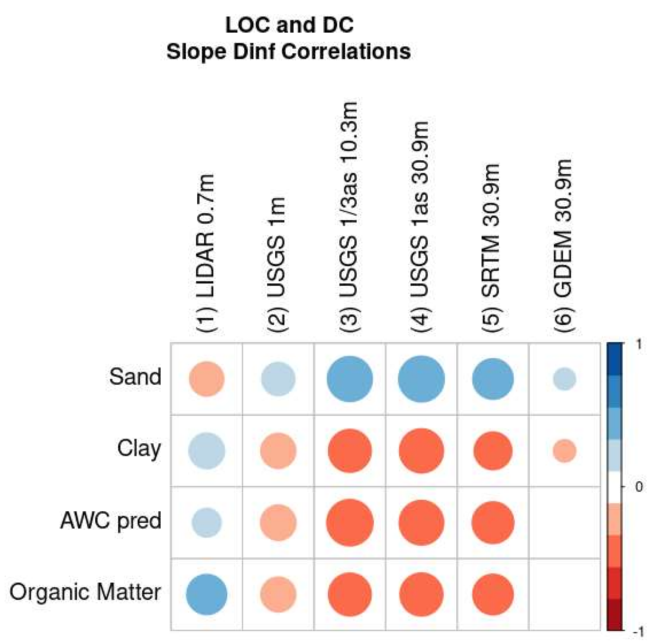

Figure 3-3 Measured soil properties correlated with DEM derived slope for the Dinf algorithm

Similar to figure 3-2, figure 3-3 is a correlation plot that compares all measured soil properties (sand, clay, predicted AWC, and organic matter) to all DEMs (LIDAR, 1m USGS, ⅓ as USGS, 1 as USGS, SRTM, and GDEM) for slope Dinf. This section aims to investigate the relationship between slope resolution and their ability to accurately describe soil properties.

Generally, slopes from coarse resolution DEMs outperform slopes from a finer resolution DEM (figure 3-3). For slope, all strongest correlations were found when comparing 1as or ⅓ as slopes to measured soil. Of note, the SRTM 30m resolution raster did quite well when considering the raster's reported errors (table 3-1; USGS 1as: 4.1m, SRTM: 9.7m). Slope correlations for the GDEM raster performed the worst (table 3-1; GDEM: 12.1m). This could be the result of two things (1) the threshold for error with respect to this application is between 9.7m and 12.1m vertical uncertainty (expressed as a standard deviation; table 3-1) or (2) the methodology of generating DEMs using stereographic imagery via satellite images is not good at accurately representing the landscape relative to the InSAR method. All best correlation magnitudes between measured soil properties and slope fell between 0.42 and 0.52.

Slope correlations for the LiDAR (0.7m) are large in magnitude but they disagree directionally from all other correlations when comparing the LiDAR column (1) to all other columns (2-6). When considering if there is a "right" and "wrong" correlation sign for each soil property, one must consider how said soil property would be expected to relate to slopes. Consider relating clay to the slope of a location. Locations with high slopes can be expected to transport clay away from that location, whereas locations with low slopes can be expected to deposit clay. Both organic matter and AWC can be expected to be large where there is a wet location in the watershed. Most typically, wet locations occur on flat ground. Lastly, sand is likely to be high at high slopes because of the relative absence of clay. As such, it is expected that all measured soil properties aside from sand are negatively related to slope. When considering this, LiDAR performs worse than the coarser resolutions. Similarly, 1m USGS do not correlate strongly with measured soil properties as well as its coarser counterparts. It is certainly surprising that the most recent, highest resolution data is performing poorly for slopes.

3.3.2.2.1 Distinguishing between DEM resolution and DEM generation method

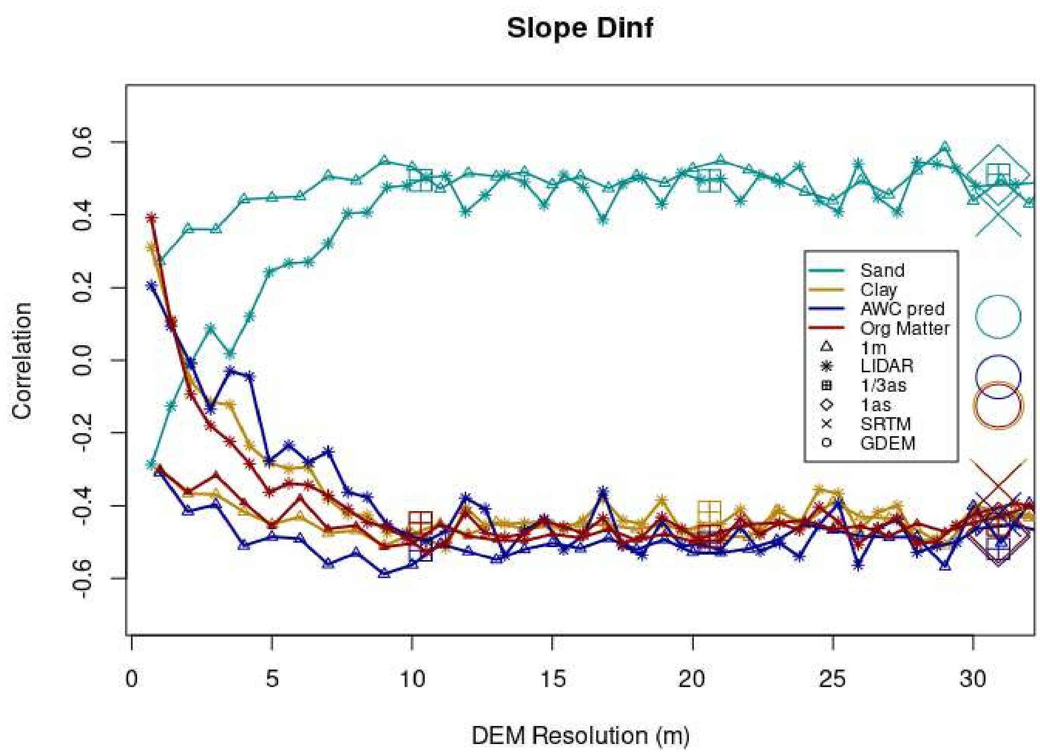

Figure 3-4 LiDAR, 1m, and 1/3as DEMs are aggregated to generate slopes derived from increasingly coarse resolution data. Correlations from derived data are plotted.

To further investigate the pattern observed in figure 3-3, we isolate effect of resolution from generation method, by using a single fine resolution DEM (LiDAR, 1m, and ⅓ as) to generate increasingly coarse DEMs. The effect of this coarsening is then observed against measured soil property correlations (figure 3-4).

As the LiDAR DEM raster is coarsened the slope correlations strengthen and plateau at resolution equivalent to 11m. This pattern is observed strongly throughout all 4 measured soil properties. This plateau extends well past the region displayed in figure 3-4; when the resolution considered is expanded, 300m rasters consistently correlate stronger with measured soils than slopes derived from fine resolution (0.7m to 4.9m) rasters (data not shown). This is particularly notable because scientists frequently choose the finest resolutions for the majority of applications, however, in this case, considering a slope derived from 300m DEM to inform the distribution of soils yields better results than choosing slopes derived from 5m DEM.

Additionally, the increasingly coarsened slope resulting from LiDAR approaches the plateau slower than that of 1m DEM. This is particularly of interest because this effect cannot be explained by resolution size alone. To further explore this anomaly, the distribution of extracted slopes for the 59 data points are observed in figure 4-5. Figure 4-5 displays an explanation for why slopes at low resolutions are not correlating well with soil properties: slopes for small resolutions are often zero. This is especially true for the LiDAR DEM and this issue propagates through several iterations of aggregation. Small resolutions effectively assign more of the watershed rasters zeros. As a result, small rasters assign select rasters higher slopes than their coarser counterparts. This finding is consistent with Sørensen & Seibert (2007) who finds that smaller rasters have higher variance when compared to their coarse counterparts. As resolution increases in size, slopes become more typically nonzero, and thus have a better potential for describing soils in a watershed using traditional correlation techniques.

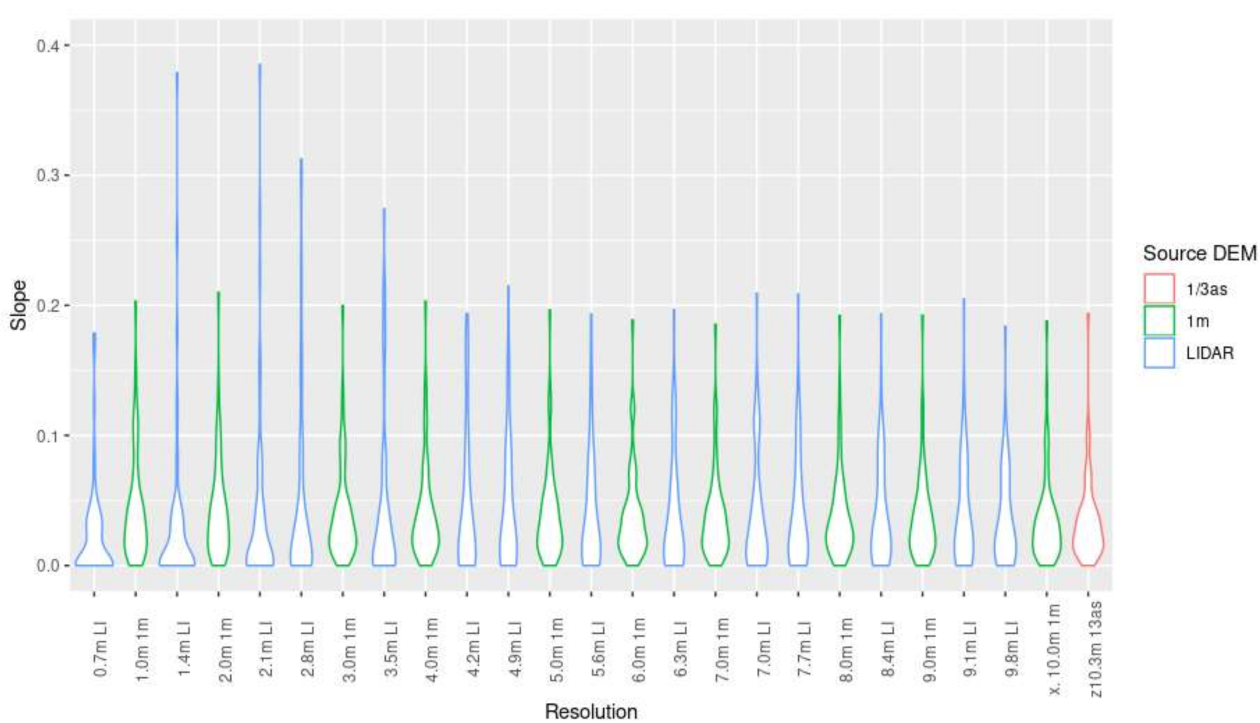

Figure 3-5 Distribution of extracted slopes found in the aggregation of LiDAR and 1m DEMs

3.3.3 Specific catchment area

The methods applied to section 3.3.2 to slope are now applied to SCA.

3.3.3.1 Flow direction algorithm

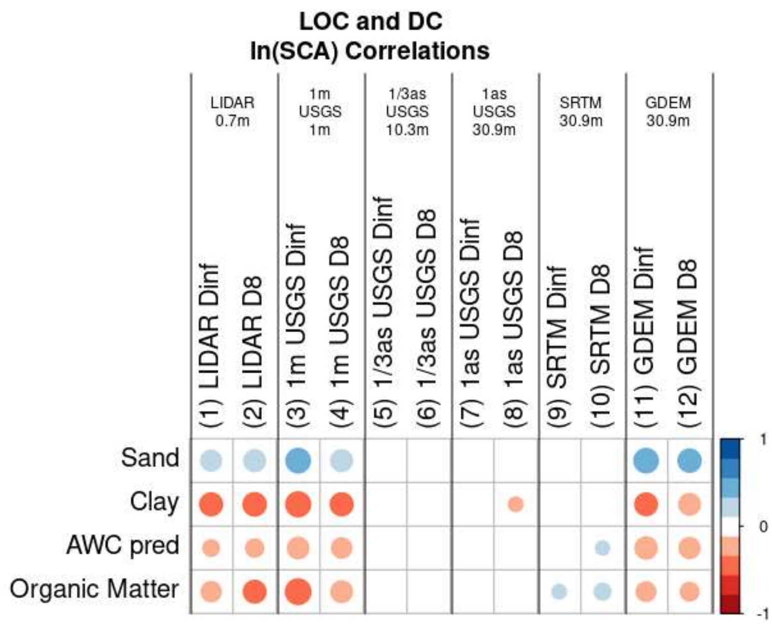

Figure 3-6 Correlations between measured soil properties and SCA derived from multiple DEMs and flow directions

When considering the directionality of the correlations for SCA, the displayed results in figure 3-6 are opposite of the patterns expected. For example, when considering the distribution of clay, one would expect for SCA to relate positively with this value, i.e. the larger the area that drains to a location the more likely that location is going to have clay deposited. However, consider a scenario where the locations of interest lie on top of tile drainage. A location with a large SCA is likely to be targeted for tile drainage installation. Such a location would actively drain any excess water. This could result in leaching of clay, and result in low organic matter content due to its relative dryness. We believe this may be occurring in our watershed resulting in a flipping of expected correlation signs. A brief exploration of aerial photos indicates that tile drainage is likely present in some fields in the region, though it is unknown the extent of their installation.

When comparing flow direction algorithms (figure 3-6 comparing odd columns to even columns), generally, the coarser resolution datasets are similarly correlated while the finer resolutions have more variability. For example, consider columns 11 and 12: the correlations observed in column 11 are nearly identical to the correlations observed in column 12. However, when fine resolutions are considered (columns 3 and 4) there is a considerable difference in the strength of correlations when comparing the two flow direction algorithms to measured organic matter. Dinf (column 3) performs better for 1m USGS than its D8 counterpart (column 4). The opposite relationship is observed for LiDAR (columns 1 and 2).

3.3.3.2 Digital elevation models

SCA 1m Dinf outperforms all other SCA combinations for the six measured soil properties (figure 3-6). All correlation magnitudes between measured soil properties and 1m Dinf ln(SCA) fell between 0.30 and 0.43. Though the general trend observed here is not as clear to interpret as that of figure 3-5 (slopes), there are still important insights that can be drawn from figure 3-7 (lnSCA Dinf) and 3-S2 (lnSCA D8). In figure 3-7, we see that the SCAs derived from resolutions less than 5 meters have a high potential to predict soil characteristics but prediction value is not robust to resolution change. SCAs derived from resolutions above 5 meters are not very useful and have low correlations. When comparing figure 3-S2 to figure 3-7, we see that D8 does not have as many high magnitude correlations below the 5-meter resolution implying that Dinf is a better choice than D8. Interestingly, we see that GDEM is predicting soil characteristics well when compared to the aggregated DEMs and other 30m DEMs. Unfortunately, these results do not paint as clear a picture as to what resolution to choose. It is likely that the fine DEM SCAs are best but they also result in highly variable correlations for soil properties. For the coarser DEMs, we see general agreement that there is little prediction power for soil characteristics except for the GDEM DEM.

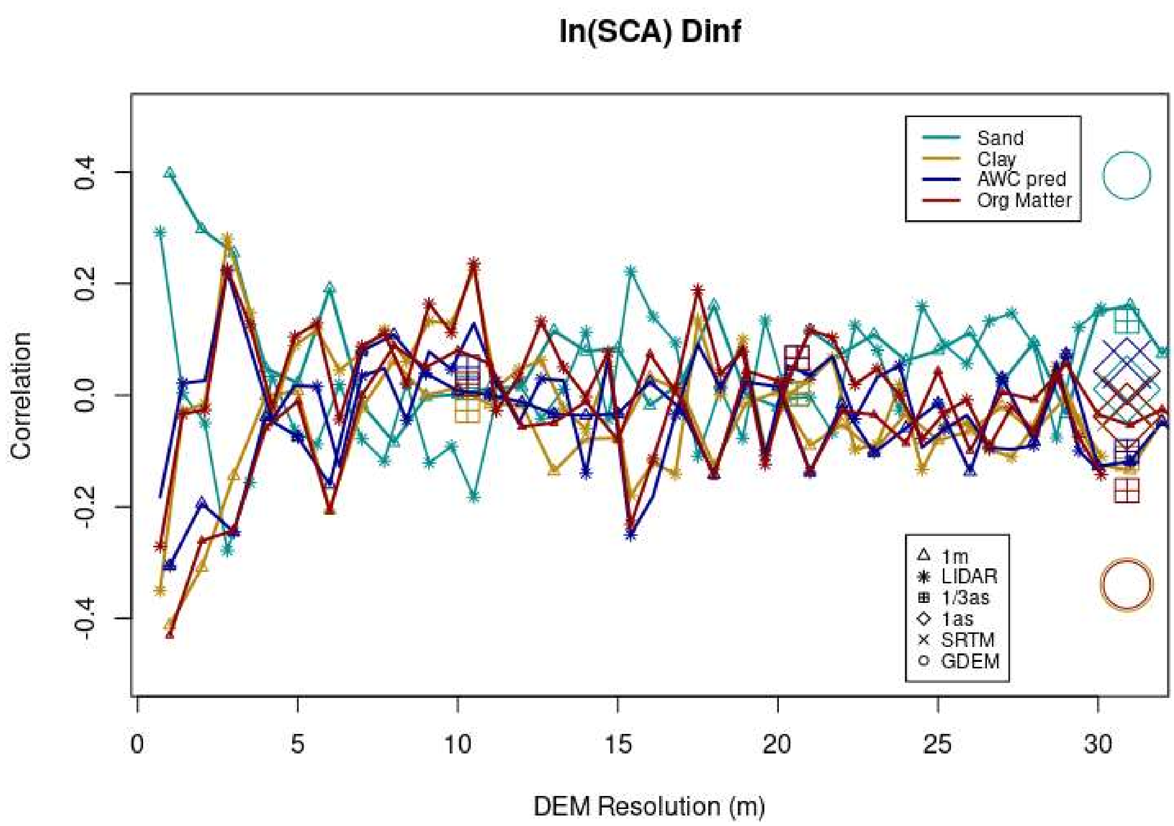

Figure 3-7 LiDAR, 1m, and ⅓ as DEMs are aggregated to generate ln(SCAs) Dinf derived from increasingly coarse resolution data. Correlations from derived data are plotted.

3.3.4 Considering multiple DEMs to distribute soils

3.3.4.1 Informing multiple DEM pairings

It is likely that slope and SCA have different information to offer in distributing soils and thus, a two-input regression analysis is implemented to use two inputs (slope and SCA) to predict the distribution of one output (measured soil property) using the methods described in section 3.2.5 and equation 3-1. Regression pairings (a single input from slope and ln(SCA)) are displayed in figure 3-8. The best correlating slopes and ln(SCA)s are selected by the automated process described in section 3.2.5 to yield a 2 input, and in all cases, a multidem regression. For all 4 measured soil properties, inputs derived from two different DEMs (a coarse resolution DEM for slope and the 1m Dinf ln(SCA)) result in the most advantageous combinations. For all displayed regression pairing, the slope regressor was the more significant of the two regressors. With these regressions, an alternative to topographic wetness is proposed that combines 2 DEM attributes to find a proxy for combining the knowledge that slope and SCA have to offer in distributing measured soil properties without constraining them and their relative importance or directionality with the TIV calculation.

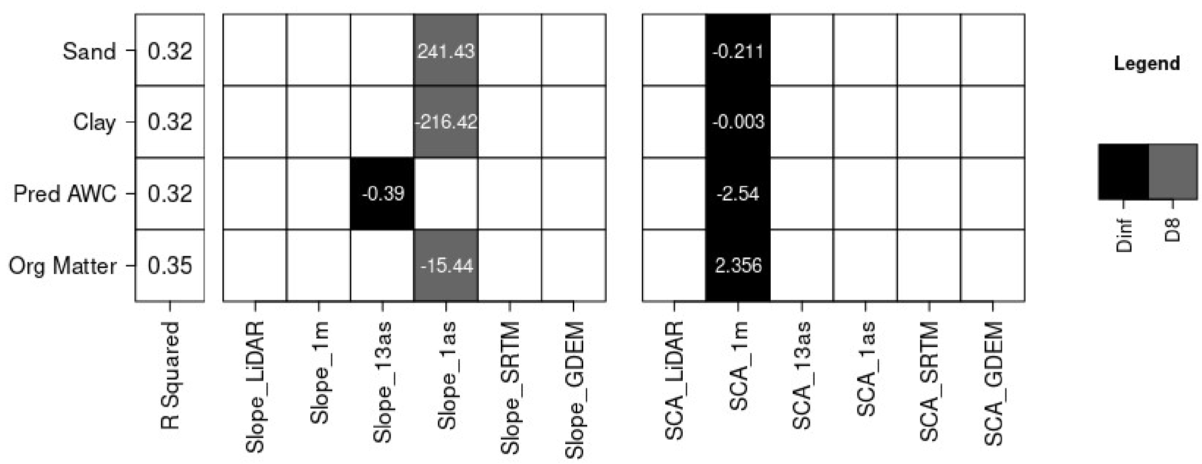

Figure 3-8 Multiple regression correlations and corresponding inputs. Resulting regressions had p-values < 0.05.

3.3.4.2 Contextualizing multidem findings with current soil distribution method

Often, researchers use the SSURGO database to distribute soils and it is important in our research to contextualize our method to the standard method. The spatial attributes selected for prediction of each soil property can be found in figure 3-9. Reported R^2 values are calculated constraining both scenarios to the identity line. SSURGO does quite poorly for all soil properties and yields a negative R^2 (figure 3-9). This means that using the average measured soil characteristic for each respective graph is a better predictor than SSURGO predicted soils. R^2 is calculated using the following equation: R^2 = 1-sum of squared error/sum of squared total. From this equation we can see that once R^2 go negative they can get quite large in magnitude quite quickly. As such, the interpretation of these results puts little emphasis of the magnitude of negative R^2s. In contrast, the DEM distributed clays predict with some success. It should be noted that SSURGO can be expected to predict measured soils better than an average case in figure 3-9 because there is an unusually high density of pedons (that inform SSURGO) surrounding the measurement locations (Nemecek, 2020).

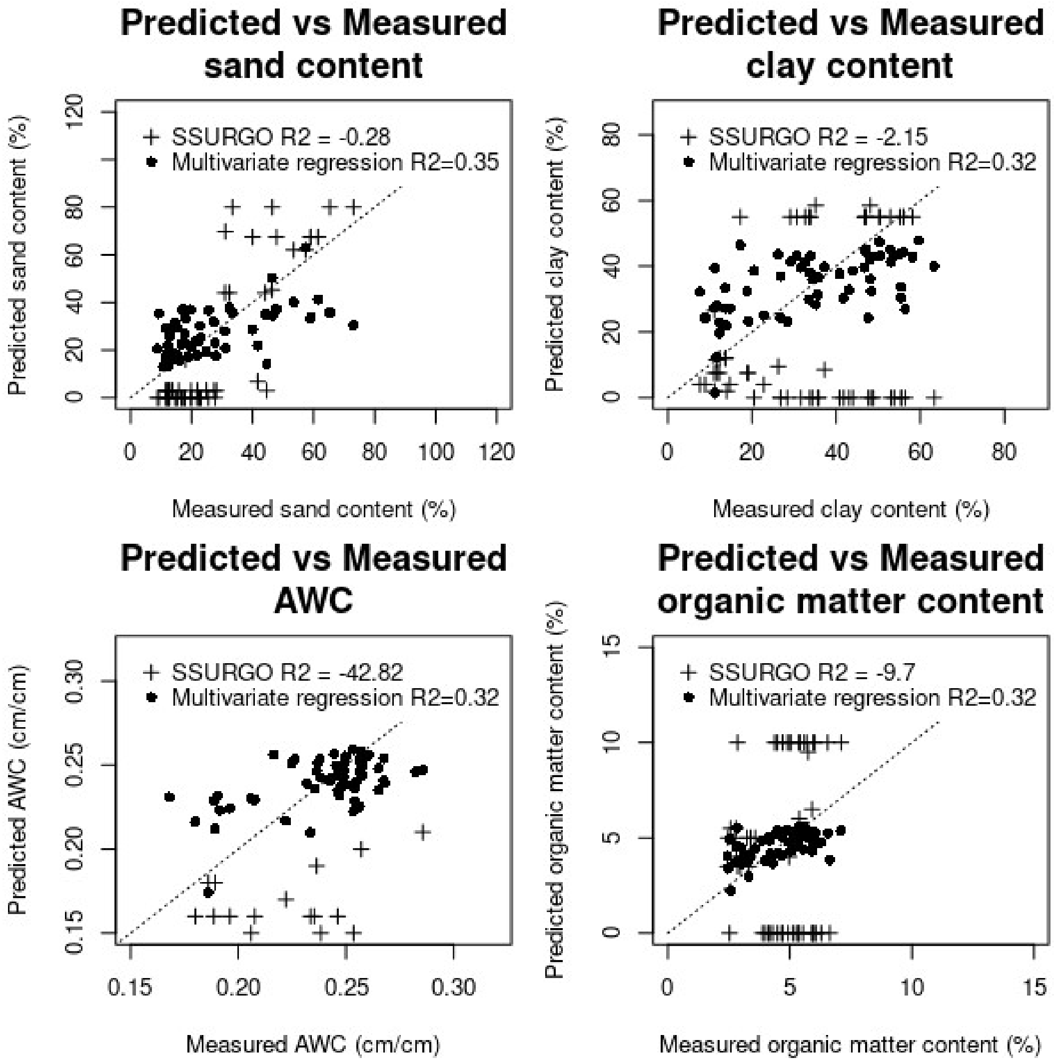

Figure 3-9 Measured soil properties compared to SSURGO and multiple regression derived soils content. R^2 displayed are calculated using the identity line (drawn) as the input model.

3.3.4.3 Distributing soil properties

Typically, scientists gravitate towards the newest, highest resolution data. In this section this default method is compared to informed DEM selection (figure 3-8). The 59 data points were split into two subsets: training and testing. Regression coefficients are generated using the training dataset and this regression fit is applied to the testing dataset and corresponding fit statistics are extracted. This is done recursively in a cross validation analysis as described in section 3.2.7. Please note that synthetically coarsened DEMs from section 3.3.3.1 is not considered for soil property distribution. Section 3.3.3.1 is executed for data exploration and is not appropriate for predicting soil distributions without careful consideration.

The multidem multivariate regression outperforms the default finest resolution regression (figure 3-10, column A). To distribute the soil properties for the multidem regression (B1-B4; D1-D4), the respective average coefficient and intercept resulting from each cross validation is used. Then, using the two rasters that informed this regression analysis (figure 3-8), a raster of distributed soil property content is created. When comparing the best regression to the SSURGO, continuous gradients of soil property change is observed more often in the multivariate regression case. Effectively, this means that when traversing from one location to another, it is likely that a gradual change in measured soil property is observed. This is more realistic than the abrupt soil property changes observed by SSURGO.

One aspect that SSURGO has a large advantage over our proposed method is observed when bedrock is present. Locations with bedrock areas often have dramatic slopes well above the range of calibration for input slopes and as a result soil property prediction for the proposed method is likely to do poorly on bedrock outcrops.

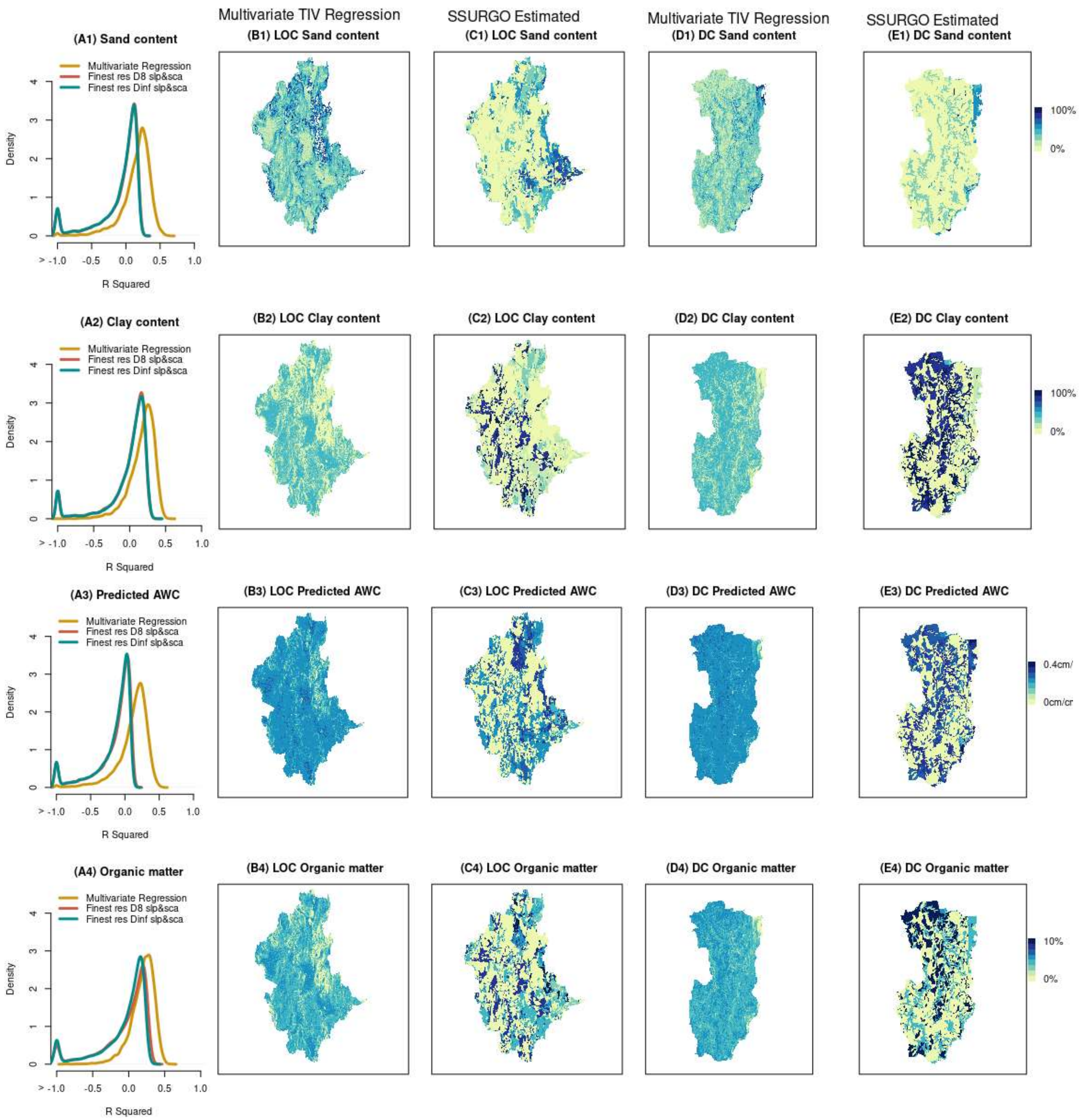

Figure 3-10 Probability density plots of the Monte Carlo test data for individual R2 for multivariate regressions in Figure 3-8 and finest resolution case for LOC sand content (A1), LOC clay content (A2), LOC predicted available water content (A3), and LOC organic matter content (A4); LOC sand content (B1), LOC clay content (B2), LOC predicted available water content (B3), and LOC organic matter content (B4) map from the multivariate regression; and LOC sand content (C1), LOC clay content (C2), LOC predicted available water content (C3), and LOC organic matter content (C4) maps from SSURGO. DC sand content (D1), DC clay content (D2), DC predicted available water content (D3), and DC organic matter content (D4) map from the multivariate regression; and DC sand content (E1), DC clay content (E2), DC predicted available water content (E3), and DC organic matter content (E4) maps from SSURGO.

3.4 Discussion

3.4.1 Topographic wetness

The findings presented in this research discuss the multiple shortcomings of using topographic wetness to distribute soils: (1) Topographic wetness classes can only appropriately be applied within watershed, and (2) Topographic wetness did not provide additional information to soil property distribution despite containing more information than its individual inputs. The second issue could be a function of multiple issues that were evident in this research.

SCA was found to be oppositely correlated than expected. We suspect this may be attributed to the presence of tile drainage. Areas with high SCAs are likely targets of tile drainage and thus can be expected to artificially present soil properties associated with dry soil. Leaching of nutrients through tile drainage has been widely documented in research (Randall & Iragavarapu, 1995; Dinnes, 2002; Moriasi et al., 2013). Because slope and SCA were correlated directionally the same, topographic wetness did not strengthen correlations between measured soil properties.

Similarly, the topographic wetness provides a rigid framework for how soil wetness is distributed. As a result, topographic wetness sets the relative importance of slope and SCA. Often, SCA is the main driver in the topographic wetness calculation due to its wide range of values. In this research, we found slope to be more strongly related to soil properties. It is likely that even if the SCA correlations were consistent directionally to our perceived knowledge, topographic wetness would still not do as well because SCA is emphasized more than slope despite slope being a stronger in predictor of soil properties, much like the results presented in chapter 2 of this dissertation. To overcome this, multiple regression for an SCA and slope collection are considered to best distribute soil properties.

3.4.2 Effect of flow routing algorithm

Flow direction algorithm did not make a large impact on our findings. As is consistent with the findings in chapter 2, flow direction algorithm choice did not considerably impact slope results. Flow direction algorithm choice did affect the SCAs correlations (as expected) for the finer resolutions, but not enough evidence was presented to definitively indicate whether Dinf or D8 was preferred. It is possible that the extra complexity added by the possible presence of tile drainage has made the results from the SCAs less informative.

3.4.3 Effect of resolution

Slopes derived from coarse resolution data outperformed their finer resolution counterparts. The optimal slope for correlating slopes between measured soil properties was typically 30m. Both LiDAR and the 1m resolutions did poorly. To further investigate this relationship, several DEMs were recursively coarsened, and correlations at each coarsening were observed. The optimal resolution derived from resolution differences (and not generation method) occurred at resolution greater than 10m. This plateau extends past 300m; of note is that slope rasters generated from 300m rasters are preferred to those generated from rasters less than 5m. This relationship is attributed to the assigned slopes for small rasters which are, in many cases, zero. Datasets that contain multiple zeros do not have the opportunity to correlate well due to the dataset distribution. This relationship became a non-issue for raster resolutions greater than 10m. Both Wolock & Price (1994) and Sørensen et al., (2006) find that resolution size can greatly affect the distributions of slopes and discuss this in more detail.

In this case, it is likely that all derivations of slope are appropriate representations of the landscape (aside from slopes derived from DEMs with large errors i.e., GDEM). Gillin et al., (2015) discusses how slopes derived from DEMs should consider the application of the slope information. For example, if slope is being used to evaluate farm equipment use, slopes derived from DEMs that have raster sizes similar to the size of the equipment may be most applicable, as that is the slope that the farm equipment is likely to experience. Applying similar logic, we must consider the resolution driving the slope processes that distribute soils. In this instance, a 30m slope (for 3 of 4 measured properties) was most advantageous.

The 1m Dinf SCA outperforms all other combinations for the six measured soil properties. There were no strong relationships that could explain this favorability. The possible presence of tile drainage and the biased soil sampling could massively affect this lack of finding. In future studies, information regarding drainage and a broader range of land uses for soils samples is recommended.

3.4.4 Advantages of pairing multiple DEMs

Slope and SCA both have different information to offer to those looking to understand the driving processes behind the geomorphologic distribution of soils. As is such, pairing these two landscape drivers together, much like topographic wetness, has the opportunity to further inform our understanding of soil property distribution. Currently, there is extensive research on ways to better distribute soils (Ibáñez et al., 2009; Chaney et al., 2019), but seldom are the processes that drive these distributions considered. This is especially problematic considering the relative densities of sampled DEMs and soils (i.e., the sampling density of DEMs is far denser than the sampling density of soils). Distributed soil maps have vast applications (Di Luzio et al., 2004; Anderson et al., 2006) and bettering them can benefit a wide range of research. The research presented here found that multiple DEMs were most advantageous in all 4 properties examined. In all cases, slopes derived from coarse resolutions were most informative, while SCAs derived from 1m Dinf were best. When comparing the ideal pairings to SSURGO and LiDAR, the ideal pairings were more robust to testing and better predictors of measured soil properties. By using multiple DEMs to distribute soil properties, we are allowing the representation of multiple geomorphic process scales to inform the distribution of soil properties.

3.4.5 Contextualizing process with standard procedure: SSURGO

SSURGO was found to distribute soil properties poorly which is consistent with Moore et al., (1993), Collick et al., (2015), Fuka et al., (2016), and Cole (2017). The map of SSURGO distributed soil properties was realistic, though abrupt changes of measured soil property were observed. This was likely the main issue driving SSURGO's poor prediction of measured soil characteristics. SSURGO will likely outperform our proposed method when exposed bedrock is present. There is certainly an opportunity to capitalize on the strengths of SSURGO, such as identifying surface level geologic formations.

3.4.6 Future work: consider geomorphology and climate

If we were going to apply the findings presented here, it is likely that our findings would not translate well to another physiographic region. Different physiographic regions would have different climates, topography, feature size, and vegetation. These factors would directly affect the mechanisms of landscape change such as erosion and deposition. In flatter locations, slope will likely not be a large driver of geomorphology. In dry locations, flow paths will likely be considerably more important. In mountainous, temperate locations, considering aspect for distribution could be fairly advantageous because of differences in wetness on sun-facing slopes as displayed by Gibson et al., (2021). There is certainly an opportunity to supplement and improve SSURGO distributed soils as displayed by Moore et al., (1993), Collick et al., (2015), Fuka et al., (2016), and Cole (2017). However, developers must consider a balance between complete modeling of geomorphic processes and overly constrained models. It is likely that we would not have to consider some inputs such as soil parent material because we could overcome these variables by using existing pedons. Even without having to understand the geologic time scale processes, modeling soil distributions using landscape attributes is daunting. Evaluating the best resolution for soils and hydrologic processes has been somewhat researched (Wolock & Price, 1994; Zhang & Montgomery, 1994; Hancock et al., 2006; Sørensen et al., 2006; Schumann et al., 2008; Vaze et al., 2010; Buchanan et al., 2014; Gibson et al., 2021). Between these papers and this research, there is considerable disagreement between what the best resolution is. In reality, the true answer is unlikely to be the same for all regions studied and is likely to not be consistent across different soil properties and hydrologic measurements. The proposed framework of considering multiple DEMs has a great deal of flexibility, and as a result could be applied widely to multiple physiographic regions. However, this widespread application should not be done haphazardly but done with consideration to the true geomorphic processes that created the properties we are looking to understand.

3.5 Conclusions

We identify coarse resolution slopes for this landscape as the best distributors of measured soil properties. Using this information, combined with the information from calculated SCAs, we are able to better predict soil properties than conventional SSURGO distributed soils. Our principle findings include:

1. The rigidity of the traditional topographic wetness calculation, combined with conventional methods of using SCAs and slopes from a single DEM resulted in topographic wetness being non-advantageous for this application.
2. Choosing the finest resolution DEM for all applications is ill-advised.
3. Considering multiple DEMs allows for flexibility when applying these findings across multiple physiographic regions.

References

Abrams, M., Crippen, R., METI, NASA, Jet Propulsion Laboratory/California Institute of Technology, 2019. ASTER GDEM V3 (ASTER Global DEM).

Anderson, R.M., Koren, V.I., Reed, S.M., 2006. Using SSURGO data to improve Sacramento Model a priori parameter estimates. J Hydrol 320, 103–116.

Arundel, S.T., Archuleta, C.-A.M., Phillips, L.A., Roche, B.L., Constance, E.W., 2015. 1-Meter Digital Elevation Model Specifications, 11. USGS.

Azizian, A., Brocca, L., 2020. Determining the best remotely sensed DEM for flood inundation mapping in data sparse regions. Int. J. Remote Sens. 41, 1884–1906. https://doi.org/10.1080/01431161.2019.1677968

Buchanan, B.P., Fleming, M., Schneider, R.L., Richards, B.K., Archibald, J., Qiu, Z., Walter, M.T., 2014. Evaluating topographic wetness indices across central New York agricultural landscapes. Hydrol Earth Syst Sci 18, 3279–3299.

Celis, J.A., Moreno, H.A., Basara, J.B., McPherson, R.A., Cosh, M., Ochsner, T., Xiao, X., 2021. From Standard Weather Stations to Virtual Micro-Meteorological Towers in Ungauged Sites: Modeling Tool for Surface Energy Fluxes, Evapotranspiration, Soil Temperature, and Soil Moisture Estimations. Remote Sens. 13, 1271. https://doi.org/10.3390/rs13071271

Chaney, N.W., Minasny, B., Herman, J.D., Nauman, T.W., Brungard, C.W., Morgan, C.L.S., McBratney, A.B., Wood, E.F., Yimam, Y., 2019. POLARIS soil properties: 30-m probabilistic maps of soil properties over the contiguous United States. Water Resour Res 55, 2916–2938.

Cole, S.A., 2017. Comparing SSURGO data versus geospatial field measurements to estimate soil texture and infiltration rate classes in glaciated soils (PhD Thesis). Clemson University.

Collick, A.S., Fuka, D.R., Kleinman, P.J.A., Buda, A.R., Weld, J.L., White, M.J., Veith, T.L., Bryant, R.B., Bolster, C.H., Easton, Z.M., 2015. Predicting phosphorus dynamics in complex terrains using a variable source area hydrology model. Hydrol. Process. 29, 588–601. https://doi.org/10.1002/hyp.10178

Di Luzio, M., Arnold, J.G., Srinivasan, R., 2004. Integration of SSURGO maps and soil parameters within a geographic information system and nonpoint source pollution model system. J Soil Water Conserv.

Dinnes, C.A., Karlen, D.L., Jaynes, D.B., Kaspar, T.C., Hatfield, J.L., Colvin, T.S., Cambardella, C.A., 2002. Review and Interpretation: Nitrogen Management Strategies to Reduce Nitrate Leaching in Tile-Drained Midwestern Soils. Agron. J.

Easton ZM, Fuka DR, Walter MT, Cowan DM. 2008. Re-conceptualizing the soil and water assessment tool (SWAT) model to predict runoff from variable source areas. *Journal of* Available at: https://www.sciencedirect.com/science/article/pii/S0022169407005756

Farr, T.G., Kobrick, M., 2000. Shuttle Radar Topography Mission produces a wealth of data. Eos Trans. Am. Geophys. Union 81, 583–585.

Farr, T.G., Rosen, P.A., Caro, E., Crippen, R., Duren, R., Hensley, S., Kobrick, M., Paller, M., Rodriguez, E., Roth, L., 2007. The shuttle radar topography mission. Rev. Geophys. 45.

Fuka, D.R., Collick, A.S., Kleinman, P.J.A., Auerbach, D.A., Harmel, R.D., Easton, Z.M., 2016. Improving the spatial representation of soil properties and hydrology using topographically derived initialization processes in the SWAT model.

Gibson, A.J., Hancock, G.R., Bretreger, D., Cox, T., Hughes, J., Kunkel, V., 2021. Assessing digital elevation model resolution for soil organic carbon prediction. Geoderma 398, 115106.

Gillin, C.P., Bailey, S.W., McGuire, K.J., Prisleyt, S.P., 2015. Evaluation of Lidar-derived DEMs through Terrain Analysis and Field Comparison. Photogramm. Eng. Remote Sens. 81, 387–396.

Goyal, R., Featherstone, W.E., Dikshit, O., Balasubramania, N., 2021. Comparison and Validation of Satellite-Derived Digital Surface/Elevation Models over India. J. Indian Soc. Remote Sens. 49, 971–986. https://doi.org/10.1007/s12524-020-01273-7

Guth, P.L., Van Niekerk, A., Grohmann, C.H., Muller, J.-P., Hawker, L., Florinsky, I.V., Gesch, D., Reuter, H.I., Herrera-Cruz, V., Riazanoff, S., López-Vázquez, C., Carabajal, C.C., Albinet, C., Strobl, P., 2021. Digital Elevation Models: Terminology and Definitions. Remote Sens. 13. https://doi.org/10.3390/rs13183581

Han, L., Wang, C., Liu, Q., Wang, G., Yu, T., Gu, X., Zhang, Y., 2020. Soil Moisture Mapping Based on Multi-Source Fusion of Optical, Near-Infrared, Thermal Infrared, and Digital Elevation Model Data via the Bayesian Maximum Entropy Framework. Remote Sens. 12. https://doi.org/10.3390/rs12233916

Hancock, G.R., Martinez, C., Evans, K.G., Moliere, D.R., 2006. A comparison of SRTM and high-resolution digital elevation models and their use in catchment geomorphology and hydrology: Australian examples. Earth Surf Process. Landf. 31, 1394–1412.

Haneberg, W.C., 2006. Effects of Digital Elevation Model Errors on Spatially Distributed Seismic Slope Stability Calculations: An Example from Seattle, Washington. Environ. Eng. Geosci. 12, 247–260. https://doi.org/10.2113/gseegeosci.12.3.247

Holmes, K.W., Chadwick, O.A., Kyriakidis, P.C., 2000. Error in a USGS 30-meter digital elevation model and its impact on terrain modeling. J Hydrol 233, 154–173.

Homer, C., Huang, C., Yang, L., Wylie, B., Coan, M., 2004. Development of a 2001 National Land-Cover Database for the United States. Photogramm. Eng. Remote Sens. 70, 829–840. https://doi.org/10.14358/PERS.70.7.829

Hutsul, T., Smirnov, Y., 2017. Comparative accuracy assessment of global DTM and DTM generated from Soviet topographic maps for the purposes of road planning. Geod. Cartogr. 43, 173–181. https://doi.org/10.3846/20296991.2017.1412638

Ibáñez, J.J., Pérez-Gómez, R., San José Martínez, F., 2009. The spatial distribution of soils across Europe: A fractal approach. Ecol Complex 6, 294–301.

Jancewicz, K., Migoń, P., Kasprzak, M., 2019. Connectivity patterns in contrasting types of tableland sandstone relief revealed by Topographic Wetness Index, Science of The Total Environment 656, 1046-1062. https://doi.org/10.1016/j.scitotenv.2018.11.467.

Karney, C.F.F., 2013. Algorithms for geodesics. J Geod. 87, 43–55.

Kopecký, M., Macek, M., Wild, J., 2021. Topographic Wetness Index calculation guidelines based on measured soil moisture and plant species composition. Sci. Total Environ. 757, 143785. https://doi.org/10.1016/j.scitotenv.2020.143785

Lyon SW, Walter TM, Gérard-Marchant P, Steenhuis TS. 2004. Using a Topographic Index to Distribute Variable Source Area Runoff Predicted With the SCS-Curve Number Equation. *Hydrological processes* **18** (15): 2757–2771 DOI: 10.1002/hyp.1494

Miller, C.L., 1958. The theory and application of the digital terrain model (PhD Thesis). Massachusetts Institute of Technology.

Moebius-Clune, B.N., Moebius-Clune, D.J., Gugino, B.K., Idowu, O.J., Schindelbeck, R.R., Ristow, A.J., van Es, H.M., Thies, J.E., Shayler, H.A., McBride, M.B., Kurtz, K.S.M., Wolfe, D.W., Abawi, G.S., 2016. Comprehensive Assessment of Soil Health – The Cornell Framework, 3.2. ed. Cornell University, Ithaca, NY.

Moore, I.D., 1991. DIGITAL TERRAIN MODELING: A REVIEW OF HYDROLOGICAL, GEOMORPHOLOGICAL, AND BIOLOGICAL APPLICATIONS. Hydrol. Process. VOL 5, 3–30.

Moore, I.D., Gessler, P.E., Nielsen, G.A., Peterson, G.A., 1993. Soil Attribute Prediction Using Terrain Analysis. Soil Sci. Soc. Am. J. 57, 443–452. https://doi.org/10.2136/sssaj1993.03615995005700020026x

Moriasi, D.N., Gowda, P.H., Arnold, J.G., Mulla, D.J., Ale, S., Steiner, J.L., 2013. Modeling the impact of nitrogen fertilizer application and tile drain configuration on nitrate leaching using SWAT. Agric Water Manage 130, 36–43.

Muthusamy, M., Casado, M.R., Butler, D., Leinster, P., 2021. Understanding the effects of Digital Elevation Model resolution in urban fluvial flood modelling. J. Hydrol. 596, 126088. https://doi.org/10.1016/j.jhydrol.2021.126088

Nabiollahi, K., Golmohamadi, F., Taghizadeh-Mehrjardi, R., Kerry, R., Davari, M., 2018. Assessing the effects of slope gradient and land use change on soil quality degradation through digital mapping of soil quality indices and soil loss rate. Geoderma 318, 16–28. https://doi.org/10.1016/j.geoderma.2017.12.024

NASA, METI, AIST, Japan Spacesystems, U.S./Japan ASTER Science Team, 2019. ASTER Global Digital Elevation Model V003. https://doi.org/10.5067/ASTER/ASTGTM.003

Nemecek, J., 2020. National Cooperative Soil Survey (NCSS) Soil Characterization database: The National Cooperative Soil Survey (NCSS) Soil Characterization Database contains the analytical results from the Kellogg Soil Survey Laboratory (KSSL) at the NCSS.

Odeh, I.O.A., Chittleborough, D.J., McBratney, A.B., 1991. Elucidation of soil-landform interrelationships by canonical ordination analysis. Geoderma 49, 1–32. https://doi.org/10.1016/0016-7061(91)90089-C

Odeha, I.O.A., McBratney, A.B., Chittleborough, D.J., 1994. Spatial prediction of soil properties from landform attributes derived from a digital elevation model. Geoderma 63, 197–214. https://doi.org/10.1016/0016-7061(94)90063-9

Paz-Kagan, T., Ohana-Levi, N., Herrmann, I., Zaady, E., Henkin, Z., Karnieli, A., 2016. Grazing intensity effects on soil quality: A spatial analysis of a Mediterranean grassland. CATENA, Dan H. Yaalon Memorial Issue 146, 100–110. https://doi.org/10.1016/j.catena.2016.04.020

Portet, S., 2020. A primer on model selection using the Akaike Information Criterion, Infectious Disease Modelling. 5, 111-128. https://doi.org/10.1016/j.idm.2019.12.010.

Quantum Spatial, 2018. Western Vermont 2017 QL2 LiDAR Project Report. Quantum Spatial, Inc.

Quantum Spatial, 2016. Rutland, VT 2015 QL2 LiDAR Project Report. Quantum Spatial, Inc.

Raduła, M.W., Szymura, T.H., Szymura, M., 2018. Topographic wetness index explains soil moisture better than bioindication with Ellenberg's indicator values. Ecol. Indic. 85, 172–179. https://doi.org/10.1016/j.ecolind.2017.10.011

Randall, G.W., Iragavarapu, T.K., 1995. Impact of long-term tillage systems for continuous corn on nitrate leaching to tile drainage. J Env. Qual 24, 360–366.

Reuter, H.I., Neison, A., Strobl, P., Mehl, W., Jarvis, A., 2009. A first assessment of ASTER GDEM tiles for absolute accuracy, relative accuracy and terrain parameters, in: 2009 IEEE International Geoscience and Remote Sensing Symposium. IEEE, p. V–240.

Schumann, G., Matgen, P., Cutler, M.E.J., Black, A., Hoffmann, L., Pfister, L., 2008. Comparison of remotely sensed water stages from LiDAR, topographic contours and SRTM. ISPRS J Photogramm Remote Sens 63, 283–296.

Sørensen, R., Seibert, J., 2007. Effects of DEM resolution on the calculation of topographical indices: TWI and its components. J. Hydrol. 347, 79–89. https://doi.org/10.1016/j.jhydrol.2007.09.001

Sørensen, R., Zinko, U., Seibert, J., 2006. On the calculation of the topographic wetness index: evaluation of different methods based on field observations. Hydrol Earth Syst Sci 10, 101–112.

Steger, C., Nigussie, G., Alonzo, M., Warkineh, B., Van Den Hoek, J., Fekadu, M., Evangelista, P., Klein, J., 2020. Knowledge coproduction improves understanding of environmental change in the Ethiopian highlands. Ecol. Soc. 25. https://doi.org/10.5751/ES-11325-250202

Stoker, J., Harding, D., Parrish, J., 2008. The need for a national LIDAR data set. Photogramm. Eng. Remote Sens. 74, 1066–1068.

Tachikawa, T., Kaku, M., Iwasaki, A., Gesch, D.B., Oimoen, M.J., Zhang, Z., Danielson, J.J., Krieger, T., Curtis, B., Haase, J., Abrams, M., Carabajal, C., 2011. ASTER Global Digital Elevation Model Version 2 - summary of validation results (Federal Government Series), ASTER Global Digital Elevation Model Version 2 - summary of validation results. NASA.

Tarboton, D.G., 1997. A new method for the determination of flow directions and upslope areas in grid digital elevation models. Water Resour Res 33, 309–319.

Tarboton DG. 2014. TauDEM. Github. Available at: https://github.com/dtarb/TauDEM [Accessed 25 January 2021]

Telak, L.J., Dugan, I., Bogunovic, I., 2021. Soil Management and Slope Impacts on Soil Properties, Hydrological Response, and Erosion in Hazelnut Orchard. Soil Syst. 5, 5. https://doi.org/10.3390/soilsystems5010005

Thomas, I.A., Jordan, P., Mellander, P.-E., Fenton, O., Shine, O., hUallacháin, D. Ó., Creamer, R., McDonald, N.T., Dunlop, P., Murphy, P.N.C., 2016. Improving the identification of hydrologically sensitive areas using LiDAR DEMs for the delineation and mitigation of critical source areas of diffuse pollution, Science of The Total Environment, 556, 276-290. https://doi.org/10.1016/j.scitotenv.2016.02.183.

USDA NRCS, 2019. USDA Announces Water Quality Study in Vermont's Lake Champlain Basin | NRCS [WWW Document]. URL https://www.nrcs.usda.gov/wps/portal/nrcs/detail/national/newsroom/releases/?cid=NRCSEPRD1495437 (accessed 4.8.22).

USGS, 1993. "Digital Elevation Models: Data Users Guide." 507 National Center Reston, Virginia 22092 : U.S. Geological Survey. https://pubs.usgs.gov/dug/0005/dug0005.pdf.

USGS, 1994. USGS Water Data for the Nation [WWW Document]. URL http://dx.doi.org/10.5066/F7P55KJN (accessed 12.1.21).

USGS, 2019, 3D Elevation Program Digital Elevation Model. URL https://www.usgs.gov/the-national-map-data-delivery

Vaze, J., Teng, J., Spencer, G., 2010. Impact of DEM accuracy and resolution on topographic indices. Environ. Model. Softw. 25, 1086–1098.

VCGI, NRCS, USGS, VT ANR, VTRANS, UVM-SAL, 2018. ElevationDEM_DEMHF0p7M2017. Quality Levels 2 & 3 Lidar Digital Elevation Model (DEM) data from the 3D Elevation Program (3DEP).

VCGI, NRCS, USGS, VT ANR, VTRANS, UVM-SAL, 2016. ElevationDEM_DEMHF0p7M2013. Quality Levels 2 & 3 Lidar Digital Elevation Model (DEM) data from the 3D Elevation Program (3DEP).

Wilson, J. P., and J. C. Gallant. 2000. "Digital Terrain Analysis." *Terrain Analysis: Principles and*. https://www.researchgate.net/profile/John-Wilson-14/publication/303543739_Digital_terrain_analysis/links/57d0467108ae0c0081dea6a6/Digital-terrain-analysis.pdf.

Wolock, D.M., Price, C.V., 1994. Effects of digital elevation model map scale and data resolution on a topography-based watershed model. Water Resour Res 30, 3041–3052.

Wei, W., Yan, F., Zhengyin, W., Hongbin, L,. 2008. Assessing effects of digital elevation model resolutions on soil–landscape correlations in a hilly area, Agriculture, Ecosystems & Environment. https://doi.org/10.1016/j.agee.2008.01.026.

Zhang, K., Gann, D., Ross, M., Robertson, Q., Sarmiento, J., Santana, S., Rhome, J., Fritz, C., 2019. Accuracy assessment of ASTER, SRTM, ALOS, and TDX DEMs for Hispaniola and implications for mapping vulnerability to coastal flooding. Remote Sens. Environ. 225, 290–306. https://doi.org/10.1016/j.rse.2019.02.028

Zhang, S., Ma, Y., Chen, Fu, Liu, J., Chen, Fulong, Lu, S., Jiang, L., Li, D., 2020. A new method for supporting interpretation of paleochannels in a large scale — Detrended Digital Elevation Model Interpretation. Geomorphology 369, 107374. https://doi.org/10.1016/j.geomorph.2020.107374

Zhang, W., Montgomery, D.R., 1994. Digital elevation model grid size, landscape representation, and hydrologic simulations. Water Resour. Res. 30, 1019–1028. https://doi.org/10.1029/93WR03553

Supplemental Materials

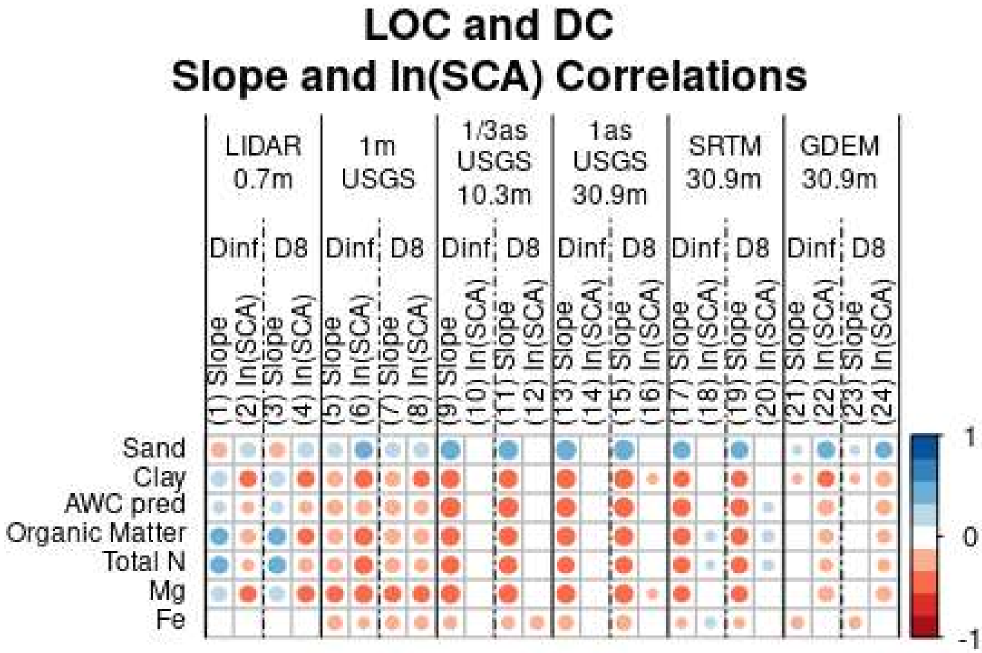

Figure 3-S1 Correlations between extracted slopes and SCAs and measured soil properties

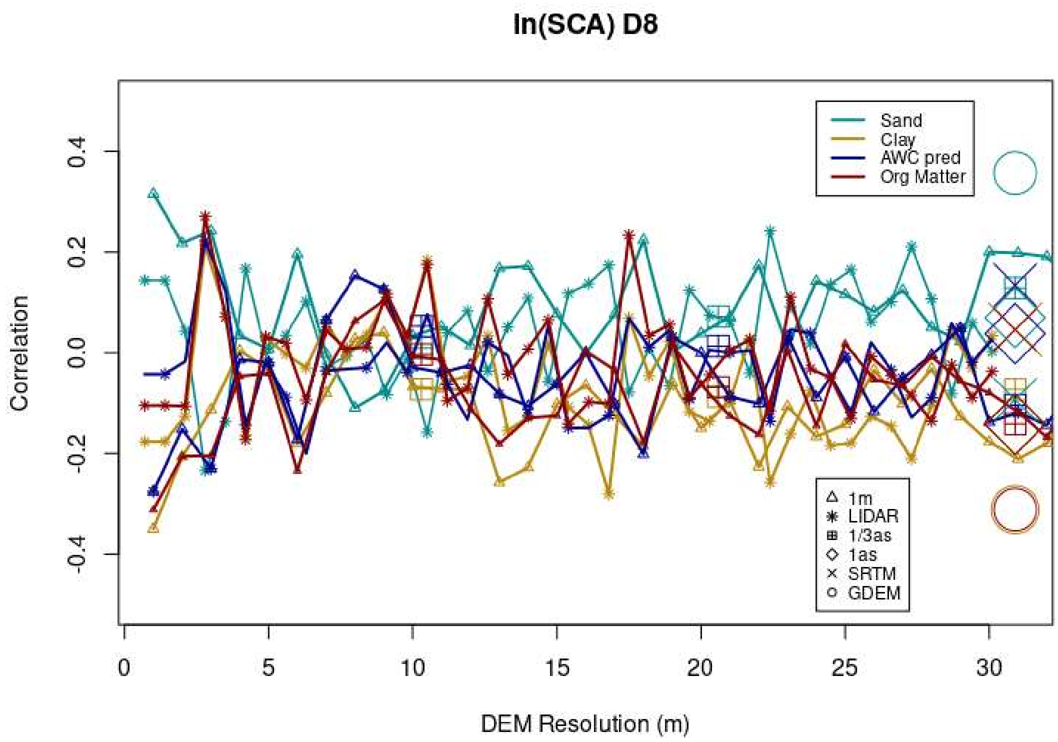

Figure 3-S2 LiDAR, 1m, and 1/3as DEMs are aggregated to generate ln(SCAs) D8 derived from increasingly coarse resolution data. Correlations from derived data are plotted.

Chapter 4: Characterization of Nitrate Removal in a Spring Fed Bioreactor

Elyce Buell[a], Kurt Stephenson[b], Daniel R. Fuka[a], Sabrina Mehzabin[a], Zachary M. Easton[a]

[a] Department of Biological Systems Engineering, Virginia Tech, Blacksburg, VA, USA
[a] Department of Agricultural and Applied Economics, Virginia Tech, Blacksburg, VA, USA

Keywords: bioreactors, legacy nitrogen, best management practices

Abstract

Groundwater contaminated with nitrogen (commonly referred to as legacy nitrogen) is a widespread issue and is cited as being a major issue plaguing water quality managers. Investigators employ a novel method: installation of a bioreactor fed by a nutrient rich spring located in Northern Virginia. The spring and bioreactor effluent are monitored for 10 months and bioreactor efficiency is quantified using a suite of inputs including hydraulic residence time, bioreactor bed temperature, and bioreactor age. A model driven by the governing equation for first order kinetics is used to predict load removal ($g/m^3/d$). The spring fed bioreactor removed 21% or 1.5 $g/m^3/d$ of nitrogen on average. The spring fed system, when compared to an edge of field system, provided a stable environment for microbial activity, however, the spring fed system was also considerably colder and thus less efficient.

4.1 Introduction

Legacy nutrients, resulting from excess anthropogenic inputs and subsequent storage in soil, sediment, or groundwater, introduce a critical time lag between changes in nutrient inputs and observable reductions in loads delivered to downstream waters and often prevent the attainment of water quality improvement goals (Sharpley et al., 2013). The accumulated stores of legacy nutrients have been identified as an important factor that accounts for the lack of observable water quality improvement in many regions (Sharpley et al., 2013; Kleinman et al., 2019; Stackpoole et al., 2019; Noe et al., 2020).

In the Chesapeake Bay watershed recent studies have shown elevated concentrations of nitrogen (N) stored in groundwater (Greene et al., 2005), and Van Meter & Basu (2017) found that legacy N is a large component of contemporary N load, contributing nearly 50% of the N load in the Susquehanna River Basin. Furthermore, a National Research Council report cautioned that achievement of Bay water quality objectives could be significantly delayed by legacy nutrients (NRCS, 2011). Nitrogen leached to groundwater may take decades to centuries to be discharged to surface waters. In the Chesapeake Bay region, lag times for legacy nitrogen are reported to be between less than a year to more than 50 years (Lindsey, 2003; Phillips & Lindsey, 2003; Sanford & Pope, 2007; Meals et al., 2010). Thus, legacy N continues to contribute to surface water impairment even if contemporary N loads are reduced or eliminated. However, little research has been devoted to developing practices to treat legacy nutrients and few existing agricultural or urban best management practices (BMPs) can remediate these nutrient reservoirs (Chen et al., 2018).

Emergent groundwater, often expressed as springs or seeps, offers a unique and unrealized opportunity to treat legacy N because they are points of concentrated groundwater discharge that can transport significant N loads. Indeed, Easton et al., (2019), analyzing data on spring flows and N concentrations in the Mid-Atlantic, suggest that the quantity of legacy N released via identified springs is in excess of 3,690 kg/yr. Springs provide an opportunity to remediate legacy N, not only due to the magnitude of the nutrient loads they export (Easton et al., 2019), but also because their concentrated flow makes them amenable to treatment by existing BMPs. Denitrifying bioreactors hold promise to address concerns derived from legacy N, as they have demonstrated performance as a BMPs to treat agricultural drainage in a range of conditions. Bioreactors are lined, organic carbon substrate (typically woodchips) filled receptacles, designed to intercept nitrogen-rich water. Woodchips act as a carbon based electron donor that fuels microbial denitrification.Woodchip bioreactors typically remove 15-50% of the nitrogen at a rate of 0.5 to 22 $g/m^3/d$ of N (Schipper et al., 2010; Christianson et al., 2012; Bock et al., 2015; Easton et al., 2015; Bock et al., 2018). Similar performance was verified by Easton et al., (2019) in the first reported application of bioreactor to remove N from a pilot-scale (32 m^3) spring bioreactor in Southwest Virginia. The spring had an estimated median NO_3-N flux of 0.23 kg/d with an estimated 41% NO_3-N load reduction annually (range of removal: 5-88%), and often achieved reductions of greater than 65% during the warmer summer months.

Variability in N removal rates in bioreactors is largely attributable to influent N concentrations, temperature, and hydraulic residence time (HRT). The characteristics and influence of these factors, however, can differ between bioreactors that treat agricultural drainage and those that treat spring flow. Several studies have shown that bioreactors can effectively remove nitrogen in fluctuating systems (Schipper et al., 2010; Christianson et al., 2017; Hassanpour et al., 2017; Rosen & Christianson, 2017; Bock et al., 2018). However, the relative stability of spring flow and nitrogen loading compared to that of agricultural drainage systems suggests spring bioreactors may outperform their edge-of-field counterparts.

Indeed, Christianson et al., (2011) demonstrated that constant influent flow rates result in greater N removal in bioreactors than fluctuating flow rates. Targeting high N flux springs could provide opportunities for a single bioreactor to treat significantly greater N loads more cost-effectively. Temperature is a significant factor influencing N removal rates and water temperatures from groundwater discharge may be lower and show less variation than water with greater influence of ambient air temperature. For example, Christianson et al., (2012), Christianson (2013), and Hassanpour et al., (2017) indicate that N removal rates show relatively little influence from other factors (HRT for example) when water temperature is below 16 C.

Both influent N concentrations and temperature are (largely) properties of the system and are therefore difficult to control (Chun et al., 2010). Hydraulic residence time, however, is a function of the bioreactor size and the volume of water treated, both to some extent controllable, either by adjusting effective bioreactor volume and/or the amount of water treated (Chun et al., 2010; Moorman et al., 2015). Since many springs may have relatively constant flow, the volume of water diverted to spring bioreactors could be actively managed to improve N removal rates after construction. Studies by Hassanpour et al., (2017), Bock et al., (2018), and Coleman et al., (2019) report significant HRT effects on bioreactor removal rates, with N removal rates declining as HRT increases across the range of HRTs evaluated (3 to 65 hrs across the three studies). Although, all three studies (Hassanpour et al., 2017; Bock et al., 2018; Coleman et al., 2019) note that influent N concentration and temperature had significant interaction effects with HRT on N removal rates. Notably the effect of both influent concentration and temperature on N removal rates were found to decrease as HRT increased.

This study evaluates the N removal performance of a first of its kind large scale spring bioreactor in the Shenandoah Valley, Virginia (Smith Creek). The objectives of this work are to:

1. Quantify the effect of N loading and hydrologic regime (flow permanence and variability) on N removal rate from a spring bioreactor.
2. Characterize the effect of variable environmental conditions (temperature, influent N concentration) on bioreactor N removal rates.
3. Evaluate which observed HRTs results in the highest load removal.

4.2 Materials and methods

4.2.1 Site description and bioreactor design

A spring fed denitrifying bioreactor, located outside of Harrisonburg, Virginia (38.473893, -78.774883) was constructed during the summer of 2020 (figure 4-1). The bioreactor measures approximately 50x15x1 m and largely follows NRCS bioreactor construction guidelines, including a flow control structure to control flow, a liner to prevent exchange of groundwater and treated flow, and 0.3 m of topsoil overtopping the bioreactor (NRCS, 2015). Water from the spring is routed via 6” PVC pipe from the spring head to the inlet of the bioreactor (figure 4-1). To minimize preferential flow, the spring influent is distributed across the top of the bioreactor by a 15 cm PVC manifold that spans the width of the bed. A water-level control structure (AgriDrain Corp.) governs flow at the outlet of the bioreactor by positioning removable stoplogs. During installation, the bed was filled with locally sourced mixed hardwood wood chips with a porosity of 0.58.

USGS sampling of spring flow at the Smith Creek (n=23) from 2012 to 2019 ranged from 460 m3/d to 6750 m3/d with a median flow of 3,200 m3/d. The bioreactor size was based on achieving 4-12 HRT under the assumption of diverting 40-50% of spring flow. A 612 m3 bioreactor would achieve a 4 HRT the last quartile of sampled flow while a minimum 12 hr HRT would treat 75% of treated flow.

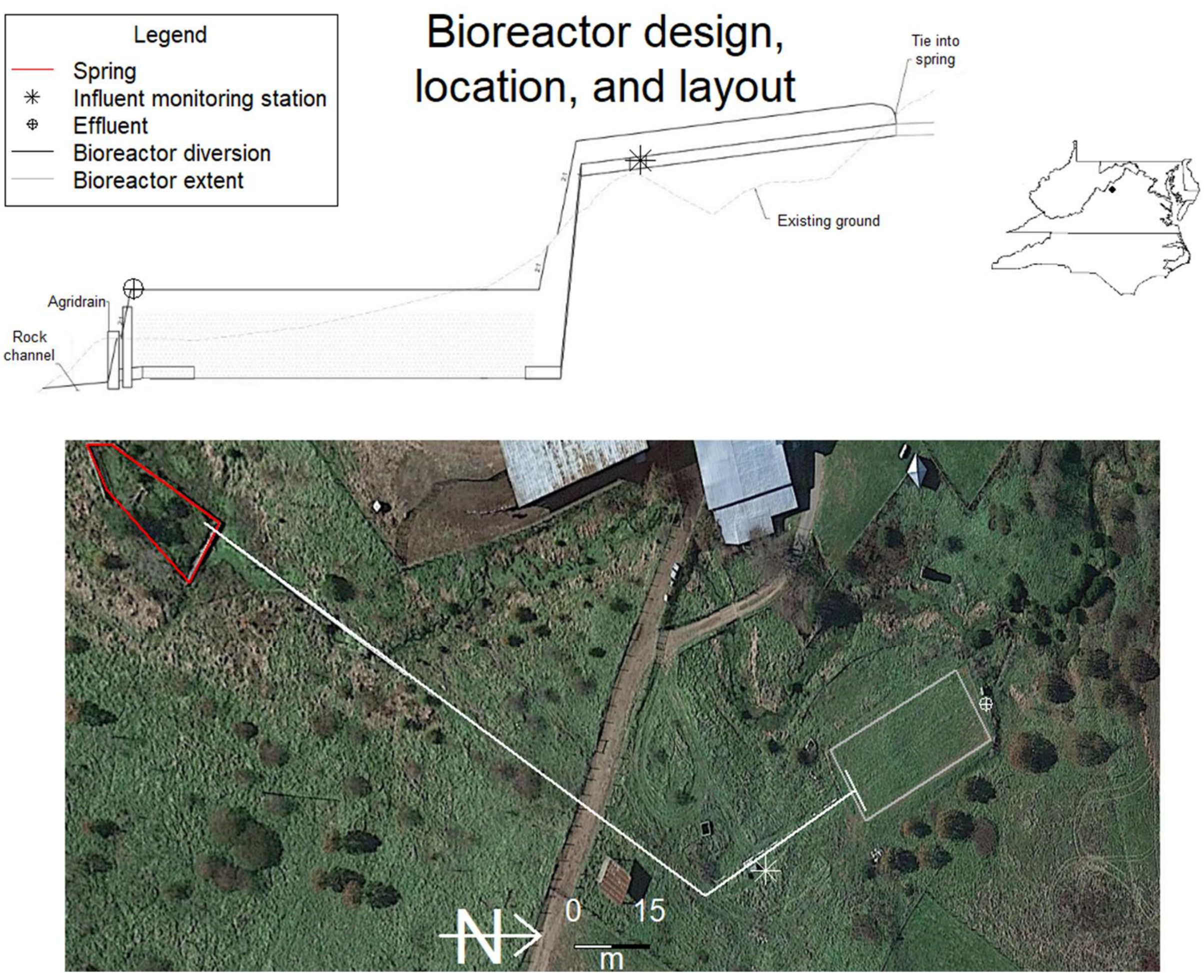

Figure 4-1 Bioreactor location and physical layout

4.2.2 Data Collection

All data is collected by the investigators using the methods described hereafter. Flow was measured using a pressure transducer (720 module, Teledyne ISCO) installed in the outlet control structure; and a power source consisting of three deep cycle marine batteries in parallel recharged by a 150-W solar panel. Flow was recorded on 15-min intervals. Since the bioreactor largely operates under steady state conditions we assumed inflow is equal to outflow.

Bioreactor bed data was recorded on 15-minute intervals using a TROLL 9500 multiparameter water quality monitoring instrument (In-Situ Inc.) equipped with temperature, dissolved oxygen (DO), oxidation-reduction potential (ORP), and pH measurement capacity. The probe was placed 8m from the outlet of the bioreactor at a depth of 0.6m below the surface of the bioreactor. The data was stored locally on the ISCO autosampler. Roughly 30% of the bed temperature data was missing due to outages in the TROLL probe. To fill in this bed data, air temperature from a weather station located 9 km northwest of the bioreactor was is used. This is downloaded using the rnoaa package in R (Chamberlain, 2021). We developed a rolling 3-day average smoothing spline to approximate bed temperature (R^2: 0.99, data not shown).

Aqueous samples were collected at the inlet and outlet using a 24-bottle autosampler (6712, Teledyne ISCO). Outlet samples are collected at intervals of 100 and 350 m^3/d, depending on season, and whether any changes to HRT were made. Inlet samples were collected at 200 m^3/d intervals (approximately equal to ¼ d intervals). At both the inlet and outlet four 200 mL samples were aggregated into a single 1 L autosampler bottle. Autosampler bottles were prepared with 5 mL of 10% sulfuric acid to achieve a sample pH < 2 and prevent degradation at ambient temperature following the method of Burke et al., (2002) and Dunderman et al., (2019). Samples were retrieved from the field bi monthly and new bottles with sulfuric acid are placed in the field every two weeks. Prior to analysis, samples were neutralized using 5-15 M sodium hydroxide (NaOH) and filtered with 0.45 micrometer nylon filters. Often, during the aforementioned process, samples are again frozen until nutrient analysis is conducted. Samples were analyzed using a flow injection analysis (FIA, QuikChem 8500, Lachat Instruments) with the cadmium reduction method for NOx (Lachat method 10- 107-04-1-A). Following analysis, all samples were stored at -10C to ensure QAQC standards were met. All numeric results reported pass the following QAQC standards: (1) all blanks (filtered in lab, filtered in field or unfiltered) result in a concentration that is below the detection limit, (2) matrix spikes are 100% +/- 15% recovery from the control sample and the known added amount of NOx-N and (3) all check samples are within +/- 0.5 mg/L of known concentration. All lab analysis described is conducted by the investigators.

4.2.3 Data processing and Calculations

While data collection began in 2020, the startup phase of bioreactor operation was not representative of long term, steady state conditions of interest for this research. Therefore, the data subjected to analysis began in July 2021. All calculations and subsequent statistical analyses were performed using the R language and environment for statistical computing (R Core Team, 2022).

4.2.3.1 Nutrient Loading and Removal

Nutrient loading and removal were assessed for a 10-month period beginning 10 months after bioreactor installation, beginning July 2021. Inlet and outlet measurements are paired using a 12 hr

moving window, resulting in 203 paired observations. If multiple outlet concentration measurements were available for a given inlet pairing, the average outlet concentrations were used for calculations.
To enable measurement of the bioreactor flow rate, the outlet drainage control structure was fitted with an AgriDrain 45° v-notch weir and rectangular weir (AgriDrain Corp), enabling quantification of flow up to 880 m^3/d. Flows above 880 m^3/d are measured by treating the drainage control structure above the v-notch as a rectangular weir (Rosen & Christianson, 2017; Shokrana & Ghane, 2021).

$$Q = \begin{cases} 1.079 * h^{2.5} & h \leq 20cm \\ 1.079 * 20^{2.5} + 158832 * (\frac{l}{100} - 0.2 * (\frac{h}{100} - \frac{20}{100})) * (\frac{h}{100} - \frac{20}{100})^{1.5} & h > 20cm \end{cases} \quad \text{Eq. 4-1}$$

Where Q is flow (m3/d), h is hydraulic head (cm), and l is length of weir crest (cm) (l = 16cm) when the v-notch weir is full. Average daily flow is calculated by averaging the 15-minute flow measurements for 24 hours centered around the average sampling time of the inlet and outlet samplings. Nutrient loading and removal rates were calculated by multiplying average daily flow by influent concentration or influent less effluent concentration, respectively, normalized to total bed volume (612 m3).

Hydraulic residence time (HRT), or the average time influent remains in contact with bioreactor media was determined assuming ideal plug-flow using the equation for theoretical HRT:

$$HRT = \rho\, V/Q \quad \text{Eq. 4-2}$$

where HRT is in hr, ρ is the media porosity (m^3/m^3), V is the saturated media volume/bed volume (m^3), and Q is the flow rate (m^3/hr). Nitrogen removal rates were calculated from the time series of flow, N concentration measurements, and bioreactor characteristics described above collected during the second year of operation. The statistical significance and 95% confidence intervals of mean removal rates and removal efficiencies were determined with one-sample t-tests.

$$RE = 100*(1- C_{out}/C_{in}) \quad \text{Eq. 4-3}$$

Where RE is removal efficiency expressed in percent, C_{out} and C_{in} are effluent and influent concentration, respectively (mg/L).

Initial exploration of the data revealed that effluent concentrations were explained well by a first order kinetics relationship with HRT as follows:

$$C_{out} = C_{in} * e^{-kt} \quad \text{Eq. 4-4}$$

Where *k* is the reaction rate (1/hr), and *t* is the HRT (hr). This assumption of first order kinetics is consistent with Lepine et. al (2016) and Chun et. al (2010). The reaction constant, *k,* is influenced by both bioreactor bed temperature and bioreactor age therefore it follows that *k* can be further partitioned as:

$$C_{out} = C_{in} * e^{-HRT*(k_1+k_2*temp+k_3*age)} \quad \text{Eq. 4-5}$$

Where *temp* is bioreactor bed temperature (°C); *age* is bioreactor age (days); k_1 is the baseline reaction rate for *temp = 0* and *age = 0;* k_2 is the reaction rate increase when *temp* increases by 1 °C; and k_3 is the reaction rate increase when *age* increases by one day. Rearranging Eq. 4-4 to isolate the reaction constants (k_1, k_2, k_3) gives:

$$-ln(\frac{C_{out}}{C_{in}})/HRT = k_1 + k_2 * temp + k_3 * age$$ Eq. 4-6

Assessment of the linear model residuals for Eq. 4-5 yielded strong autocorrelation in time and thus first order autoregressive model (AR1), similar to that applied in Bock et al. (2018) was deemed most appropriate:

$$-ln(\frac{C_{out}^t}{C_{in}^t})/HRT_t = k_1 + k_2 * temp_t + k_3 * age_t + AR1 * e_{t-1}$$ Eq. 4-7

Where e_{t-1} is the error term at *t-1* and *AR1* is the regression coefficient on e_{t-1}. The response was determined to be appropriately represented by an AR1 model because their autocorrelation for lags 1-4 and lags 6-25is less than 0.14 which corresponds to the $a = 0.05$ significance level. Lag 5 had an autocorrelation of 0.21. Because there is no physical reason that might explain why lag 5 is important but lags 1-4 aren't, and because this autocorrelation value is small we do not include this in our regression. Reaction constants in Eq. 4-6 were determined by linear regression of the negative natural log of the ratio of inlet and outlet concentrations normalized by HRT against k_1, k_2, and k_3. Please note that the dependent variable in Eq. 4-6 is used for the sole purpose of approximating the coefficients k_1, k_2, k_3, and *AR1.* Once these estimates are known, the load removal equation expressing load removed results in:

$$LR = Q * C_{in}/V * (1 - e^{-HRT*(k_1+k_2*temp+k_3*age+AR1*e_{t-1})})$$ Eq. 4-8

Where *LR* is load removed in (g/m^3/d), and *Q* is flow (m^3/d). Substituting $Q = \rho V/HRT$ from Eq. 2 into Eq. 7*,* and noting *V* cancels, this can be rewritten as:

$$LR = C_{in}\rho/HRT * (1 - e^{-HRT*(k_1+k_2*temp+k_3*age+AR1*e_{t-1})})$$ Eq. 4-9

Thus, Eq. 4-9 relates the load removed by the bioreactor to the influent concentration and hydraulic residence time modified by bioreactor age and temperature dependent processes, similar to models proposed by Bock et al. (2018), Christianson et al. (2012), Lepine et al. (2016) and Povilaitis & Matikienė (2020). The model was fit using 299 days of data. Model parameters were selected by evaluating model residuals, term significance, and model interpretability consistent with Bock et al. (2018), Christianson et al., (2012), Hassanpour et al., (2017), and Lepine et al., (2016). Homoscedasticity in residuals was verified visually. A Shapiro-Wilks test indicates that the model residuals are normally distributed with a p-value = 1.987e-08.

4.3 Results

4.3.1 Bioreactor Performance Summary

Nutrient loading to the bioreactor averaged 7.7 g/m^3/d. The bioreactor cumulatively removed an estimated 21% of the influent N at an average rate of 1.5 g/m^3/d (table 4-1). A one sample t-test indicates that the true average removal efficiency and load removed observed is significantly different than zero (95% confidence interval: 20.3% to 22.0%, or 1.47 to 1.56 g/m^3/d, respectively). The mean influent concentration of the bioreactor was 6.5 mg/L and the concentrations were fairly consistent, ranging between 5.6 and 7.4 mg/L. The average HRT and bioreactor bed temperature was 13.3 hours and 11.8 ^{o}C, respectively. Please note that the reported flows, HRTs, and temperatures are reported on a 15-minute interval. Average daily values are used for the regression analysis. Time series data is plotted in figure 4-2. Figure 4-3 explores the relationship between load removal and inputs including HRT, bioreactor temperature, and bioreactor age.

Table 4-1: Summary statistics of bioreactor conditions and performance

	Minimum	1st Quartile	Mean	Median	3rd Quartile	Maximum	Variance	N
Load removed (g/m3/d) [kg/d]	0.43 [0.26]	1.34 [0.82]	1.47 [0.91]	1.53 [0.94]	1.68 [1.04]	2.96 [1.82]	0.12 [0.05]	203
Removal efficiency (%)	5.27	16.86	21.14	21.33	24.55	37.08	35.72	203
Influent concentration (mg/L)	5.61	6.24	6.48	6.52	6.82	7.43	0.19	203
Effluent concentration mg/L)	3.86	4.67	5.10	5.14	5.60	6.59	0.41	203
Influent load (g/m3/d) [kg/d]	3.43 [2.11]	6.75 [4.16]	7.66 [4.72]	7.44 [4.58]	8.55 [5.27]	9.82 [6.05]	2.3 [0.87]	203
Effluent load (g/m3/d) [kg/d]	2.41 [1.48]	5.26 [3.24]	5.97 [3.68]	5.92 [3.64]	6.98 [4.3]	8.51 [5.24]	2.21 [0.84]	203
Flow (m3/d)	346	625	711	688	813	911	23822	34285
HRT (hours)	9.41	10.55	12.06	13.31	13.73	24.77	14.99	34285
Bed temperature (deg C)	9.10	11.30	11.80	12.08	12.90	15.10	1.34	25267

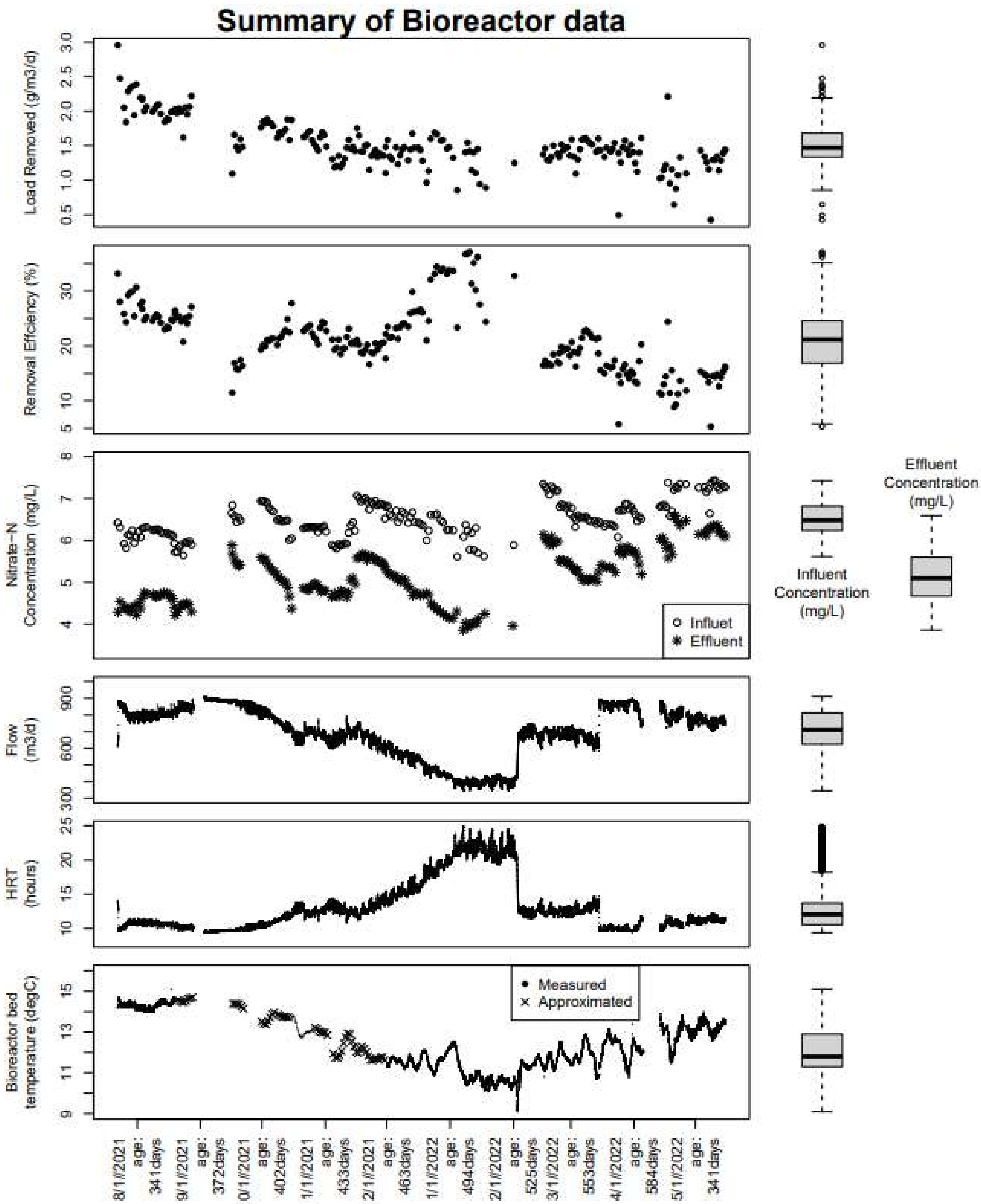

Figure 4-2 Summary of bioreactor performance; on the x-axis is date and corresponding bioreactor age

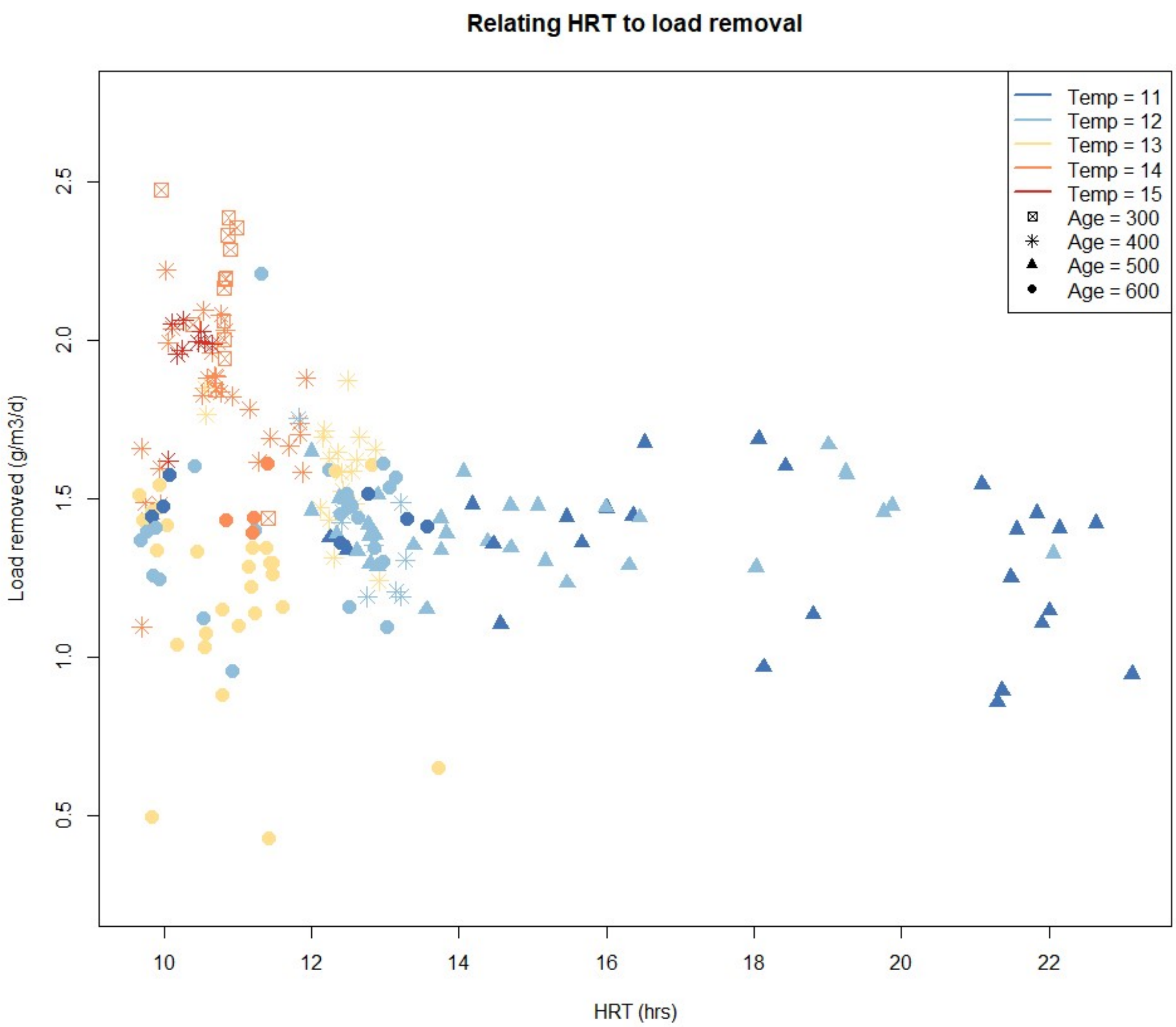

Figure 4-3: Relating load removal to HRT (x-axis), bioreactor temperature (represented in color, rounded to the nearest whole ºC), and bioreactor age (represented in point shape, rounded to the nearest hundred days)

4.3.2 Estimating bioreactor performance

4.3.2.1 Secondary analysis: finding reaction rate k

Eq. 4-7 is used to determine values for k_1 - k_3 and the *AR1* coefficients (Table 4-2).

Table 4-2: Approximating reaction rates resulting from regression analysis of Eq. 4-7

	Multiple regression results
k1	0.027
k2	8.81E-04
k3	-3.95E-05
AR1	0.472

4.3.2.2 Estimation of load removal

In this section we apply the deductions found in 4.3.2.1, ARIMA regression, to eq. 4-9. In doing so, we find that the autocorrelation issues are satisfied by the inclusion of the AR1 coefficient. This model results in an R^2 of 0.63 (figure 4-3), when comparing predicted load removal to measured load removal. Using the range of values observed in the bioreactor, an hour increase of HRT results in a decrease of between 0.004 g/m^3/d (for low load removal conditions) and 0.03 g/m^3/d (for high load removal conditions). A single degree increase in temperature can be found to increase load removed between 0.06 g/m^3/d (for low load removal conditions: old bioreactor and large HRT) and 0.08 g/m^3/d (for high load removal conditions). Similarly, a single day increase in bioreactor age can be found to decrease load removed between 0.002 g/m^3/d (for low load removal conditions) and 0.003 g/m^3/d (for high load removal conditions). Lastly, an increase of 1 mg/L of nitrogen inlet concentration results in between 0.13 g/m^3/d (for low load removal conditions) and 0.33 g/m^3/d (for high load removal conditions).

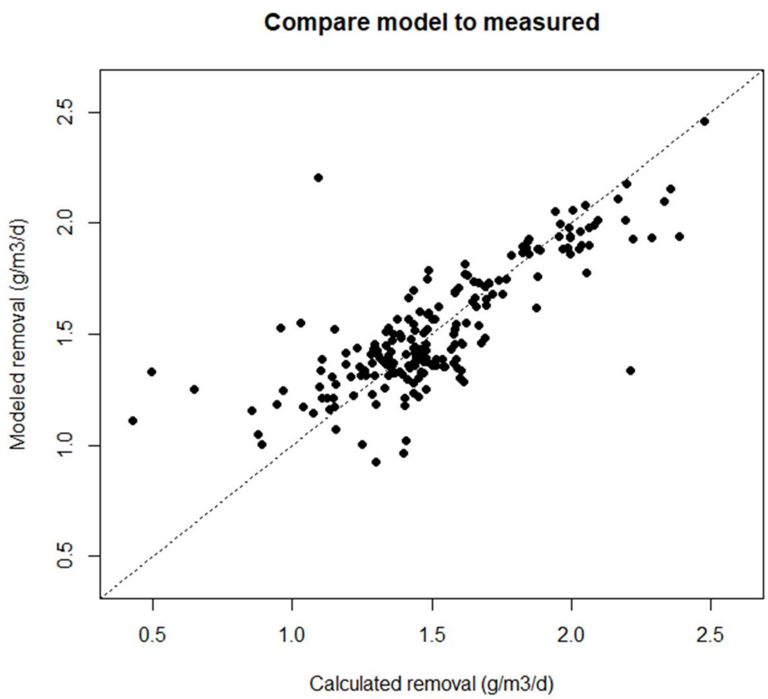

Figure 4-4 Comparing modeled and measured load removal

From looking at figure 4-4, we see that the model is able to predict load removal with some success. To visualize specifically the effects that bioreactor conditions have on load removal, figure 4-4 is generated. Please note that a generalized reaction constant *k* will be explored in figure 4-4 such that: $k = k_1 + k_2*temp + k_3*age + AR1*e_{t-1}$

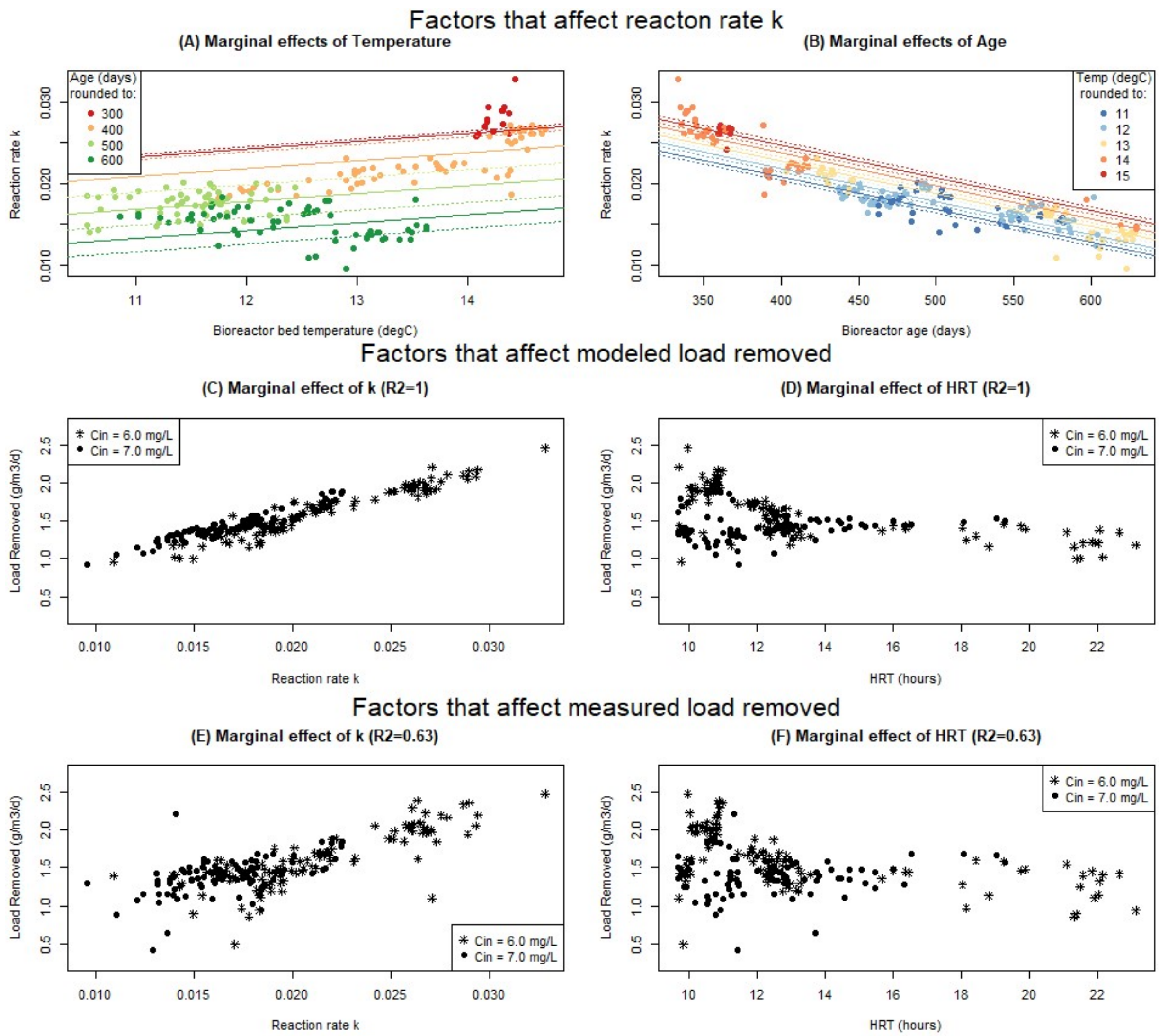

Figure 4-5 Visualization of how bioreactor conditions affect load removal via the relationship explained by eq. 4-9

Please note that the graphics displayed are condensing several dimensions into fewer dimensions. For example, reaction rate (k) is linearly related to bioreactor age, temperature, and the e_{t-1}. Plots (A) and (B) are visual representations of how much the ARIMA method affects the relationship between input bed temperature and bioreactor age respectively. For figure 4-5(A), the colors represent all the data points that have bioreactor ages corresponding to the legend; the solid line represents the trend for the average bioreactor age in each category and the dotted lines represent the trend for the maxima and minima of the bioreactor age in each category. If no ARIMA method was used, all data points would fall between the dotted lines of their respective color. The ARIMA method is displayed as affecting the values of reaction rate k a good deal. This effectively makes relationships between modeled output and inputs more difficult to evaluate.

In figure 4-4(C) and (D) we see how much variability these visualizations show when condensing higher dimensional data. Both (C) and (D) are representations of the model output plotted against a model input (i.e. $R^2 = 1$). When comparing figure 4-4(C) and (D) to figure 4(E) and (F) we see some additional noise appear in both graphics that can be attributed to model prediction error. Generally, additional noise is present for small reaction constants (k) and for large HRTs. The additional error associated with large HRTs may be an artifact of HRTs being difficult to calculate (Christianson et al., 2011) and a small error in calculation results in a large HRT error when HRTs are large.

4.4 Discussion

4.4.1 Modeling load removal

In this research we found that by using a physically based regression model, we were able to predict load removal of nitrogen with moderate success ($R^2 = 0.63$). There is some agreement that denitrifying bacteria adhere to first order reaction kinetics (Chun et al., 2009; Christianson et al., 2012; Lepine et al., 2016) [eq. 3], and we used this principle to derive a multivariate linear regression model [eq. 7]. The aforementioned regression model is then directly applied to load removal [eq. 9]. The resulting equation formation agreed with the general consensus between Christianson et al. (2012), Lepine et al. (2016), and Povilaitis & Matikienė (2020) that load removal decreases exponentially as HRT increases.

Contextualizing the resulting specific coefficient is difficult, because few have specified a model similar to this research. The formulation proposed by Lepine et al. (2016) was similar to our final results, as both formulas related load removal to Euler's number (*e*) to the power of -HRT; though Lepine et al. (2016) relates this term to load removed via a straight regression. Though the resulting equation from Lepine et al. (2016) poses a striking similarity, it is constrained by static coefficients when compared to the proposed model. As such, the value that would correspond to the reaction rate constant (k) would likely be considerably different if the model was respecified identically to the model proposed in this paper. However, this issue should not entirely preclude the comparison of the models. Lepine et al. (2016) finds $k = 0.22$; when the values from table 4-2 are used to calculate k using average temperature and bioreactor age for the "loading test period" in this study (~12.5 ^{o}C and 218 days, respectively), the result is $k=0.028$. It should be noted that (1) Lepine et al. (2016) is modeling a considerably different system; the bioreactor N loading is substantially larger, and (2) the calculated reaction rate constant for the proposed method is extrapolated slightly for bioreactor age (bioreactor age_{min} = 332 days).

4.4.2 What affects load removal

4.4.2.1 HRTs

Over the range of inputs, a single hour increase in HRT resulted in a decrease of between 0.004 and 0.03 g/m^3/d. This result is relatively consistent with the literature. Bock et al. (2018) finds an hour increase in HRT results in a decrease of 0.06 g/m^3/d when load removal is linearly related to HRT. Christianson et al. (2012) finds an hour increase results in a decrease of 0.03 g/m^3/d (for the Pekin bioreactor which is most similar to the N influent concentrations examined in this paper) when load removed is linearly related to HRT. Povilaitis & Matikienė (2020) finds an hour increase in HRT results in a maximum of 0.056 g/m^3/d (for inputs that correspond to the aforementioned 0.03 g/m^3/d removal) when load removed is related via LR~HRT^-constant. Please note that: (1) both Bock et al. (2018) and Christianson et al. (2012) contain additional linear inputs that relate to HRT, so these comparisons could change considerably in a differently specified model and (2) the range of HRTs evaluated in Povilaitis & Matikienė (2020) (2-9.5 hrs) is entirely below the range of HRTs evaluated in this investigation, and thus the aforementioned comparison is lightly extrapolated ($LR_{HRT=10}$ - $LR_{HRT=11}$).

This analysis was largely driven by finding the best HRTs to maximize load removal. We found that load removal was maximized at HRT = HRT_{min} for all bioreactor conditions evaluated. This contradicts Addy et al. (2016) and Christianson et al. (2012), who suggest that optimal HRTs depend on bioreactor conditions. Prima facie, our findings disagree with well-established research, however, these two ideas are not mutually exclusive. Given the proposed equation [eq. 9], maximal load removal occurs at HRT = 0 hours. Though this is certainly counterintuitive, the range of HRTs evaluated were not near HRT = 0 hours (HRT_{min} = 9.4 hours [table 4-1]), and thus drawing this conclusion so far outside of the observed data is ill-advised. This presents an obvious opportunity to refine this investigation: test lower HRTs to see when the assumption of first order reactions is no longer advantageous for model prediction. We anticipate there to be a single nonzero HRT (less than HRT_{min}) that would correspond to a maximal load removal, and the optimal HRT value would depend on bioreactor conditions. Thus, this corroborates the ideas put forward by Addy et al. (2016) and Christianson et al. (2012).

Despite the investigators' best efforts, smaller HRTs could not be obtained due to deteriorated construction of the concrete that contained the spring. The bioreactor was designed to field an estimated 40-50% of the spring flow (median flow: 3,200 m^3/d), but investigators could not divert more than 20% consistently to the bioreactor. With these design constraints, the designed bioreactor ultimately was too large to treat typical flows in the desired HRT range (4-8hrs). Lastly, it is also important to note that theoretical calculations can often be fairly erroneous when compared to true HRTs (Christianson, 2013). This study would have benefitted from a tracer test to corroborate the true HRT of the system.

4.4.2.2 Temperature

Spring fed bioreactors are expected to have colder bed temperatures (especially in the summer) relative to their surface fed counterparts. It is well established that lower temperatures inhibit bioreactor efficiency (Christianson et al., 2012; Hoover et al., 2016; Hassanpour et al., 2017; Bock et al., 2018; Povilaitis & Matikienė, 2020); this is corroborated by our findings. We find that a single ^{o}C increase in temperature corresponds to an increase of load removal between 0.06 and 0.08 $g/m^3/d$ (for low and high removal rate conditions, respectively). Bock et al. (2018) found, for the same inputs that correspond to the 0.08 $g/m^3/d$, a single ^{o}C increase in temperature corresponds to an increase of load removal of 0.16 $g/m^3/d$.

We could seek to increase bioreactor temperature thus increase load removal via the following untested ideas: adding black geotextile fabric to the bioreactor surface (to both decrease the surface albedo and eliminate plant growth, thus reducing transpiration [an endothermic process]), or increasing piping length. However, bioreactor managers and designers should be cognizant of the surface water standards (Surface Water Standards with General, Statewide Application; 9VAC25-260-60. Rise above Natural Temperature, 1992, Surface Water Standards with General, Statewide Application 9VAC25-260-70. Maximum Hourly Temperature Change, 1992) that specify modifications to effluents cannot warm the overall system. The temperature was measured at the spring, bioreactor outlet, and downstream of the merging of the bioreactor effluent and bypass stream twice. This indicated (albeit weak because of small sample size; n=2) that the bioreactor had a cooling effect (if any) on the smith creek for the evaluated reactor.

4.4.2.3 Bioreactor age

In this study, we found that a single day increase in bioreactor age decreased load removal by between 0.002 and 0.003 $g/m^3/d$. This is somewhat similar to the findings of Christianson et al. (2012). When the bioreactor age was increased by a single day, the Green county and Hamilton county bioreactor load removal decreased by 0.004 and 0.003 $g/m^3/d$, respectively. It should be noted that these bioreactors were selected for comparison over the Pekin bioreactor because the evaluation period for both Green and Hamilton county were much closer to that of the bioreactor studied.

There is a concern for this bioreactor's longevity in particular because the nitrifiers were fixing nitrogen in cold temperatures. Maxwell et al. (2020) finds that the long-term decline is more rapid for colder reactors when compared to an otherwise equal warmer reactor. This is especially true when a bioreactor is subjected to both cold temperature and HRTs < 20 hours which was found to accelerate organic carbon losses (Jéglot et al., 2022). Povilaitis & Matikienė (2020) notes that biochar addition may help particularly cold reactors (*temp* < 10ºC), while it's been found to be largely non-advantageous for warm systems. Thus, addition of biochar could help combat the aforementioned shortened longevity associated with cold water bioreactors, though more research is needed to confirm the validity of this strategy.

4.4.2.4 Other predictors (not found to be significant in proposed model)

Predictors that we found to be insignificant for modeling but were collected included pH, DO (dissolved oxygen), and ORP (oxidative redox potential). pH data ranged from 7.0 to 7.8. It is understandable that pH played a nonsignificant role in the effect of denitrification given the results from Antoniou et al. (1990) who found that an optimum denitrifying pH occurred at 7.8, and the difference in expected denitrification for the temperature range observed in our system was small. The karst nature of this location makes bioreactor installation especially advantageous because of high pHs relative to other systems (typical ranges between 5-7) (Bock et al., 2018; Povilaitis & Matikienė, 2020).

DO concentrations were zero for 99.1% of data points. The high instances of zeros make this a poor predictor for bioreactor performance. In addition, these values indicate optimal DO conditions as defined by Metcalf et al. (1991). There is certainly an opportunity to evaluate the fluxes of DO as the treated water moves towards the outlet much like the experiment constructed by Christianson et al. (2013). As water enters the bioreactor, the DO will not instantaneously become zero. A setup such as this could help us identify the critical distance between the beginning of the bioreactor and the DO measurement such that DO measurements are mostly nonzero. This would produce data that could have potential to inform load removal models.

4.4.3 Advantages and disadvantages of spring fed over traditional edge of field bioreactors

It is most typically recommended that the design of the bioreactor revolves around mitigating issues that arise from unsteady systems (Christianson, 2013). For example, bioreactors must be designed around peak flows (NRCS, 2015) because a high flow could result in flooding and adverse destruction for a bioreactor that is undersized. However, if a bioreactor dries out completely, aerobic nitrification can lead to increased leaching of dissolved organics, and hydrogen sulfide production (Lopez-Ponnada et al., 2017). Currently, the research specifies bioreactor sizing to be mostly related to these two adverse effects, and the majority of field scale studies are constrained by these. However, for spring fed bioreactors, wetting-drying cycles are rare (for nonseasonal springs), and flows are typically semi-uniform. As a result, the optimal design of a spring fed bioreactor could considerably deviate from the conventional design specifications. Arguably, designing a spring fed system is straightforward relative to its surface water counterpart because of semi-uniform input conditions. If the bioreactor design is simplified for spring bioreactors, it will be considerably easier to design a system around targeted HRTs. Spring fed bioreactors provide an interesting niche that can allow researchers to explore small HRTs. Currently there is some consensus that load removed relates to HRTs as an exponentially decaying function (Christianson et al., 2012; Lepine et al., 2016; Povilaitis & Matikienė, 2020). However, this does not make physical sense at the HRT = 0 boundary condition, where theoretical load removed would also be zero. There is a clear need to evaluate the relationships between load removed and HRT for small HRT in a field setting. This campaign can be uniquely applied to spring fed bioreactors because their design is arguably much simpler and does not rely on nonuniform flow conditions for design.

In addition to the possible simplification of bioreactor design, semi-uniform inputs result in favorable denitrification conditions. Traditional applications of bioreactors are complicated by fluctuating systems. A spring fed system eliminates wetting and drying cycles, providing a more stable environment for denitrifying microbes. In fact, Hassanpour et al. (2017) finds, at their Chemung county site, that semi-uniform flow provides stable conditions for denitrifiers and found this site in particular to be considerably more efficient with respect to HRT when compared to two other bioreactors.

Though the uniform conditions of bioreactor inputs are advantageous in many ways, this was also disadvantageous for this study because a small range of bioreactor treatments and performance resulted in a small application range of the resulting model. When referring to table 4-1, we see that a small range of removal efficiencies and bioreactor conditions are explored relative to other studies. Hassanpour et al. (2017), Lepine et al. (2016), Christianson et al. (2012), Povilaitis & Matikienė, (2020), and Christianson, et al. (2012) evaluate bioreactor efficiencies between 0-100%, 0-100%, 7-100%, 10-80%, 12-76%, respectively. These ranges of explored removal efficiencies are considerably larger than the removal efficiencies reported in this study (5-37%). In consideration of a future study, it is important to design the bioreactor such that a wider range of HRTs and possibly other inputs, such as inlet concentrations and bed temperature, can be evaluated.

In addition to the aforementioned benefits, spring fed bioreactors provide a unique opportunity to address legacy nitrogen. Legacy nitrogen is a widespread, difficult water quality issue to address (Lindsey, 2003; Phillips & Lindsey, 2003; Sanford & Pope, 2007; NRCS, 2011; Easton et al., 2019). Both Easton et al. (2019) and Stephenson et al. (2021) have identified spring fed bioreactors as a unique way to address prevalent high N loadings of springs in the Chesapeake Bay.

4.5 Conclusions

Results presented herein indicate that the reaction kinetics model is a successful predictor of load removal, and all the marginal effects of temperature, bioreactor age, and HRT were well aligned with existing research. Our principle findings include:

1. The spring fed bioreactor studied adheres to first order reaction kinetics, and the reaction kinetics equation was successfully applied to modeling bioreactor performance via load removal.
2. Spring fed bioreactors have their advantages (stable environment for denitrifying microbes) and disadvantages (colder and therefore less efficient).

Future studies should seek to design a spring fed system such that a greater variety of bioreactor states can be explored. Additionally, spring fed bioreactors could provide a unique opportunity for economic solutions proposed by Jones et al. (2010), McKibben (2022), and Stephenson et al. (2021) that pay constituents who implement best management practices based on the amount of contaminant they are able to remove. Spring fed bioreactors are somewhat predictable (relative to edge-of-field systems), and thus quantifying performance may be easier in a system such as this.

References

Addy, K., Gold, A. J., Christianson, L. E., David, M. B., Schipper, L. A., Ratigan, N.A. 2016. Denitrifying Bioreactors for Nitrate Removal: A Meta-Analysis. *Journal of Environmental Quality*, *45*(3), 873–881. https://doi.org/10.2134/jeq2015.07.0399

Antoniou, P., Hamilton, J., Koopman, B., Jain, R., Holloway, B., Lyberatos, G., Svoronos, S. A. 1990. Effect of temperature and ph on the effective maximum specific growth rate of nitrifying bacteria. *Water Research*, *24*(1), 97–101. https://doi.org/10.1016/0043-1354(90)90070-M

Bock, E. M., Coleman, B. S. L., Easton, Z. M. 2018. Performance of an under-loaded denitrifying bioreactor with biochar amendment. *Journal of Environmental Management*, *217*, 447–455. https://doi.org/10.1016/j.jenvman.2018.03.111

Bock, E., Smith, N., Rogers, M., Coleman, B., Reiter, M., Benham, B., Easton, Z. M. 2015. Enhanced nitrate and phosphate removal in a denitrifying bioreactor with biochar. *Journal of Environmental Quality*, *44*(2), 605–613. https://doi.org/10.2134/jeq2014.03.0111

Burke, P. M., Hill, S., Iricanin, N., Douglas, C., Essex, P., Tharin, D. 2002. Evaluation of preservation methods for nutrient species collected by automatic samplers. *Environmental Monitoring and Assessment*, *80*(2), 149–173. https://doi.org/10.1023/a:1020660124582

Chamberlain, S. (2021). *rnoaa: "NOAA" Weather Data from R. R package version 1.3.4*. https://CRAN.R-project.org/package=rnoaa

Chen, D., Shen, H., Hu, M., Wang, J., Zhang, Y., Dahlgren, R. A. 2018. Chapter Five - Legacy Nutrient Dynamics at the Watershed Scale: Principles, Modeling, and Implications. In D. L. Sparks (Ed.), *Advances in Agronomy* (Vol. 149, pp. 237–313). Academic Press. https://doi.org/10.1016/bs.agron.2018.01.005

Christianson, L. (2013). Modeling and Calibration of Drainage Denitrification Bioreactor Design Criteria. *Journal of Irrigation and Drainage Engineering*, *139*(9), 699–709. https://doi.org/10.1061/(ASCE)IR.1943-4774.0000622

Christianson, L., Bhandari A., Helmers, M.J. 2011. Pilot-Scale Evaluation of Denitrification Drainage Bioreactors: Reactor Geometry and Performance. *Journal of Environmental Engineering*, *137*(4), 213–220. https://doi.org/10.1061/(ASCE)EE.1943-7870.0000316

Christianson, L, Bhandari, A., Helmers, M., Kult, K., Sutphin, T., Wolf, R. 2012. PERFORMANCE EVALUATION OF FOUR FIELD-SCALE AGRICULTURAL DRAINAGE DENITRIFICATION BIOREACTORS IN IOWA. *American Society of Agricultural and Biological Engineers*, *55*(6). https://vt.hosts.atlas-sys.com/illiad/illiad.dll?Action=10&Form=75&Value=1611795

Christianson, L. E., Collick, A. S., Bryant, R. B., Rosen, T., Bock, E. M., Allen, A. L., Kleinman, P. J. A., May, E. B., Buda, A. R., Robinson, J., Folmar, G. J., Easton, Z. M. 2017. Enhanced denitrification bioreactors hold promise for mid-Atlantic ditch drainage. *Agricultural & Environmental Letters*, *2*(1), 170032. https://doi.org/10.2134/ael2017.09.0032

Chun, J. A., Cooke, R. A., Eheart, J. W., Cho, J. 2010. Estimation of flow and transport parameters for woodchip-based bioreactors: II. field-scale bioreactor. *Biosystems Engineering*, *105*(1), 95–102. https://doi.org/10.1016/j.biosystemseng.2009.09.018

Chun, J.A., Cooke, R.A., Eheart, J.W., Kang, M.S. 2009. Estimation of flow and transport parameters for woodchip-based bioreactors: I. Laboratory-scale bio- reactor. Biosyst. Eng. 104:384–395. doi:10.1016/j.biosystemseng.2009.06.021

Coleman, B. S. L., Easton, Z. M., Bock, E. M. 2019. Biochar fails to enhance nutrient removal in woodchip bioreactor columns following saturation. *Journal of Environmental Management*, *232*, 490–498. https://doi.org/10.1016/j.jenvman.2018.11.074

Dunderman, L., Verma, S., Davidson, P. 2019. Evaluation of Sodium Omadine for Short-Term Preservation of Nitrate-N and Orthophosphate in Water Samples. *NATO Advanced Science Institutes Series E: Applied Sciences*, *9*(7), 1450. https://doi.org/10.3390/app9071450

Easton, Z. M., Bock, E., Stephenson, K. 2019. Feasibility of Using Woodchip Bioreactors to Treat Legacy Nitrogen to Meet Chesapeake Bay Water Quality Goals. *Environmental Science & Technology*, *53*(21), 12291–12299. https://doi.org/10.1021/acs.est.9b04919

Easton, Z. M., Rogers, M., Davis, M., Wade, J., Eick, M. 2015. Mitigation of sulfate reduction and nitrous oxide emission in denitrifying environments with amorphous iron oxide and biochar. *Ecological*. https://www.sciencedirect.com/science/article/pii/S0925857415300446

Greene, E. A., LaMotte, A. E., Cullinan, K.-A. 2005. *Ground-water vulnerability to nitrate contamination at multiple thresholds in the mid-Atlantic region using spatial probability models* (No. 2004-5118). https://doi.org/10.3133/sir20045118

Hassanpour, B., Giri, S., Pluer, W. T., Steenhuis, T. S., Geohring, L. D. 2017. Seasonal performance of denitrifying bioreactors in the Northeastern United States: Field trials. *Journal of Environmental Management*, *202*(Pt 1), 242–253. https://doi.org/10.1016/j.jenvman.2017.06.054

Hoover, N. L., Bhandari, A., Soupir, M. L., Moorman, T. B. 2016. Woodchip Denitrification Bioreactors: Impact of Temperature and Hydraulic Retention Time on Nitrate Removal. *Journal of Environmental Quality*, *45*(3), 803–812. https://doi.org/10.2134/jeq2015.03.0161

Jéglot, A., Miranda-Velez, J. F., Plauborg, F., Elsgaard, L. 2022. Nitrate removal and environmental side-effects controlled by hydraulic residence time in woodchip bioreactors treating cold agricultural drainage water. *Environmental Technology*, 1–10. https://doi.org/10.1080/09593330.2022.2091482

Jones, C. Y., Branosky, E., Selman, M., Perez, M. 2010. *How nutrient trading could help restore the Chesapeake bay*. https://cbf.typepad.com/files/wripaper.pdf

Kleinman, P. J. A., Fanelli, R. M., Hirsch, R. M., Buda, A. R., Easton, Z. M., Wainger, L. A., Brosch, C., Lowenfish, M., Collick, A. S., Shirmohammadi, A., Boomer, K., Hubbart, J. A., Bryant, R. B., Shenk, G. W. 2019. Phosphorus and the Chesapeake Bay: Lingering Issues and Emerging Concerns for Agriculture. *Journal of Environmental Quality*, *48*(5), 1191–1203. https://doi.org/10.2134/jeq2019.03.0112

Lepine, C., Christianson, L., Sharrer, K., Summerfelt, S. 2016. Optimizing Hydraulic Retention Times in Denitrifying Woodchip Bioreactors Treating Recirculating Aquaculture System Wastewater. *Journal of Environmental Quality*, *45*(3), 813–821. https://doi.org/10.2134/jeq2015.05.0242

Lindsey, B. D. 2003. *Residence times and nitrate transport in ground water discharging to streams in the Chesapeake Bay Watershed*. https://books.google.ca/books?hl=en&lr=&id=R1_gRUymuA4C&oi=fnd&pg=PA1&ots=XcXTc2j4xx&sig=7ieFfFSHQNyr6Jz6ANdz1SqEuf4

Lopez-Ponnada, E. V., Lynn, T. J., Peterson, M., Ergas, S. J., Mihelcic, J. R. 2017. Application of denitrifying wood chip bioreactors for management of residential non-point sources of nitrogen. *Journal of Biological Engineering*, *11*, 16. https://doi.org/10.1186/s13036-017-0057-4

Maxwell, B. M., Díaz-García, C., Martínez-Sánchez, J. J., Birgand, F., Álvarez-Rogel, J. 2020. Temperature sensitivity of nitrate removal in woodchip bioreactors increases with woodchip age and following drying–rewetting cycles. *Environmental Science: Water Research & Technology*, *6*(10), 2752–2765. https://doi.org/10.1039/D0EW00507J

McKibben, P. A. 2022. *Using Monte Carlo Analysis to Assess Outcome-based Payment for Environmental Services for Denitrifying Bioreactors in the Chesapeake Bay* [Virginia Tech]. https://vtechworks.lib.vt.edu/handle/10919/107419

Meals, D. W., Dressing, S. A., Davenport, T. E. 2010. Lag time in water quality response to best management practices: a review. *Journal of Environmental Quality*, *39*(1), 85–96. https://doi.org/10.2134/jeq2009.0108

Metcalf, L., Eddy, H. P., Tchobanoglous, G. 1991. *Wastewater engineering : treatment, disposal, and reuse*. library.wur.nl. https://library.wur.nl/WebQuery/titel/1979505

Moorman, T. B., Tomer, M. D., Smith, D. R., Jaynes, D. B. 2015. Evaluating the potential role of denitrifying bioreactors in reducing watershed-scale nitrate loads: A case study comparing three Midwestern (USA) watersheds. *Ecological Engineering*, *75*, 441–448. https://doi.org/10.1016/j.ecoleng.2014.11.062

Noe, G. B., Cashman, M. J., Skalak, K., Gellis, A., Hopkins, K. G., Moyer, D., Webber, J., Benthem, A., Maloney, K., Brakebill, J., Sekellick, A., Langland, M., Zhang, Q., Shenk, G., Keisman, J., Hupp, C. 2020. Sediment dynamics and implications for management: State of the science from long-term research in the Chesapeake Bay watershed, USA. *WIREs. Water*, *7*(4). https://doi.org/10.1002/wat2.1454

NRCS. 2011. *Achieving Nutrient and Sediment Reduction Goals in the Chesapeake Bay* (Committee on the Evaluation of Chesapeake Bay Program Implementation for Nutrient Reduction to Improve Water Quality, Water Science and Technology Board, & Division on Earth and Life Studies (eds.)). The National Academes Press. https://www.chesapeakebay.net/channel_files/21727/2011_nas_report.pdf

NRCS. 2015. *Natural Resources Conservation Service CONSERVATION PRACTICE STANDARD DENITRIFYING BIOREACTOR* (Version 605-CPS-1). NRCS.

Phillips, S., Lindsey, B. D. 2003. The influence of ground water on nitrogen delivery to the Chesapeake Bay. In *Fact Sheet*. US Geological Survey. https://doi.org/10.3133/fs09103

Povilaitis, A., Matikienė, J. 2020. Nitrate removal from tile drainage water: The performance of denitrifying woodchip bioreactors amended with activated carbon and flaxseed cake. *Agricultural Water Management*, *229*, 105937. https://doi.org/10.1016/j.agwat.2019.105937

R Core Team. 2022. *R: A Language and Environment for Statistical Computing*. https://www.R-project.org/

Rosen, T., Christianson, L. 2017. Performance of Denitrifying Bioreactors at Reducing Agricultural Nitrogen Pollution in a Humid Subtropical Coastal Plain Climate. *WATER*, *9*(2), 112. https://doi.org/10.3390/w9020112

Sanford, W., Pope, J. P. 2007. *A simulation of groundwater discharge and nitrate delivery to chesapeake bay from the lowermost delmarva peninsula, USA*. https://www.semanticscholar.org/paper/3239453cadd422beb67af4e70d650eb580cdf55d

Schipper, L. A., Cameron, S. C., Warneke, S. 2010. Nitrate removal from three different effluents using large-scale denitrification beds. *Ecological Engineering*, *36*(11), 1552–1557. https://doi.org/10.1016/j.ecoleng.2010.02.007

Sharpley, A., Jarvie, H. P., Buda, A., May, L., Spears, B., Kleinman, P. 2013. Phosphorus legacy: overcoming the effects of past management practices to mitigate future water quality impairment. *Journal of Environmental Quality*, *42*(5), 1308–1326. https://doi.org/10.2134/jeq2013.03.0098

Shokrana, M. S. B., Ghane, E. 2021. An empirical V-notch weir equation and standard procedure to accurately estimate drainage discharge. *Applied Engineering in Agriculture*, *37*(6), 1097–1105. https://doi.org/10.13031/aea.14617

Stackpoole, S. M., Stets, E. G., Sprague, L. A. 2019. Variable impacts of contemporary versus legacy agricultural phosphorus on US river water quality. *Proceedings of the National Academy of Sciences of the United States of America*, *116*(41), 20562–20567. https://doi.org/10.1073/pnas.1903226116

Stephenson, K., Ferris, W., Bock, E., Easton, Z. M. 2021. Treatment of Legacy Nitrogen as a Compliance Option to Meet Chesapeake Bay TMDL Requirements. *Environmental Science & Technology*, *55*(20), 13593–13601. https://doi.org/10.1021/acs.est.1c04022

Surface Water Standards with General, Statewide Application; 9VAC25-260-60. Rise above natural temperature, no. §§ 62.1-44.15(3) and (10) of the Code of Virginia., Virginia Administrative Code 1992. https://law.lis.virginia.gov/pdf/admincode/9/25/260/60/

Surface Water Standards with General, Statewide Application 9VAC25-260-70. Maximum hourly temperature change, no. 62.1-44.15(3a) of the Code of Virginia, Virginia Administrative Code 1992. https://law.lis.virginia.gov/pdf/admincode/9/25/260/70/

Van Meter, K. J., Basu, N. B. 2017. Two centuries of nitrogen dynamics: Legacy sources and sinks in the Mississippi and Susquehanna River Basins. Global Biogeochemical Cycles. https://doi.org/10.1002/2016GB005498

Chapter 5: Conclusions

5.1 Distributing soil maps (Chapter 2 & 3)

In the United States the finest nationally available classifications of soil physical properties is the SSURGO database. The SSURGO database distributes soils based on a database of roughly 20,000 pedons that spans all American states and most territories (Nemecek 2020). On average, this is a sampling density of roughly 1 pedon for every 350 to 500 km^2.Though much of the continental United States exceeds this density, realistic sampling densities are still fairly sparse. Soil sampling is expensive, and the density is unlikely to change drastically in a small amount of time. SSURGO is unlikely to make the strides needed in this area to compensate for its shortcomings given this current metric of soil classification. Currently, this distribution of soils is the gold standard for several applications but describes landscape soils poorly as seen in chapters 2 & 3 as well as in multiple other studies (Moore et al., 1993; Collick et al., 2015; Fuka et al., 2016). These studies represent multiple geographic locations (Colorado, Vermont, New York, Pennsylvania, Texas and Virginia), implying that this issue is potentially widespread.

Because soil properties relate strongly to landscape (Stolt et al., 1993; Zhi et al., 2008), DEMs and derivatives thereof can help predict soil properties (Moore et al., 1993; Gessler et al., 2000; Rezaei & Gilkes, 2005; Thompson et al., 2006; Collick et al., 2015). Because DEMs are important for a broad range of applications, innovations in this area of research will continue to surge. As a result, tying research to an innovative field with abundant diverse datasets is advantageous. In comparing the DEM sampling density (as small as a sample for every $0.09m^2$) to the SSURGO soil sampling density (as small as a sample for every ~1e+8 m^2), it is clear that including DEMs for soil map creation can provide additional information. It is important to note that, though the sampling for DEMs is up to a billion times more dense, DEMs are not direct representations of soil, unlike the SSURGO soil samples.

Chapter 2 of this dissertation found that SSURGO did not relate to any measured soil properties in a small watershed in southwest Virginia. Between the four DEMs examined, large (+/- 1m) spatially dependent disagreements between two DEMs were common. These disagreements propagated into derived spatial data; this finding is consistent with Wolock & Price (1994) and Sørensen & Seibert (2007). A single slope and SCA are selected to spatially distribute soil properties via multiple regression. The selected resolutions for the regressions were not homogenous for each soil property (i.e., there was no clear best resolution for distributing soil properties); five of six measured soil properties selected mixed resolution DEMs to best distribute soil properties. This resulted in soil maps with gradual changes for soil properties relative to the SSURGO distributed maps. Additionally, the proposed multiple regression did better than regression with LiDAR slopes and SCAs as inputs. Ultimately, this chapter found that both coarse and fine resolution DEMs showed promise in soils distribution.

Chapter 3 focused on the relationship between resolution size and soil characteristics in addition to much of the analysis done in chapter 2. When fine resolution data was recursively coarsened, a plateau for high slope correlations is found at DEMs greater than 11m in size. A finer resolution than this correlates poorly with measured soil properties. When the same is evaluated for SCA, not much is gleaned. This research found (much like in the previous chapter) that spatial attributes derived from multiple DEMs are advantageous for all four soil properties explored. Similar to the chapter 2 findings, resulting soil maps were gradual with respect to the soil distribution relative to SSURGO, and the proposed multiple regression outperformed the LiDAR multiple regression. The proposed regression models did not pick slopes derived from DEMs less than 10m, implying that slopes derived from small resolutions are poor predictors for this application.

5.2 Future work: Distributing soil maps (Chapter 2 & 3)

It is likely that the chapter 2 & 3 findings would not translate well to different physiographic regions. Physiographic regions have variable climates, topography, feature size, and vegetation. These factors would directly affect the mechanisms of landscape change such as erosion and deposition. Moore et al., (1993), Collick et al., (2015), Fuka et al., (2016), and the results discussed in chapters 2 & 3 display that there is certainly an opportunity to supplement and improve SSURGO distributed soils. There is considerable disagreement between previous research that evaluates best DEM resolutions for soils and hydrologic processes (Wolock & Price, 1994; Zhang & Montgomery, 1994; Hancock et al., 2006; Sørensen et al., 2006; Schumann et al., 2008; Vaze et al., 2010; Buchanan et al., 2014; Gibson et al., 2021). The true best DEM is unlikely to be the same for all the regions or applications studied. Additional studies with diverse response variables and regions would be integral in understanding the resolution size and spatial attributes that best represent processes.

5.3 Conclusions: Spring fed bioreactors (Chapter 4)

Legacy nitrogen is a widespread, difficult to address issue that is arguably preventing attainment of water quality goals (NRCS, 2015). Easton et al., (2019) investigates the prevalence and the expected mass nitrogen exported. They found that nutrient heavy springs could be responsible for 3,690 kg/yr of nitrogen. The concentrated sources of nitrogen provide a unique opportunity to apply an emerging technology to treat nitrogen: bioreactors. Bioreactors are most typically installed edge-of-field and treat highly variable flow and nitrogen load. The consistency in loading and flow provide a uniquely stable environment for denitrifiers. A spring in northern Virginia is outfitted with a bioreactor, and bioreactor bed temperature, flow, influent, and effluent concentrations are measured for 10 months. Bioreactor efficiency is quantified and modeled using a first order reaction driven model. Marginal effects of bioreactor bed temperature, age, and HRT are found to be consistent with Bock et. al, (2018), Christianson et al., (2012), Povilaitis & Matikienė (2020) and Lepine et al., (2016). This project discusses the benefits, including lack of drying-wetting cycles; eliminates bioreactor specific concerns regarding toxic effluent; and drawbacks, including colder water temperature resulting in a less efficient system relative to edge-of-field counterparts, of implementing spring bioreactors.

5.4 Future work: Spring fed bioreactors (Chapter 4)

The consistency in spring fed bioreactor performance would allow economists to implement pay for performance systems with ease relative to edge-of-field counterparts. This idea consists of paying bioreactor managers for demonstrated performance of their bioreactor. The spring bioreactor efficiency was modeled successfully using woodchip age, bioreactor, flow and temperature (which could effectively be modeled by environmental temperature). As such, modeling bioreactor performance is attainable for a system such as this with fewer data points when compared to the more chaotic edge-of-field system.

References

Bock, E.M., Coleman, B.S. L., Easton, Z.M. 2018. "Performance of an under-Loaded Denitrifying Bioreactor with Biochar Amendment." *Journal of Environmental Management* 217 (July): 447–55.

Buchanan, B. P., Fleming, M., Schneider, R. L., Richards, B. K., Archibald, J., Qiu, Z., Walter, M. T. 2014. "Evaluating Topographic Wetness Indices across Central New York Agricultural Landscapes." *Hydrology and Earth System Sciences* 18 (8): 3279–99.

Christianson, L, Bhandari, A., Helmers, M., Kult, K., Sutphin, T., Wolf, R., 2012. "PERFORMANCE EVALUATION OF FOUR FIELD-SCALE AGRICULTURAL DRAINAGE DENITRIFICATION BIOREACTORS IN IOWA." *American Society of Agricultural and Biological Engineers* 55 (6). https://vt.hosts.atlas-sys.com/illiad/illiad.dll?Action=10&Form=75&Value=1611795.

Collick, A.S., Fuka, D.R., Kleinman, P.J.A., Buda, A.R., Weld, J.L., White, M.J., Veith, T.L., Bryant, R.B., Bolster, C.H., Easton, Z.M. 2015. "Predicting Phosphorus Dynamics in Complex Terrains Using a Variable Source Area Hydrology Model: MODELLING P DYNAMICS IN COMPLEX TERRAINS." *Hydrological Processes* 29 (4): 588–601.

Easton, Z.M., Bock, E., Stephenson, K. 2019. "Feasibility of Using Woodchip Bioreactors to Treat Legacy Nitrogen to Meet Chesapeake Bay Water Quality Goals." *Environmental Science & Technology* 53 (21): 12291–99.

Fuka, D.R., Collick, A.S., Kleinman, P.J.A., Auerbach, D.A., Harmel, R.D., Easton, Z.M. 2016. "Improving the Spatial Representation of Soil Properties and Hydrology Using Topographically Derived Initialization Processes in the SWAT Model," November. https://doi.org/10.1002/hyp.10899.

Gessler, P. E., Chadwick, O.A., Chamran, F., Althouse, L., Holmes, K. 2000. "Modeling Soil-Landscape and Ecosystem Properties Using Terrain Attributes." *Soil Science Society of America Journal. Soil Science Society of America*, SSSA Spec. Publ. 33, 64 (6): 2046–56.

Gibson, A.J., Hancock, G. R., Bretreger, D., Cox, T., Hughes, J., Kunkel, V. 2021. "Assessing Digital Elevation Model Resolution for Soil Organic Carbon Prediction." *Geoderma* 398 (September): 115106.

Hancock, G. R., Martinez, C., Evans, K.G., Moliere, D.R. 2006. "A Comparison of SRTM and High-Resolution Digital Elevation Models and Their Use in Catchment Geomorphology and Hydrology: Australian Examples." *Earth Surface Processes and Landforms* 31 (11): 1394–1412.

Lepine, C., Christianson, L., Sharrer, K., Summerfelt, S. 2016. "Optimizing Hydraulic Retention Times in Denitrifying Woodchip Bioreactors Treating Recirculating Aquaculture System Wastewater." *Journal of Environmental Quality* 45 (3): 813–21.

Moore, I.D., Gessler, P.E., Nielsen, G.A., Peterson, G.A. 1993. "Soil Attribute Prediction Using Terrain Analysis." *Soil Science Society of America Journal*. https://doi.org/10.2136/sssaj1993.03615995005700020058x.

Nemecek, J. 2020. "National Cooperative Soil Survey (NCSS) Soil Characterization Database: The National Cooperative Soil Survey (NCSS) Soil Characterization Database Contains the Analytical Results from the Kellogg Soil Survey Laboratory (KSSL) at the NCSS." September

9, 2020.
https://nrcs.maps.arcgis.com/home/item.html?id=65ffa754044548919781c0f0136aec88.

NRCS. 2015. "Natural Resources Conservation Service CONSERVATION PRACTICE STANDARD DENITRIFYING BIOREACTOR." NRCS.

Povilaitis, A., Matikienė, J. 2020. "Nitrate Removal from Tile Drainage Water: The Performance of Denitrifying Woodchip Bioreactors Amended with Activated Carbon and Flaxseed Cake." *Agricultural Water Management* 229 (February): 105937.

Rezaei, S.A., Gilkes, R.J. 2005. "The Effects of Landscape Attributes and Plant Community on Soil Physical Properties in Rangelands." *Geoderma* 125 (1): 145–54.

Schumann, G., Matgen, P., Cutler, M.E.J., Black, A., Hoffmann, L., Pfister, L. 2008. "Comparison of Remotely Sensed Water Stages from LiDAR, Topographic Contours and SRTM." *ISPRS Journal of Photogrammetry and Remote Sensing: Official Publication of the International Society for Photogrammetry and Remote Sensing* 63 (3): 283–96.

Sørensen, R., Seibert, J. 2007. "Effects of DEM Resolution on the Calculation of Topographical Indices: TWI and Its Components." *Journal of Hydrology* 347 (1): 79–89.

Sørensen, R., Zinko, U., Seibert, J. 2006. "On the Calculation of the Topographic Wetness Index: Evaluation of Different Methods Based on Field Observations." *Hydrology and Earth System Sciences* 10 (1): 101–12.

Stolt, M.H., Baker, J.C., Simpson, T.W. 1993. "Soil-Landscape Relationships in Virginia: II. Reconstruction Analysis and Soil Genesis." *Soil Science Society of America Journal. Soil Science Society of America* 57 (2): 422–28.

Thompson, J.A., Pena-Yewtukhiw, E.M., Grove, J.H. 2006. "Soil–landscape Modeling across a Physiographic Region: Topographic Patterns and Model Transportability." *Geoderma* 133 (1): 57–70.

Vaze, J., Teng, J., Spencer, G. 2010. "Impact of DEM Accuracy and Resolution on Topographic Indices." *Environmental Modelling & Software* 25 (10): 1086–98.

Wolock, D.M., Price, C.V. 1994. "Effects of Digital Elevation Model Map Scale and Data Resolution on a Topography-Based Watershed Model." *Water Resources Research* 30 (11): 3041–52.

Zhang, W., Montgomery, D.R. 1994. "Digital Elevation Model Grid Size, Landscape Representation, and Hydrologic Simulations." *Water Resources Research* 30 (4): 1019–28.

Zhi, L.I., Wen-zhao. L.I.U., Qiu-xian, W. 2008. "Effects of Land Use Type and Slope Position on Soil Physical Properties in Loess Tableland Area." *Chinese Journal of Applied Ecology* 19 (06): 1303.